UiT
THE ARCTIC UNIVERSITY OF NORWAY

Faculty of Science and Technology - Department of Geosciences

Environmental impact of sediment-hosted stratiform iron deposits: an on-land vs. submarine tailing simulation

A study of the stratiform iron mineralization in Dunderland Valley

—

Birgitte Andrea Fagerheim

Master's thesis in Geology GEO-3900

May 2019

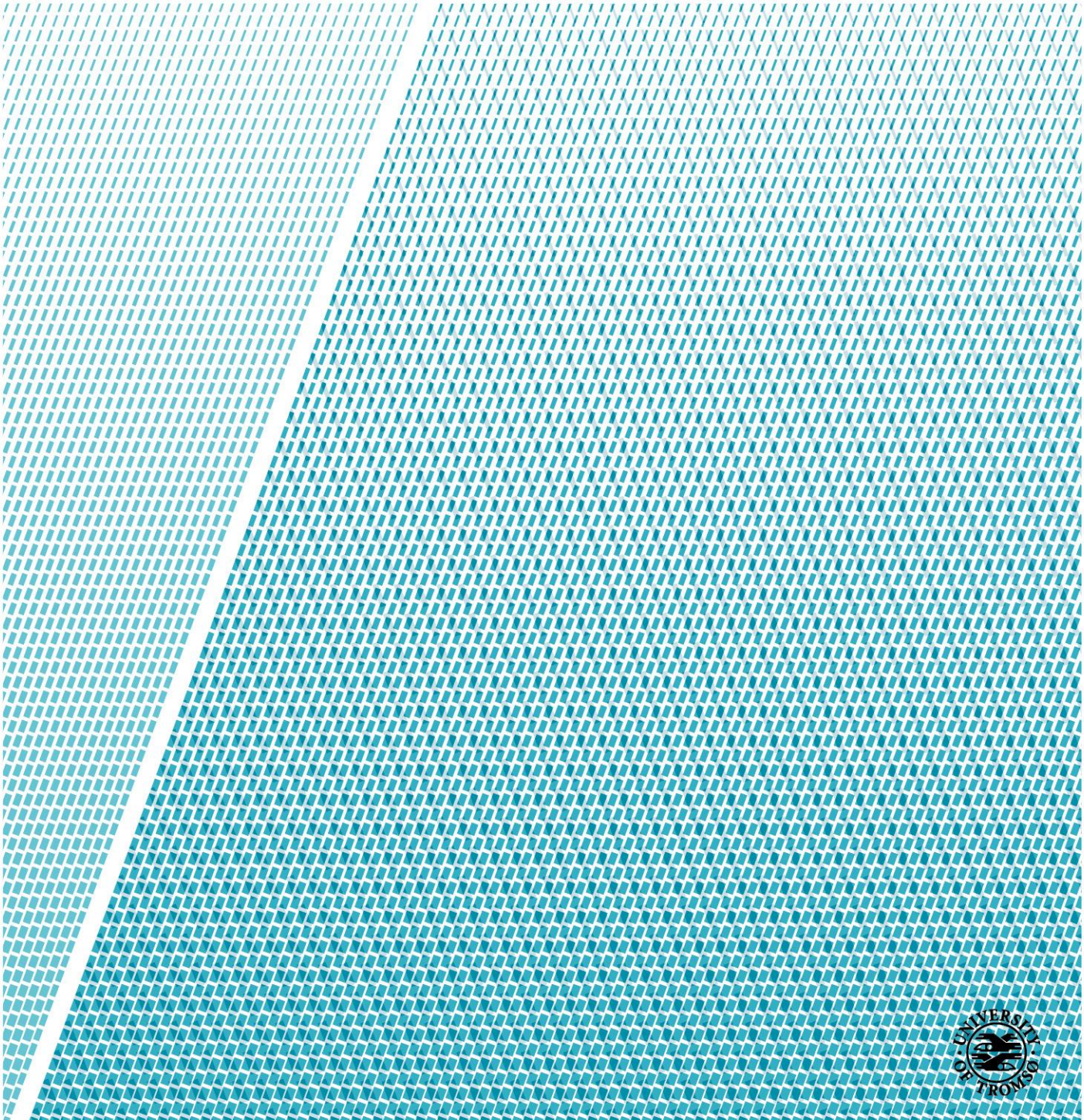

UiT - The Arctic University of Norway

Faculty of Science and Technology

Department of Geosciences

GEO-3900

Master thesis in Hard Rock Geology

❖

Environmental impact of sediment-hosted stratiform iron deposits: an on-land vs. submarine tailing simulation.

A study of the stratiform iron mineralization in Dunderland Valley.

❖

Submitted by: Birgitte Andrea Fagerheim

Supervisor: Sabina Strmic Palinkaš

Abstract

This thesis studies possible environmental impacts of tailings from the stratiform iron deposits. The study was conducted on selected mineralized samples from the Dunderland Valley, Nordland, simulating on-land and submarine tailing disposal conditions.

The Dunderland Valley mineralization is hosted by Neoproterozoic (Tonian, 800-730 Ma) meta-sedimentary sequence of the Caledonian Uppermost Allochthon. The main ore minerals are hematite and magnetite, with quartz and carbonates as principal gangue minerals. Locally, a manganese-rich mineralization occurs. The concentrations of sulphide in is low, with iron sulphides recorded mostly along contact of ore bodies and host rocks.

The study combines determination of mineralogical and geochemical characteristics of three main types of ore mineralization and their behaviour in a kinetic column test (12 weeks; modified EPA method 1627) simulating: 1) non-buffered on-land; 2) carbonate-buffered on-land; 3) submarine conditions. Physicochemical properties (pH, redox potential (Eh) and conductivity) of the kinetic column leachates were measured after 24 h, 48h, 1 week, 2 weeks, 6 weeks and 12 weeks. The ore samples were analysed on major and trace element composition before and after the kinetic test to determine potential geochemical changes. Thin sections of the ore samples were exposed to similar conditions as the kinetic test to trace potential mineralogical reactions. Thermodynamic modelling was performed to determine speciation of iron and manganese in on-land and submarine conditions.

Results showed that the ore samples contain mostly iron-oxides, manganese-silicates and silica, with trace values of copper in the hematite and magnetite samples, and cobalt, arsenic and antimony in the manganese rich sample. These elements are in stable mineral phases, therefore do not represent an environmental threat. Since the samples are characterized by a high Fe^{3+}/Fe^{2+} ratio, negligible amounts of sulphide minerals and abundant carbonate content, their capability to generate acid mine drainage (AMD) and mobilize heavy metals is extremely low. The resulting data from the kinetic column test showed that carbonate-buffered on-land and submarine simulated conditions had the highest pH and the least fluctuating measurements, implying that they are the most favourable conditions for storage of tailings. The lithogeochemical analysis showed some depletion of copper in the hematite sample for all conditions. The results from the thin section exposed to weathering conditions presented altered calcite grains of all samples in non-buffered on-land conditions. The speciation of iron and manganese showed that an addition of carbonates and components of the marine system do not give a significant effect to bind the iron and manganese, indicating that it will not contribute to mobilize iron and manganese.

Acknowledgements

First, I would like to thank my supervisor Sabina Strmic Palinkaš for always taking time to discuss and answer my questions, your guidance throughout the work of my thesis and your enthusiasm for research has been essential. Thank you for giving me the unique opportunity to work on this study of environmental science, a subject which I find extremely fascinating and interesting. I would like to thank Yulia Mun for help and collaboration in the lab, and Hanne-Kristin Paulsen for sampling seawater from your sailboat and guidance in CorelDraw. The laboratory staff at Institute of Geoscience, UiT, Karina Monsen, Ingvild Hald and Trine Dahl, thank you for your help and assistance.

I will like to thank Rana Gruber and Mineralklynge Norge for founding the project. A sincere thanks goes to the geologist working in Rana Gruber and to professor Steffen Bergh and fellow students Kristian Lie and Fredrik Lie for making the field work an educational and good experience.

Finally, I would like to thank family and friends, for support and encouragement through the year. Thanks to Julia, Ragnhild and Egil for tea breaks and motivation during the writing process. I'm so grateful for the proofreading from Franciszka Stopa, Johanne Hansen, and especially Ragnhild Eiesland with the kind words, support and corrections. Last, but not least, thanks to Thomas for always making me happy and for believing in me.

Birgitte Andrea Fagerheim

Tromsø, May 2019.

Table of content

Abbreviations

Minerals

Hm – Hematite

Mt – Magnetite

Mu – Muscovite

Qtz – Quartz

Cc – Chalcocite

Sps – Spessartine

Bt – Biotite

Cal – Calcite

Other

PPL – Plane polarized light

XPL – Crossed polarized light

Ma – Million years ago

Ga – Billion years ago

Glossary of Terms

Anoxic and oxygenated conditions: Refers to conditions in water with a depletion of oxygen (anoxic) and content of oxygen (oxygenated).

Storm and fair-weather wave base: In general, a wave base is the depth in the water column where there are no motions (waves). The difference between storm and fair-weather wave base is the depth of the base. The storm wave base in much deeper than the fair-weather base, since the waves cause motions in the water column deeper when it is a storm. The fair-weather wave base is beneath the average daily waves (Peters and Loss, 2012).

Euphotic zone: "*Is a layer within the water column that is close to the surface, so it receives enough light for photosynthesis to occur"(Britannica, 2018).*

Benthic community: Refers to the species living at the lowest level of a water body, in contact with the substrate (bottom of the ocean) (Britannica, 2018).

Sills: Refers to an aquatic sill, that is a barrier on the seafloor between basins.

PAHs: "*Polycyclic aromatic hydrocarbon (PAHs) are ubiquitous environmental pollutants generated primary during incomplete combustion of organic materials*" (Abdel-Shafy and Mansour, 2016).

Heavy metals: "…*any metallic chemical element that has a relatively high density and is toxic or poisonous at low concentrations. Examples of heavy metals include mercury (Hg), cadmium (Cd), arsenic (As), chromium (Cr), thallium (Tl), and lead (Pb)" (Lenntech).*

Bioaccumulation: "…*an increase in the concentration of a chemical in a biological organism over time, compared to the chemical's concentration in the environment. Compounds accumulate in living things any time they are taken up and stored faster than they are broken down (metabolized) or excreted" (Lenntech).*

Bioavailability: "*The degree to which a chemical in a potential source is free for uptake (movement into an organism)" (Newman and Jagoe, 1992 and Benson and Albert, 1992 cited in Naidu et al., 2008).*

1 Introduction and study objective

Increased industrial activities, aligned with society demands for new products, drive fundamental needs for more extensive mineral extraction and future developments in the mining sector (Vogt, 2012; Dold, 2014; Ramirez-Llodra et al., 2015). Mining related activities usually are associated with raised environmental concerns, especially if the activities results in accumulation and deposition of large amounts of tailings (i.e. residual materials after extraction of metals from mineralized rocks) (e.g. Vogt, 2013). The disposal and management of tailings can present a challenging problem for the mining industry, especially due to potential generation of acid mine drainage (AMD) and the leaching of heavy metals (Johnson and Hallberg, 2005; Akcil and Koldas, 2006). The potential environmental impact from the deposited material strongly depends on the origin of the ore mineralization, its mineral composition and chemistry of ore and gangue minerals (Australia, 2007 cited in Vogt, 2013; Dold, 2014). Traditionally, tailings have been deposited on-land, but in some countries, including Norway, disposal of tailings in marine environments is relatively common (Vogt, 2012; Ramirez-Llodra et al., 2015). Some mining companies in Norway use fjords, a submarine environment, for disposal of tailings. The environmental impacts related to disposal of tailings in fjords has not been well studied. Therefore, it is important to obtain more knowledge regarding the environmental impact related to the disposal and the behaviour of tailings in different geochemical environments. This information can be utilized to find the best method for storage of tailing that gives a minimal environmental impact (Dold, 2014).

The objective of this study is to estimate the potential environmental impact related to disposal of tailings from sediment-hosted stratiform iron deposits in on-land and submarine conditions. The study was conducted on samples collected from the stratiform iron mineralization in the Dunderland Valley in Rana municipality, Nordland. The motivation of this study is to determine the best method for deposition of the tailings that can minimize the environmental impact from the mining industry.

The mineralization is hosted by Neoproterozoic (Tonian, 800-730 Ma) meta-sedimentary sequence of the Caledonian Uppermost Allochthon (Melezhik et al., 2015). The main ore minerals are hematite (Fe_2O_3) and magnetite (Fe_3O_4) with quartz and carbonates as principal gangue minerals (Bugge, 1948; Melezhik et al., 2015). In some sections of the formation

manganese-carbonates and –silicates are present. The concentration of sulphide in the ore is low, but iron sulphides (e.g. pyrrhotite) has been recorded locally along contacts of ore bodies and host rocks (Melezhik et al., 2015).

The study combines determination of mineralogical characteristics and chemical composition of the ore mineralization with kinetic column test (12weeks; modified EPA method 1627 (EPA, 2011)) to simulate weathering of tailings in on-land and submarine conditions. The three major types of analysed samples include the Neoproterozoic hematite-, magnetite- and manganese-rich mineralization from the Dunderland Valley. On-land conditions were simulated in: a) non-buffered, chloride- and organic matter-free aqueous solutions and b) carbonate-buffered, chloride- and organic matter-free aqueous solutions. In the submarine simulated conditions, the tested samples were exposed to seawater in presence of organic rich marine sediments. Physicochemical properties of the kinetic column leachates were determined by measuring pH, redox potential (Eh) and conductivity. On the samples weathered in the kinetic column tests, lithogeochemical analysis was performed to determine the potential mineralogical changes before and after weathering. Representative thin sections of the tested samples were exposed to similar conditions as the kinetic column tests to trace potential mineral reactions. The mineralogical characteristics of the tested ore samples were determined by optical microscopy, SEM/EDS, XRD, Raman spectroscopy and lithogeochemistry. The speciation of iron and manganese in on-land and submarine conditions was determined by thermodynamic modelling.

2 Geological background

The stratiform iron mineralization in the Dunderland Valley is located in the south-central part of the Nordland county, near Mo i Rana in the Rana municipality (Fig. 1). The geology of the area has a complex history with variable deformation, metamorphism, thrusting, extension and erosion (Corfu et al., 2014). In this chapter, the geological setting of the **Scandinavian Caledonides,** the **Uppermost Allochthon** and **The stratiform iron mineralization in the Dunderland Valley** are presented.

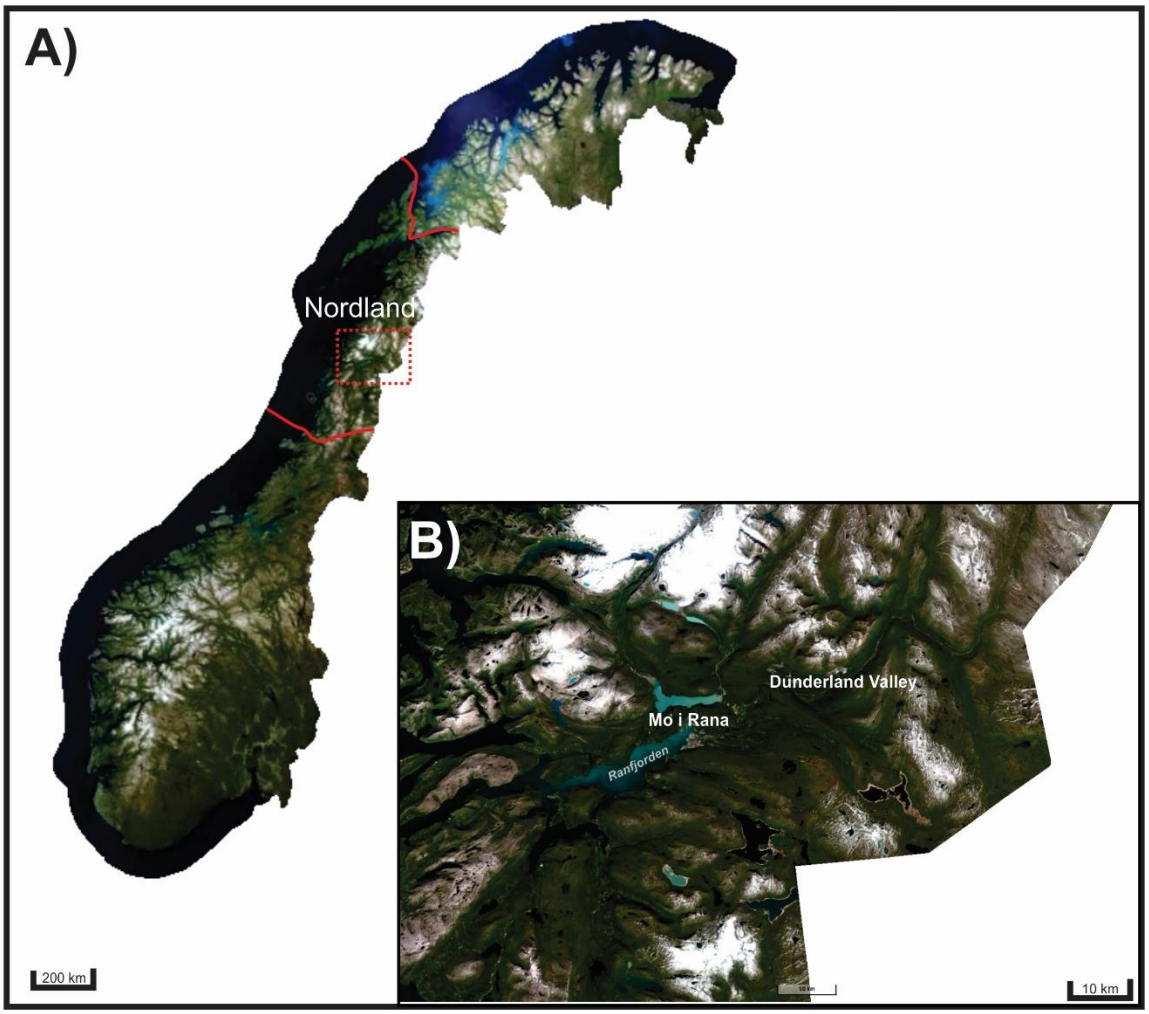

Figure 1: Overview map of A) Norway with location of Nordland county, where B) Dunderland Valley (area of study) is located, near Mo i Rana. Modified map from Norgeskart (Kartverket, 2013).

2.1 The Scandinavian Caledonides

The Scandinavian Caledonides is a mountain belt located in Norway and Sweden, extending from Ryfylkeheiene in the south to Varangerhalvøya in the north (Ramberg et al., 2013). The mountain belt was formed by a continent-continent collision that can be illustrated by the later stages of the Caledonian Wilson tectonic cycle.

The Caledonian Wilson tectonic cycle is a plate tectonic cycle characterized by several stages: **1)** rift-phase of the supercontinent Rodinia at the end of Precambrian (~700 Ma); **2)** opening and development of the Iapetus Ocean; **3)** subduction and formation of volcanic arcs (~500 Ma); **4)** closing of the Iapetus Ocean by drifting of the Laurentian margin (Greenland and North America) to the Baltican margin (northern part of Europe); and **5)** conclusively the collisional phase, where the Laurentian margin was obducted onto the Baltic margin in Silurian-Early Devonian time (~420 Ma)(Grenne et al., 1999; Roberts, 2003; Ramberg et al., 2013).

The main structures of the Scandinavian Caledonides have been characterized as successions of four allochthons (Gee and Sturt, 1985 and Roberts and Gee, 1985 cited in Melezhik et al., 2015). During the collision between the Baltican and Laurentian margin, the successions were thrusted upon each other, over a basement of sedimentary rocks of Precambrian age (Grenne et al., 1999; Melezhik et al., 2015). The allochthons originate from different geological environments, where the lowest allochthons were transported the shortest distance and the structurally highest units were transported the longest distance from their origin (Ramberg et al., 2013).

The four allochthons are described as the Lower, Middle, Upper and Uppermost Allochthon. The Lower Allochthon (LA) and the Middle Allochthon (MA) are shelf and continental rise successions derived from the margin of Baltica. The Upper Allochthon (UA) is composed of metasediments and ophiolite sequence that represents the Iapetus Ocean. The Uppermost Allochthon (UmA) is elements derived from the Laurentian margin (Fig. 2)(Stephens et al., 1985; Stephens and Gee, 1989; Roberts, 2003; Roberts et al., 2007; Gee et al., 2010; Melezhik et al., 2015).

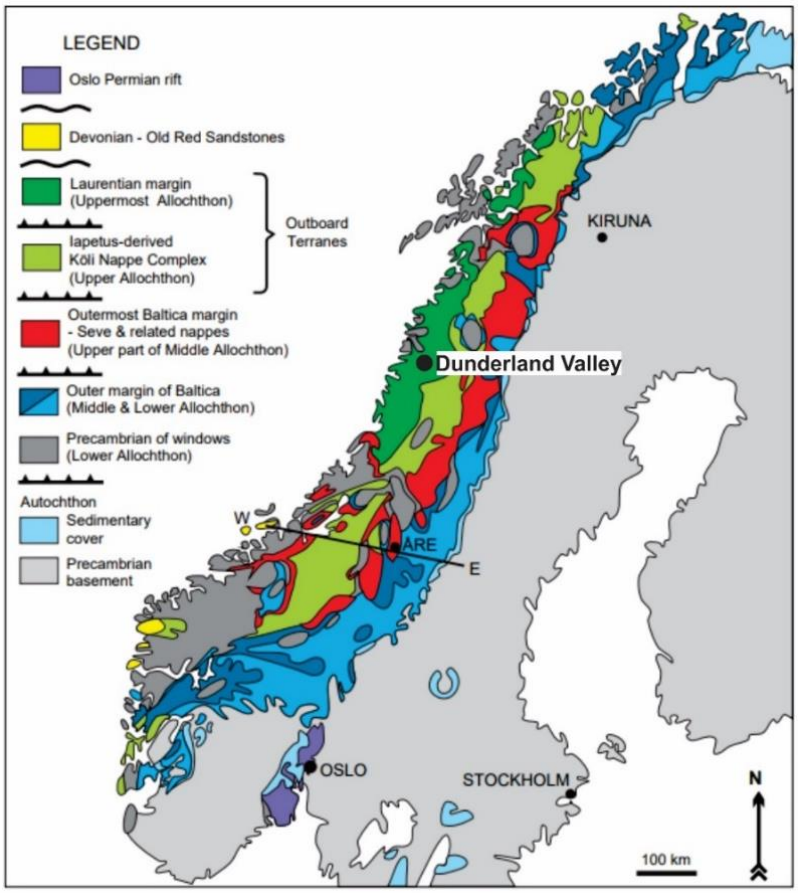

Figure 2: *Modified tectonic map of the Scandinavian Caledonides ((Gee et al., 2010), based on Gee et al. (1985)).*

2.2 The Uppermost Allochthon

During the closure of the Iapetus Ocean, the successions from the continental margin of Laurentia were thrusted upon the Baltican margin and became a part of the Scandinavian Caledonides (Roberts et al., 2007; Melezhik et al., 2015). The Laurentian derived successions are defined as the Uppermost Allochthon (UmA) (Fig 2).

In the area of study, the UmA is divided into several tectonostraigraphical units, including the Rödingsfjället Nappe Complex. The Rödingsfjället Nappe Complex is composed of two main nappes: Ravnålia Nappe and Plura Nappe. The Ravnålia Nappe is further sub-divided into Ørtfjellet group, Dunderland formation and Kjerringfjellet group (Fig. 3) (Søvegjarto et al., 1988, 1989; Gjelle et al., 1991 cited in Melezhik et al., 2015). The UmA is characterised by the presence of medium- to high-grade metasedimentary rocks, with marbles as the predominant lithology (Melezhik et al., 2015).

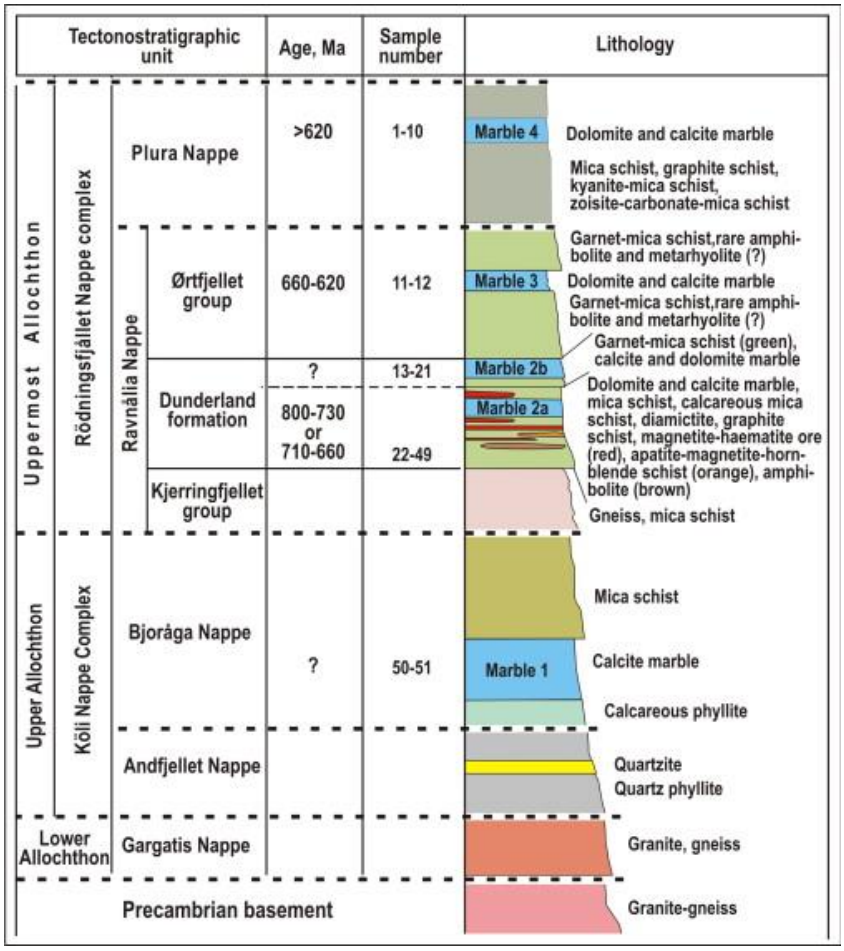

Figure 3: *Overview of the tectonostratigraphic units in Rana region, by Melezhik et al. (2015)(based on (Søvegjarto et al., 1988, 1989; Gjelle et al., 1991; Marker et al., 2012 cited in Melezhik et al., 2015)).*

2.3 The stratiform iron deposits in Dunderland Valley

The stratiform iron deposits of the Dunderland formation are situated in the Uppermost Allochthon of the north central part of the Scandinavian Caledonides (Fig. 4) (Stephens et al., 1985; Grenne et al., 1999; Melezhik et al., 2015). According to Melezhik et al. (2015), the mineralization extends between 65°20´and 69°40´ latitudes, approximately 550 km. The mineralization has an important economic role for the Rana district, where the mine has been operating for nearly a century.

The Dunderland formation consists of a large, complex, antiformal structure called the Dunderland antiform (Fig. 5) (Melezhik et al., 2015). The main lithology of the formation are metasedimentary rocks of amphibolite facies including schists and dolomitic- and calcitic-marbles, which includes various types of mica-, calcareous- and quartz-garnet-mica-schists.

The metasedimentary rocks host the stratiform iron deposits. The deposit occurs in contact with calcareous schists, marbles and diamictites (Melezhik et al., 2015). The major ore mineral is hematite and the subordinate are magnetite. The major gangue mineral is quartz, and the subordinate gangue minerals are dolomite, calcite, biotite, apatite, muscovite, amphiboles, potassic feldspars, epidote and chlorites, and garnets as an accessory mineral (NGU, 2015b). The iron ore contains an average of approx. 34wt.% iron (Bugge, 1978 cited in Melezhik et al., 2015). Hematite makes up to approx. 98% of the iron ore, while the magnetite ore bodies can vary between approx. 2-15% (RanaGruber). The magnetite-dominated ores often have a presence of amphiboles, Fe-Mn-garnets and/or apatite, while the hematite ore is often enriched in epidote (Melezhik et al., 2015). The sulphide content is generally very low in the ores, but can occur locally along mica schist-magnetite ore contacts (Melezhik et al., 2015).

The iron mineralization occurs in banded layers with host rock of carbonate-bearing quartzitic to pelitic matrix, but can also be disseminated (Melezhik et al., 2015). The contact between the host rocks and the iron mineralization is possibly tectonic or conformable (Melezhik et al., 2015). A thin layer of carbonate-mica schist that is rich in Mn-carbonates and Mn–silicates and has a low iron-oxide content, separates the iron deposit from the host-rock (Melezhik et al., 2015). The marble-unit in the Dunderland antiform has an N-S trend and a significant thickness. The marbles are gently folded and occur as calcitic and dolomitic marbles (Melezhik et al., 2015). The thickness varies from 1cm to over 10m (Fig. 5) (Melezhik et al., 2015). Diamictites occur in a conformable contact with the stratiform iron deposits in the western part of the Dunderland antiform. Melezhik et al. (2015) describes the diamictites as generally fine-grained dolostones with rare calc-silicate rocks, where the clasts are mainly rounded of possibly glaciogenic origin.

The formation age of the deposit has been discussed by several authors. Bugge (1948) suggested that the mineralization is Upper Cambrian to Lower Ordovician, while Søvegjarto et al. (1988) argued for the Late Precambrian to Cambro-Ordovician age (Bugge, 1948 and Søvegjarto et al.,1988 cited in Melezhik et al., 2015). From a chemostratigraphic research of marbles associated with the stratiform iron deposits in the Dunderland formation by Melezhik et al. (2015), the formation age of the deposit was determined to be 800-730 Ma (Mid-Late Tonian age).

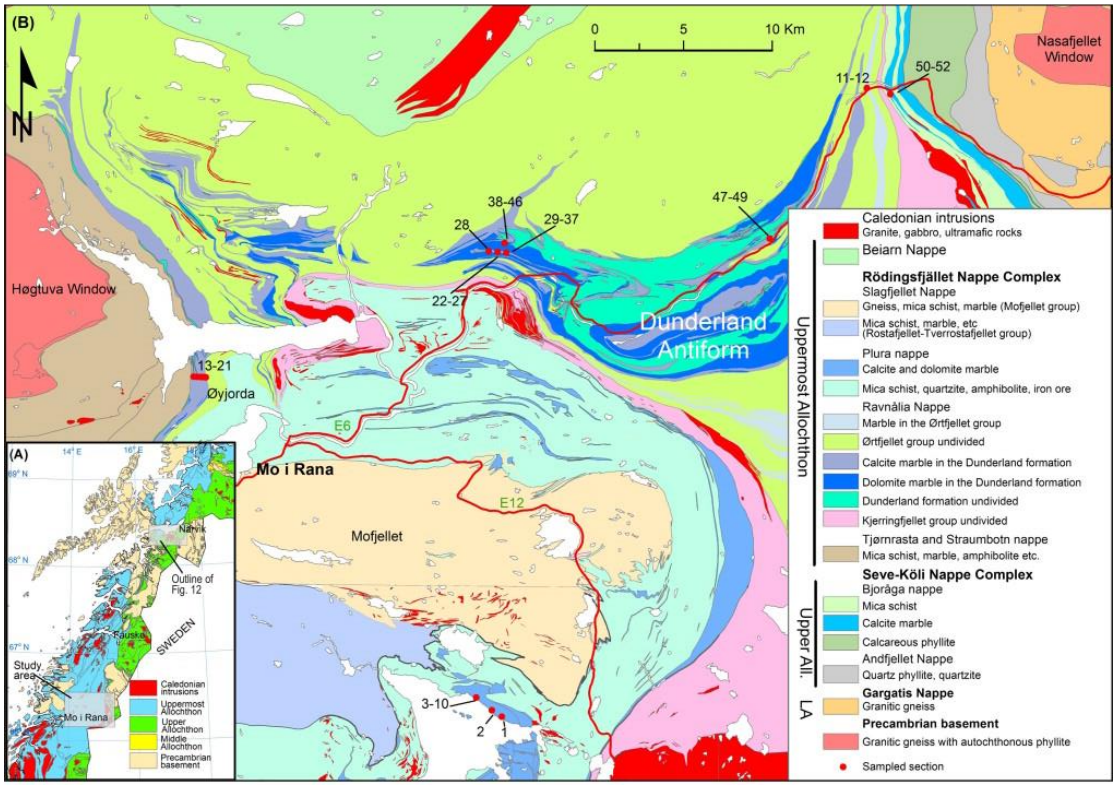

Figure 4: *(A) Geographic location of the study area. (B) Geological map of the Rana region with the Dunderland antiform and description of the nappe complexes (Melezhik et al., 2015). The red points are from another study (Melezhik et al. (2015)) and will not be used in this study. Figure from Melezhik et al. (2015).*

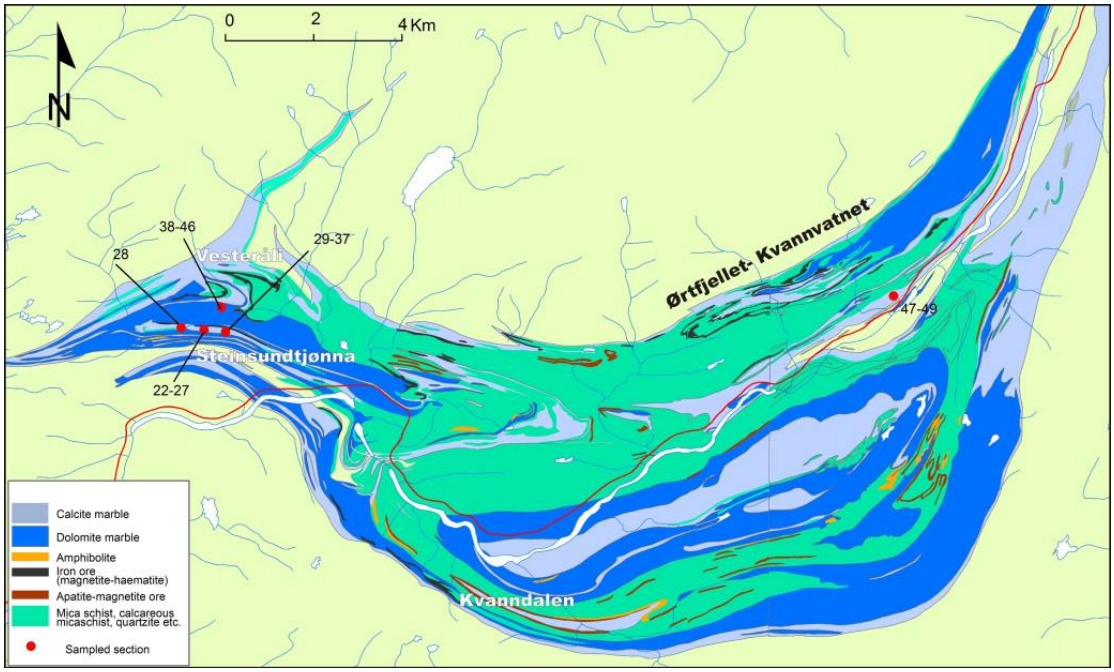

Figure 5: *The Dunderland antiform with a detailed bedrock map. The points are from another study and will not be used in this thesis. Figure from Melezhik et al. (2015).*

3 Theoretical background

This chapter summarizes present knowledge about **Stratiform iron formations**, including banded-iron formations (**BIF)**, Neoproterozoic-iron formations (**NIF)** and sedimentary-exhalative (**SedEx)** deposits. Related to the objective of this study, the **geochemical characteristics of tailing disposal** including the **disposal methods** in on-land and marine environments, **tailing disposal in Norway**, specific on **tailing disposal in Dunderland Valley** and **previous work related to disposal of tailings from Dunderland Valley** is presented**.** Additionally, the environmental issues related to tailing disposal with **mobility of metals in surficial environments** is presented as well.

3.1 Stratiform iron formation

Stratiform deposits are mineral deposits that consists of one or more mineralized sequences that are conformable with enclosing sedimentary strata. The mineralized sequences extend over the full stratigraphic thickness of one or more strata (Canavan, 1973; Skinner, 2015). Iron formations (IFs) are stratigraphic units composed of bedded, layered or laminated iron-rich rocks (15 wt.% or more iron) of a sedimentary or hydrothermal origin (James, 1954; Gross, 1996; Bekker et al., 2010; Konhauser et al., 2017).

Through the evolution of the Earth, the atmospheric conditions have changed. There have been periods with atmospheric anoxic conditions (i.e. oxygen free) dominated by CO_2 and CH_4 and more oxygenated conditions (i.e. rich in O_2) (Bekker and Kaufman, 2007). The development of IFs has been discussed in various literature, but the specific mechanism of IFs deposition has not been resolved. In earlier works, the general thought was that IFs development only came from deep marine redox evolution (events of ocean oxygenation versus sub-anoxic/anoxic conditions), and therefore can be a record of Earth's atmospheric changes (e.g. Bekker et al., 2010). The anoxic/sub-anoxic conditions can cause accumulation of ferrous iron that is stable in solution under anaerobic conditions (Hoffman et al., 1998; Bekker et al., 2010; Rickard, 2012). Some researchers believe that an additional source of iron was needed to form the large masses of IFs. The source of iron can be associated with a sub-marine hydrothermal system and hydrothermal upwelling of iron (Holland, 1973; Bekker et al., 2010; Konhauser et al., 2017) or iron can be transported from a terrestrial source (Bekker et al., 2010). The oxygen content in oceans and its role in the formation of IFs have been

discussed. Some authors suggest that the IFs are related to oxygen stratification in the oceans (oxic/anoxic layers), whereas some other argue for locally oxygenated areas (Klein and Beukes, 1989).

Mechanisms that can affect oxidation of Fe(II) and the deposition of iron hydroxide include both biological and non-biological processes (Fig. 6) (Bekker et al., 2010). The most common biological oxidation mechanism is associated with a cyanobacteria activity and Fe(II) oxidizes with oxygen produced by photosynthesis (Equation 1) (Cloud, 1973; Bekker et al., 2010). Another possible mechanism involved the metabolic iron oxidation by iron bacteria. The bacteria utilize oxygen, carbon dioxide and water to survive and produces ferric hydroxide ($Fe(OH)_3$), or by photoferrotrophy the bacteria use light, carbon dioxide and Fe(II) thereby produce Fe(III) in anoxygenic conditions (Equation 2 / Equation 3) (Ehrenreich and Widdel, 1994; Bekker et al., 2010; Konhauser et al., 2017). The non-biological oxidation mechanism is UV photooxidation of Fe(II). An ultraviolet radiation (*hv*) could have caused a photo-oxidation of ferrous iron to ferric iron (Equation 4). When the levels of oxygen in the atmosphere are low, the flux of ultraviolet radiations is high due to a lack of a protective ozone layer (Cairns-Smith, 1978; Bekker et al., 2010).

$2Fe^{2+} + 0.5O_2 + 5H_2O \leftrightarrow 2Fe(OH)_3 + 4H^+$ **(Equation 1)**

$6Fe^{2+} + 0.5O_2 + CO_2 + 16H_2O \leftrightarrow [CH_2O] + 6Fe(OH)_3 + 12H^+$ **(Equation 2)**

$4Fe^{2+} + 11H_2O + CO_2 \leftrightarrow [CH_2O] + 4Fe(OH)_3 + 8H^+$ **(Equation 3)**

$2Fe^{2+}(aq) + 2H^+ + hv \rightarrow 2Fe^{3+}(aq) + H_2$ **(Equation 4)**

The general age of the IFs is Precambrian Eon, with the peak appearance in Neoarchean to Paleoproterozoic Era (2.80 – 1.85Ga) (Bekker et al., 2010; Konhauser et al., 2017). In Precambrian Eon, the atmosphere and ocean systems were largely anoxic (Cloud, 1973; Holland, 1973). The period between approx. 1.8-0.7 Ga, IFs were absent before reappearance in the end of Neoproterozoic Era (Bekker et al., 2010). The periods with absence of IFs is probably related to complete ocean oxidation (Holland, 1973) or sulfidic conditions in deep-ocean (Canfield, 1998; Poulton et al., 2004 cited in Bekker et al., 2010; Poulton and Canfield, 2011). Kirschvink (1992) explains the reappearance of IFs in Neoproterozoic by the Snowball Earth hypothesis, based on an original idea by Harland and Rudwick (1964). The hypothesis

suggests that the Earth was covered by ice (Kirschvink, 1992). As a consequence of the oceans being covered with ice, anoxic conditions could arise, that possibly can enrich the oceans in dissolved ferrous iron (Hoffman et al., 1998; Rickard, 2012). During Phanerozoic Eon, IFs called ironstones occurred, that are relatively rare and possibly related to temporally marine anoxic events (Bekker et al., 2010; Young, 1989).

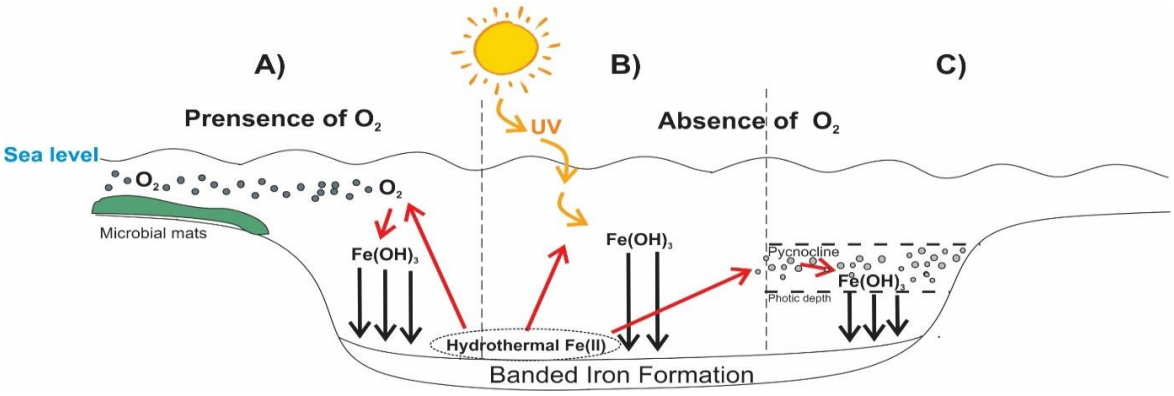

Figure 6: *Model of banded iron formation deposition in oxygenated water (A): The traditional model of BIF deposition by the production of oxygen by cyanobacteria and the release to the water column to chemically react with hydrothermal dissolved (Fe(II)). In anoxic sea water (B) abiotic Fe(II) photooxidation by UV light and (C) direct microbial Fe(II) oxidation via anoxygenic Fe(II)-oxidizing phototrophy. Remake of a model based on a model by Posth, Konkauser and Kappler (Posth et al., 2011).*

3.1.1 Banded iron formation

Banded iron formation (BIF) are repeatedly interbedded layers of iron-rich oxides and silica (Cloud, 1973). The layers have a various thickness from macrobands (meters) to mesobands (centimetres) to thinner layers (Trendall, 1973). In the least metamorphosed BIFs, the mineralogy commonly consists of a combination of chert, magnetite, hematite, carbonates and locally pyrite (Klein, 2005).

The BIFs are dominant in Neoarchean to early Paleoproterozoic Era (2.80 – 1.85 Ga) successions, but can also occur in late Neoproterozoic Era. They originate from relatively deep-water settings above storm and fair-weather wave bases, explained by a lack of evidence of wave and storm action (Simonson and Hassler, 1996; Trendall, 2002; Krapež et al., 2003 cited in Konhauser et al., 2017).

The banding is commonly explained by seasonal variations, oxic/anoxic conditions or episodic hydrothermal pulsation and upwelling of ferrous iron to depositional basins of

dissolved silica. When the ferrous iron encounters the silica, they can react and precipitate as ferrous- or ferric-silicates (Konhauser et al., 2007). The silica layers can be explained by silica-rich conditions, with a direct precipitation of amorphous silica to the basin floor (Siever, 1992; Krapež et al., 2003; Maliva et al., 2005 cited in Posth et al., 2011) or by seasonal evaporation of basin waters that can cause silicification (Holland, 1973; Garrels, 1987; Jacobsen and Pimentel-Klose, 1988; Siever, 1992 cited in Posth et al., 2011).

3.1.2 Neoproterozoic iron formations

Neoproterozoic iron formations (NIF) represent iron mineralizations that appeared in Neoproterozoic successions associated with glaciogenic deposits (Canfield, 1998; Klein, 2005; Bekker et al., 2010; Cox et al., 2013). The reappearance of IFs at the end of the Neoproterozoic indicates a return of anoxic and ferruginous ocean conditions (Bekker et al., 2010; Cox et al., 2013). Some scientists suggest that the anoxic conditions in Neoproterozoic are caused by the ice-covered Earth (Kirschvink, 1992). The anoxic conditions could have led to oceans enrich in dissolved ferrous iron (Kirschvink, 1992; Hoffman et al., 1998; Rickard, 2012). However, an additional source of iron is needed to account for the large mass of the NIF occurrence (Cox et al., 2013). Iron can possibly be sourced from a sub-marine volcanism or from sub-marine hydrothermal systems by hydrothermal upwelling of iron associated with rifting as well as of detrital origin (Cox et al., 2013).

NIFs are generally characterized by absence or poor development of banding and occurs commonly as ferruginous laminated siltstones or within a glaciogenic matrix (Cox et al., 2013). The NIFs almost exclusively consist of hematite as the principal iron-bearing phase and is enriched in phosphorus compared to older IFs (Klein and Beukes, 1993 cited in Cox et al., 2013). The enrichment of phosphorus is possible due to the higher levels of silica in the Archean and Paleoproterozoic that prevent phosphorous to co-precipitate with iron oxy-hydroxides (Cox et al., 2013).

3.1.3 Sedimentary exhalative deposits

Sedimentary exhalative (SedEx) deposits are syn-genetic deposits formed by venting of hydrothermal metal-bearing fluids onto the seafloor in rift-related settings (Fig. 7) (Sangster, 2002; Robb, 2005; Leach et al., 2010; Wilkinson, 2013; Carne and Cathro, 1982 cited in Emsbo et al., 2016). The deposits is usually formed in the advanced rifting stage of the

Wilson tectonic cycle (Palinkaš et al., 2016). The advanced rifting stage involves the divergent drifting of the margins, where there is a development of sea with continental margins (Robb, 2005). The location of the deposits is within sub-basins controlled by syn-sedimentary faults (Sangster, 2002). In the fault zones, mineralized fluids can migrate from greater depths to the host basin (Goodfellow, 1993 cited in Wilkinson, 2013).

The primary flow mechanism for the hydrothermal fluids is believed to be buoyancy driven free convection (Yang et al., 2004; Yang et al., 2006; Radulescu, 2010; Wilkinson, 2013). The buoyancy forces are a result of fluid density gradients, temperature, salinity and pressure in submarine environments (Evans and Raffensperger, 1992; Garven, 1995 cited in Radulescu, 2010). When the hydrothermal mineralized fluids are released into a seawater reservoir, stratiform precipitates due to sudden changes in physicochemical parameters is resulting (Haldar, 2013). The morphology of SedEx deposits varies between lensed and sheet-like shaped, to tabular shaped deposits (Paradis and Goodfellow, 2012).

The mineralization depends on the mineralogy and physical properties of the footwall sediments of the fault, temperature and composition of the hydrothermal fluids and water depth (Deb and Goodfellow, 2004). The host sediments are marine sedimentary rocks, and can be clastic or carbonates, with little or no association with volcanism (Leach et al., 2010; Wilkinson, 2013). The dominated metal association of SedEx deposits are zinc, lead and silver (Singer, 1995 cited in Wilkinson, 2013; Goodfellow et al., 1993 cited in Radulescu, 2010; McGoldrick and Large, 1998; Goodfellow and Lydon, 2007 cited in Emsbo et al., 2016), although some SedEx deposits may carry significant amounts of mercury (e.g. Almadén, Spain; Idrija, Slovenia) and/or iron (e.g. Vareš, Bosnia and Herzegovina; Kremikovci, Bulgaria).

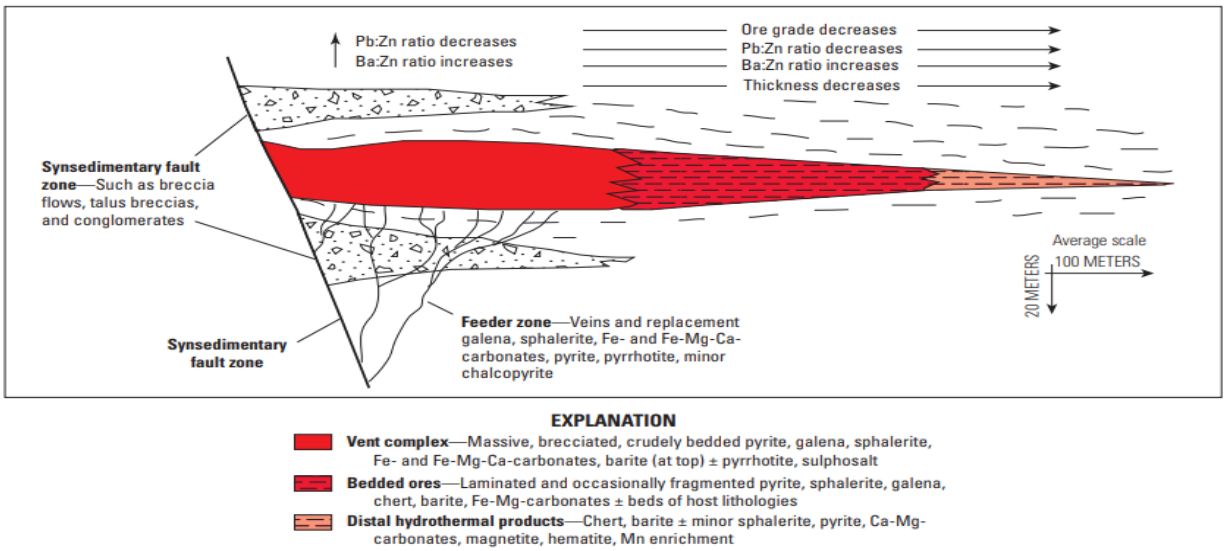

Figure 7: *Model of an idealized SedEx deposit: Cross-section showing the morphology and distribution of the ore, mineralogical and geochemical zoning ((Emsbo et al., 2016) modified from Lydon, 2004).*

3.2 Geochemical characteristics of tailing disposals

The mining industry produces a large amount of tailings, i.e. waste material after extraction of metals from ore (e.g. Vogt, 2013; Ramirez-Llodra et al., 2015). Tailings are slurry, composed of a fine-grain fraction (typically silt-sized, from 0.001-0.6 mm) and can include chemicals that were used during the process of extraction (Vogt, 2013; Ramirez-Llodra et al., 2015). The amount of tailings depends on the ore deposit type and the efficiency of the extraction process (waste/element produced ratio) (Dold, 2014). Tailings can cause a negative environmental impact by potentially generation of acid mine drainage (AMD) and leaching of heavy metals (Johnson and Hallberg, 2005; Skei, 2013; Dold, 2014). Because of the potential environmental impacts and large volume of waste produce, the disposal and management of tailings can represent a challenging problem for the mining industry (Apte and Kwong, 2004 cited in Skei, 2013).

3.2.1 Disposal methods

Tailings can be disposed in various ways depending on the tailing characteristics, climatic conditions and the location of the mining operation and processing plant (Vogt, 2013). The most common tailing disposal sites are placed on-land. However, some countries use riverine discharge (e.g. Indonesia and Papua New Guinea) and marine environments (e.g. Norway,

Turkey, Indonesia and Papua New Guinea) for disposal of tailings (Vogt, 2012; Loe and Aagaard, 2013; Ramirez-Llodra et al., 2015).

To find the best method to store tailings it is crucial to understand the behaviour of the tailings in different physicochemical conditions. Dold (2014) states the importance of detailed mineralogical and geochemical analyses of the tailings to know how the elements behave. The characteristics of the tailings vary dependent on the origin of the ore mineralization and composition of ore and gangue minerals (Australia, 2007 cited in Vogt, 2013; Dold, 2014). Since minerals can co-exists in rocks, the management of tailings is challenging because the minerals can behave different and in different environments. Skei (2013) states that the environmental affect from tailing disposals in unavoidable. Therefore, it is important to develop criteria for tailing disposal that ensure that the disposals give the minimum negative impact on the environment.

3.2.1.1 On-land

On-land tailing disposal sites can be situated above or below the water table (Loe and Aagaard, 2013). In an above the water table setup, the deposited material is exposed to oxygen and continuous infiltration of surface- and ground-water. The infiltration can cause remobilization of metals to the surrounding environment (Fig. 8a) (Loe and Aagaard, 2013). Tailings can be stored below the water table in disposal dams, lakes and raised impoundments, characterized by no direct contact of deposited material with oxygen and a lower degree of water infiltration. Consequently, the flux of metals to the environment could be prevented or minimized compared to the above the water table setup (Fig. 8b) (Loe and Aagaard, 2013; Vogt, 2013). Numerous tailings disposals in on-land environments are known for causing a major negative impact on the surrounding environment (Dold, 2014). The environmental issues are mostly associated with acidification of waters due to oxidation of sulphide minerals (AMD) and leaching of potentially toxic elements (e.g. Avoca mines, Ireland; Røros, Norway) (Johnson and Hallberg, 2005; Akcil and Koldas, 2006), or by failure of storage dams (high pore pressure and geotechnical instability) (e.g. Mount Polley, Canada; Córrego do Feijão (Brumadinho dam), Brazil) (Vogt, 2012).

Effects of carbonates

Calcareous rocks that contain dolomite ($CaMg(CO_3)_2$) or calcite ($CaCO_3$) are often used for treatment of disposals of low pH (e.g. sulphide minerals) (Miljødirektoratet, 2015) due to their ability to neutralize acidic solutions.

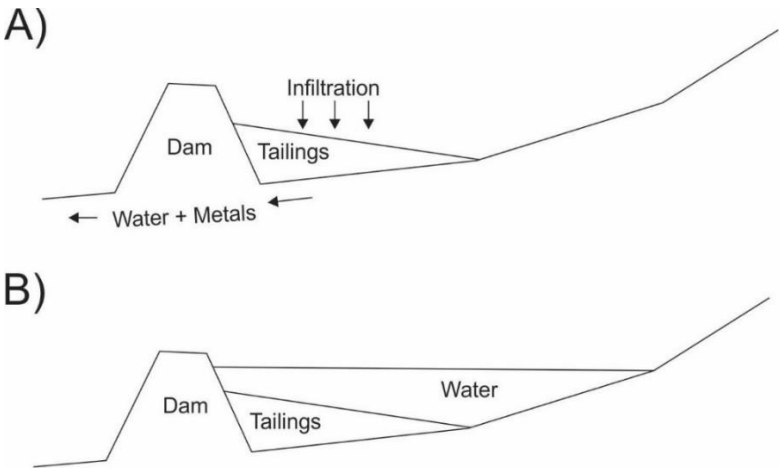

Figure 8: *Sketch over A) drained and B) water filled on-land disposal. Modified from Loe and Aagaard (2013).*

3.2.1.2 Marine

There are three main types of tailing disposals in marine environments: coastal tailing disposal (CTD), submarine tailing disposal (STD) and deep-sea tailing disposal (DSTD). CTD are placed in coastal, shallow-waters in the euphotic zone (Franks et al., 2011 cited in Ramirez-Llodra et al., 2015). STD occur in relatively shallow water (<100 m) at the submerged water depths of the euphotic zone or deeper areas below the euphotic zone (Ellis and Ellis, 1994; Shimmield et al., 2010; Vogt, 2013; Skei, 2014 cited in Ramirez-Llodra et al., 2015). DSTD are disposals placed in relatively deep waters (>100 m) below the euphotic zone (Ramirez-Llodra et al., 2015). The euphotic zone is the upper part of the water column where the primary production occurs. The depth normally varies between 0-50 m (Fig. 9). In this zone, the photosynthetic oxygen production cause high levels of dissolved oxygen (Skei, 2013).

In contrast to groundwater that controls geochemistry of on-land disposals, seawater has a slightly alkaline character and a high content of e.g. sulphate (SO_4^{2-}) and chloride (Cl^-) (Pedersen, 1984 cited in Kvassnes and Iversen, 2013).

In marine environments where oxygen is available, oxidizing conditions can occur. The oxidizing conditions are often associated with shallow marine environments i.e. areas in the euphotic zone. However, circulation in the water column can transport oxygen to deeper parts of the oceans. The oxidizing conditions can cause oxidation of some minerals that can mobilize and release potentially harmful elements (Loe and Aagaard, 2013). In the marine environment, reducing conditions can occur in the water column with limited circulation and less oxygen available.

The importance of organic matter in marine sediments

The presence of organic matter in tailings can decrease the redox potential. For oxidizable minerals (e.g. sulphides), it can result in reducing of potential for generating of acid mine drainage (AMD). Whereas, it can promote dissolution of reducible minerals (e.g. ferrihydrite, amorphous Fe/Mn oxides, goethite).

In the marine environment, the final deposition depth of the tailings is an important factor that controls their potential environmental impact (Ramirez-Llodra et al., 2015). During the process of discharge tailings usually behave like a plume that can be affected by seawater dynamics (Skei, 2013). The marine environment is a complex and dynamic environment, motions in the sea can cause erosion of disposed material and promote mobilization of fine-grain particles from tailings. According to Skei (2013), the ideal waste site in the marine environment is deep (>100 m), flat or slightly sloping bottom and the area is confined (e.g. surrounded by sills), the basin is enclosed, and sedimentation is prominent.

In general, disposal of tailings in the marine environment have not been studied in details (Hammer, 2011). In Norway, research of marine disposal of tailings has been conducted within the framework of Imptail (Improved submarine tailings placements in Norwegian fjords), EWMA (Environmental Waste Management) and NYKOS (New knowledge on sea deposits) projects. The goal of these projects was to obtain more knowledge about the environmental impacts related to tailing disposals in the marine environment and to improve

criteria that can ensure safe and environmentally friendly disposals that can facilitate for a sustainable mineral industry in Norway (Sintef).

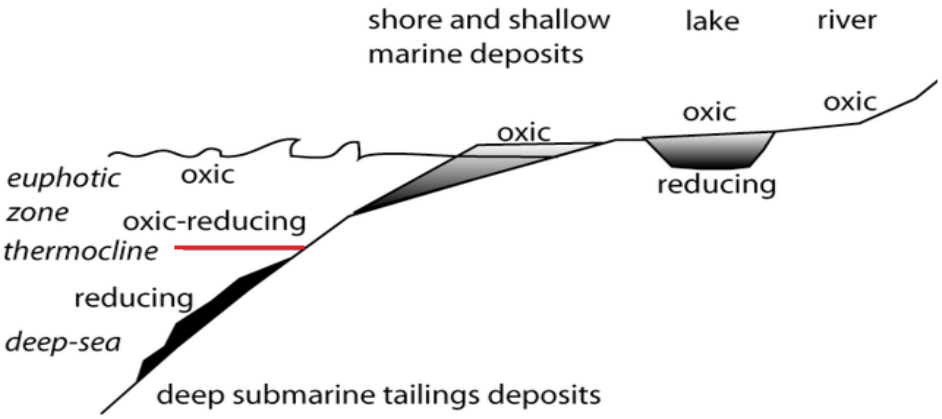

Figure 9: *Sketch of marine tailing disposals, modified by (Dold, 2014).*

3.2.2 Tailing disposal in Norway

In Norway, disposal of tailings have been placed both on-land and in marine environments (Kvassnes and Iversen, 2013; Skei, 2014). Disposals on-land have constituted challenging environmental issues by generation of AMD that can result in lowering of pH conditions, accompanied with high values of dissolved metals in ground waters (e.g. Røros, Jøssingfjorden) (NGU, 2015a). Fjord disposals is a submarine tailing disposal (STD), where the tailings are placed at the bottom of fjords in a confined area isolated by sills. The topography makes the exchange of water limited and can cause anoxic conditions in the bottom part of the water column. During the last 50 years, 26 mines have practiced STDs in Norway (Skei, 2014). The environmental issues associated with marine disposals are related to the impact of the marine ecosystem (e.g. Repparfjorden, Førdefjorden) (NGU, 2015a).

The arguments that go in a favour of tailing disposals in a marine environment are associated with the topography, climate and geology of a region. Norway has a steep and rugged topography that may affect the geotechnical stability of on-land disposal sites. The climate conditions can cause heavy rains and thereby cause floods of on-land dams (Caroletti and Barstand, 2010 cited in Kvassnes and Iversen, 2013). Additionally, there can be conflicts of land-use and the aesthetic benefits, as the waste deposited in deep fjords is not visible. The

combination of these factors makes the fjords with a confined, relatively stable and large storage area an appealing alternative for tailing disposal (Cornwall, 2013; Kvassnes and Iversen, 2013; Dold, 2014). Skei (2014) states that it is necessary to evaluate the feasibility of marine tailing disposals, since most mineral resources are located near the coastline.

In Norway, there are strict regulations on disposal of tailings in on-land and in marine environments (Kvassnes and Iversen, 2013). The discharges are regulated by a variety of laws that are set to protect the environment. The Norwegian Environment Agency (*Norwegian: Miljødirektoratet*) is the agency that regulate the disposal of tailings and the mining industry. They have a key role in shaping the Norwegian environmental policy, where they have developed a classification system to prevent spreading of toxins to the environment.

3.2.2.1 Disposal of tailings from Dunderland Valley

Tailings from Dunderland Valley are released at the bottom of Ranfjorden by Rana Gruber. The annually disposal is approx. 3 M tonnes of tailings per year (Kvassnes and Iversen, 2013; Skei, 2014; Ramirez-Llodra et al., 2015). The tailings from the mine consists of 40-50% quartz, 15-20% Fe-Al-Mg silicates (mostly micas, garnets, amphiboles and epidote) as well as some calcite, dolomite, feldspars and 6-14% hematite (Skei, 2014). According to Skei (2014), no elevated levels of trace metals have been found and the tailings contain less than 2% of particles smaller than 10 μm. The depth of discharge of the tailings has been at 125 m depth since May 2014 (Skei, 2014).

Formerly, Ranfjorden has been used as disposal site for heavy industry (Miljødirektoratet, 2012) and tailings disposal site for other mines. This waste disposal has caused the bottom of the fjord to be contaminated, causing problems related to heavy metals and polycyclic aromatic hydrocarbons (PAHs) (Skei, 2014). Ranfjorden was also used as a disposal site for tailings from several Pb, Zn and Cu sulphide deposits, including Mofjellet Gruber, Båsmoen Gruver and Bleikvassli Gruber (Kvassnes and Iversen, 2013). These mines are not active any more. According to Skei (2014), tailings from the iron deposits of the Dunderland Valley can be classified as inert due to the low release rates of materials (below detection limits) in seawater by elutriate testing. They show no toxic effects on marine diatoms and salmon smolt (Skei, 2014). Consequently, the iron deposit tailings were approved to be suitable capping material for contaminated sediments in fjords (Miljødirektoratet, 2012)

3.2.3 Previous work related to disposal of tailings from the Dunderland Valley

Previously environmental work related to the deposited tailings from the Dunderland Valley was conducted by Rana Gruber with Molab AS and NIVA (Norwegian Institute for Water research) in 2011. The analysis by Molab involved mineralogical and chemical analysis of three materials of mine waste to provide documentation to get approval to use the main waste as cover material of former polluted sediments. The materials were analysed for main element constituents and for contents of organic chemical pollutants and heavy metals. Additional analysis includes studies of the effects on biota, chemical stability and leaching properties according to the TA-2143/2005 (KLIF, 2005 cited in MOLAB, 2011). The analysis concludes that there is no indication that the material contains heavy metals or significant amount of organic chemical pollutants above defined acceptance criteria. The leaching showed a reduction in leaching metals over time and no values above acceptance criteria. The effects on biota was analysed by NIVA, where the eco-toxicological test concludes that all three materials are suitable for covering polluted sediments (MOLAB, 2011).

According to Ramirez-Llodra (2015), several of environmental surveys and assessments have been conducted since the 1960s on Ranfjorden. Some are directed towards the mining industry, some towards other pollution sources and to the general status of the fjord ecology. In 1994 and 2003, Johansen et al. (2004) and Walday et al. (2004), cited in Ramirez-Llodra et al. (2015), documented the influence by tailing discharge in the inner fjord on the soft bottom fauna. From their work, it is evident that Ranfjorden is affected by the tailing discharge, probably mainly due to the high sedimentation of particles with low organic content. It is important to have the river contribution in mind, as it can affect the supply of sediments. High levels of PAHs and metals in sediments from the inner fjord have been measured. However, the contamination is not caused by the discharge of the tailings (Ramirez-Llodra et al., 2015).

Previous studies in Ranfjorden area at UiT - The Arctic University of Norway were conducted within a framework of the NYKOS (New Knowledge on Sea Disposal) project (e.g. Haugen, 2018; Figenschau, 2018). The studies include mapping of the topography and dynamics of Ranfjorden, as well as sedimentological analysis of core samples in the fjord. The topography and dynamics of the fjord indicate that the tailings have spread throughout the majority of the inner 18km of the fjord. The bathymetry presents a large amount of erosion and accretion in channels along the innermost part of the fjord. From the core sample study, the tailings were

recognized by a dark red colour, with high iron content (iron-oxides: mainly hematite, some magnetite). This study showed that the recent iron/oxide containing tailings have an evident capping effect to the previous deposited sediments (natural, industrial and tailings), resulting in a gradual isolation of the contaminated sediments.

The disposal of tailings from Dunderland Valley show similarities with Ensenada Chapaco disposal in Northern Chile. In the bay of Ensenada Chapaco, a pellet plant have deposited tailings of several iron oxide deposits firstly at the shore since 1978 and then at 35 m depth since 1994 (Dold, 2014). The processes use a separation of ore that is based on magnetic separation, without any chemicals (González et al., 2014). The composition of tailings in Chapaco is largely inert (Nunex, 1993 cited in González et al., 2014). The tailings include iron ore and clay particles that are released in the waters of Ensenda Chapaco that cause heavy sedimentation (Stotz et al., 1994 cited in González et al., 2014). There is a scientific publication on the effects of the Ensenada Chapaco tailing disposal on the benthic community (Dold, 2014). González et al. (2014) investigated the impact of 16 years of disposal of tailings in the intertidal zone (1978-1994) on the benthic community. Their results concluded that the community suffered in abundance, species richness, diversity and high dominance caused by tailing deposition (Dold, 2014). The change of deposition depth in 1994 resulted in deposition of tailings from 35 m to 130 m depth. Dold (2014) informs of a published paper of Environmental Impact Study (EIS) with an expansion project to deep-sea tailings deposition. The study suggests that hematite-magnetite in the submarine deposited tailings at 35-130 m depth undergo reductive dissolution and release associated trace elements to the seawater.

3.3 Mobility of metals in surficial conditions

Weathering processes in surficial environments are associated with low temperatures and pressure, available free oxygen, water and carbon dioxide (CO_2), and pronounced geochemical dispersion (Rose et al., 1979). The dispersion in surficial environments is mostly driven by the mobility of elements in aqueous solutions i.e. by its ionic potential (Z) equal to the ionic charge to ionic radius ratio (Fig. 10) (Rose et al., 1979).

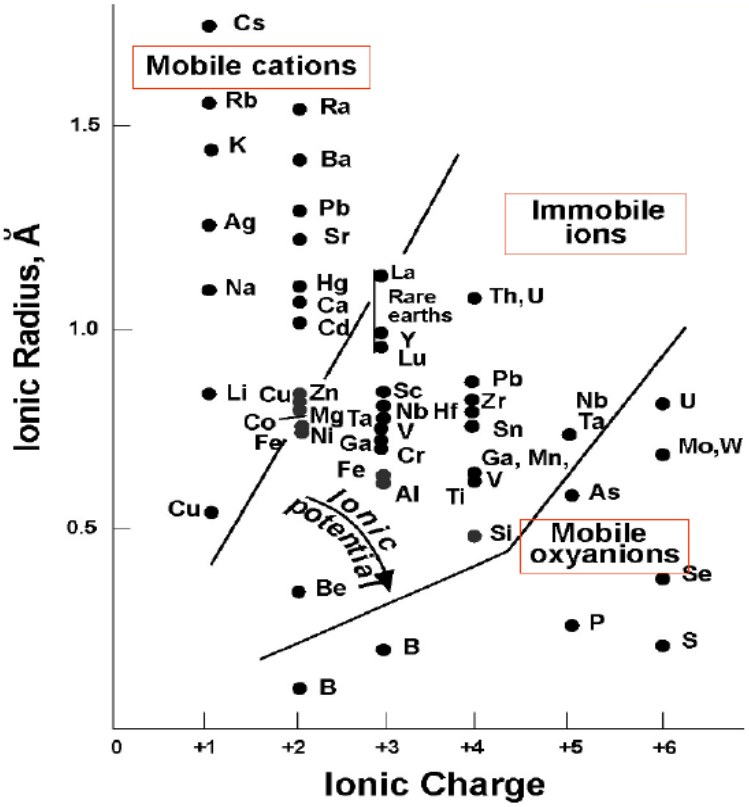

Figure 10: *Guidance of mobility of elements in surficial environments presented as ionic potential equal to ionic charge divided by ionic radius. Difference valence states give difference in mobility (e.g. Fe^{2+} / Fe^{3+}) (Smith, 2007).*

The solubility of elements in waters is highly affected by the concentrations of hydrogen ions in the solution (pH) and the redox potential (Eh) (Rose et al., 1979).

3.3.1 Iron

Iron (Fe) is a chemical element of group 8 in the periodic table. It belongs to the first transition series of elements. Iron is considered to be the most abundant element of the Earth, assuming it as one of major elements forming the Earth's core. Iron can enter different mineral group, including oxides, sulphides, silicates and carbonates. The most common Fe

oxides are hematite (Fe_2O_3), magnetite (Fe_3O_4) and goethite (FeO*OH), sulphides are pyrite (FeS_2), pyrrhotite ($Fe_{1-x}S$) and marcasite (FeS_2), and iron carbonates e.g. siderite ($FeCO_3$), Fe silicates represent a diverse group of minerals, including olivines, pyroxenes, amphiboles and chlorites, etc.

The concentrations of iron in waters are generally low (Hem, 1985). The solubility and chemical behaviour of iron in water is strongly dependent on the oxidizing potential and pH of the systems. The two most common oxidation states of iron are ferrous (Fe^{2+}) and ferric (Fe^{3+}) iron, but iron can exist in oxidation states from -2 to +7. Elevated concentrations of iron in drinking waters have no harmful effect of the majority on the population. However, high iron concentrations can cause significant aesthetic disadvantages by precipitation of red iron-oxide-hydroxide that makes the water unsuitable for e.g. human consumption, laundry and plumbing fixtures (Hem, 1985; Folkehelseinstituttet, 2018). The recommended upper limit for iron in public water supplies in Norway is 0.2 mg/L iron (Folkehelseinstituttet, 2018).

From a biological point of view, iron is an essential element in the metabolism for all living organisms, where it has many biological functions, e.g. content in haemoglobin that transports oxygen and in cell growth (Hem, 1985).

Sources, species and solubility of iron

In the igneous rock minerals, as e.g. olivines, pyroxenes, amphiboles, magnetite and biotite, the iron content is relatively high (Hem, 1985). The iron in these minerals are commonly in the ferrous (Fe^{2+}) oxidation state, and some may be present in the ferric (Fe^{3+}) oxidation state. When iron bearing minerals react with water, the iron may be released and re-precipitated (Hem, 1985). Under oxidizing conditions, the sedimentary species of iron can be in form of ferric oxides or oxyhydroxides, including e.g. hematite (Fe_2O_3) and goethite (FeOOH). Whereas under reducing conditions with sulphur available, iron can be in form as ferrous polysulphides (e.g. Pyrite (FeS_2)), and with less sulphur available iron carbonates may form (e.g. Siderite ($FeCO_3$)) (Hem, 1985). In sulphide ores of other minerals, iron is commonly a component. Ferric hydroxide ($Fe(OH)_3$) are commonly the name for newly precipitated material that do not have a fully developed crystal structure. Magnetite is often present as residual material in sediments due to the resistance of reaction with water (Hem, 1985).

The solubility and chemical behaviour of iron in aqueous solutions is strongly affected by pH and Eh conditions (the intensity of oxidation and reducing conditions of the system). The amount of dissolved ferrous iron in solution can occur in oxidative conditions by oxidation of e.g. ferrous sulphides (the sulphur is altered to sulphate, releasing the ferrous iron) or in reductive conditions by reduction of e.g. ferric oxyhydroxides (Hem, 1985).

Ferrous iron may be stable in natural waters that has no contact with air, but when exposed to air, the iron can be wholly or partly oxidized to ferric iron state (Hem, 1985). The presence of ferric iron in water are in the free ferric state in water with pH above 3.5, whereas in pH below 3.5 the ferric iron in water must be either undissolved or combined in complex ions (GeologicalSurvey et al., 1962). In most natural waters, pH is not low enough to prevent formation of iron hydroxides. When there is oxidizing conditions, almost all the iron is precipitated as ferric hydroxides $(Fe(OH)_3)(s)$ (GeologicalSurvey et al., 1962). Iron has the tendency in solution to form complex ions with inorganic and organic material. Iron complexes are considered to be more stable than free iron in solution, and therefore they may remain in solution (GeologicalSurvey et al., 1962). The complex $FeOH^+$ can be predominant with pH around 9.5. The anion complexes $Fe(OH_3)^-$ and $HFeO_2^-$ can appear in pH conditions above 11. Such pH conditions appear rarely in nature. In solutions that have more than a few hundred milligrams of sulphate per liter, an ion pair $FeSO_4(aq.)$ can be prominent (Hem, 1985).

Ferric iron can occur in solutions with low pH as Fe^{3+}, $FeOH^{2+}$, $Fe(OH)^+_2$ and polymeric hydroxide forms (Hem, 1985). The form and concentration are dependent on the pH of the system. In waters with pH above 4.8 the ferric hydroxide concentration will be less than 10 µg/l. If the amount of dissolved ferric iron exceeds 1,000 mg/l, dimeric or polymeric ferric hydroxyl cations $(Fe_2(OH)_2^{4+})$ can form, but in natural waters such iron concentrations are rare (Hem, 1985). In natural waters, a very low concentration of solid ferric oxyhydroxides and macroions or microcrystalline forms may form by polymerization, like the species $Fe(OH)_3(aq.)$. In very strong oxidizing systems at high pH the oxidation state +6 of iron can be present as FeO_4^{2-}, but it is rarely in natural systems. If the pH is 10 or greater, the anionic ferric species $Fe(OH)^{4-}$ can affect the iron solubility. Ferric iron can form varieties of inorganic complexes with many anions, where chloride, fluoride, sulphate and phosphate complexes may be important, depending on the natural system composition (Hem, 1985). The

adsorption capacity of ferric oxyhydroxide surfaces may affect the concentration of minor constituents in the water that are associated with the material. The solubility of other metal ions under some conditions are controlled by redox co-precipitation (Hem, 1997 cited in Hem, 1985).

Chemical behaviour of iron can be predicted as a function of pH and redox potential (Eh), presented in an Eh-pH diagram (Fig. 11). The diagram presents the relations of Eh and pH in the Fe-O-H-Si system. Under reducing conditions with low pH, iron is mobile as Fe^{2+}. With higher oxidation (higher Eh) the Fe^{2+} goes to Fe^{3+}. With higher pH, iron is stable as various of forms of iron oxides. In weathering conditions near surface to under surface, iron oxides are stable e.g. hematite or goethite (Brookins, 1988).

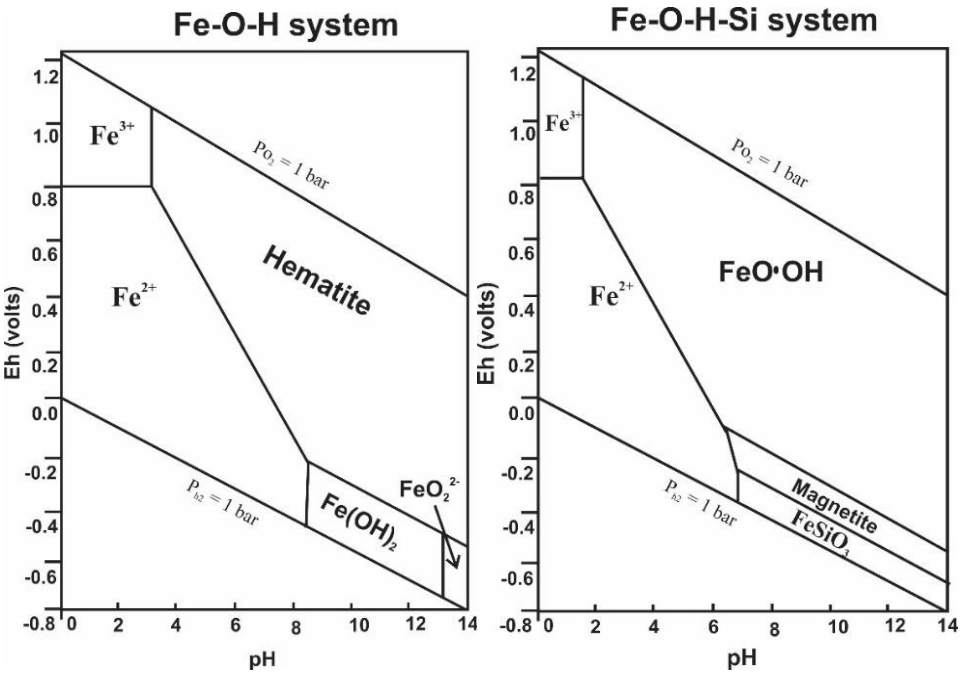

Figure 11: *Eh-pH diagram for part of the system Fe-O-H and Fe-O-H-Si (Brookins, 1988).*

3.3.2 Manganese

Manganese (Mn) is a chemical element of group 7 in the periodic table. It belongs to the first transition series of elements. Even though manganese is one of the more abundant metallic elements, the content compared to iron is only about one-fiftieth. In the more common silicate rock minerals manganese is not an essential component, but it can substitute for iron, magnesium and calcium in silicate structures (Hem, 1985). There are five common oxidation

states of manganese (2+, 3+, 4+, 6+ and 7+), where manganese can form a variety of oxides. The most economically important manganese mineral is pyrolusite (MnO_2). Other common manganese minerals are braunite ($(Mn^{2+}Mn^{3+}{}_6)(SiO_{12})$), psilomelane ($(Ba, H_2O)_2Mn_5O_{10}$), rhodochrosite ($MnCO_3$), rhodonite ($MnSiO_2$), spessartine ($Mn^{2+}{}_3Al_2(SiO_4)_3$) and johansenite ($CaMn^{2+}Si_2O_6$).

The mobility and chemical behaviour of manganese in aqueous solutions are strongly dependent on the redox potential and pH of the system. Generally, some elevated concentrations of manganese in drinking waters have no harmful effect on humans. However, the disinfection efficiency of the UV-plant can be reduced and cause the water quality to go down if manganese deposits in the water (Hem, 1985; Folkehelseinstituttet, 2018).

From an industrial point of view, practically all manganese that is produced are used in steel industry, because of the good ability to be used as alloy (Pedersen and Kofstad, 2018).

Manganese also plays an important role in biological processes, especially as an essential constituent of many enzymes. However, a large consumption of manganese can have a harmful effect on the central nervous system. The recommended upper limit of manganese in public water supplies in Norway is 0.005 mg/L manganese, based on the aspect of use (Folkehelseinstituttet, 2018).

Sources, species and solubility of manganese

Manganese is a minor constituent in many igneous and metamorphic minerals, e.g. basalt, olivines, pyroxene and amphiboles (Hem, 1985). Manganese can substitute other elements, commonly calcium in dolomite and limestones.

In natural waters, dissolved manganese will mainly be in the 2+-oxidation state. In conditions with pH higher than 10.5, the manganese hydroxide complex ($MnOH^+$) will dominate and when pH is 12.0 or higher, the anionic form of manganese will dominate. In solutions with concentrations of bicarbonates near 1,000 mg/L HCO_3^-, the complex $MnHCO_3$ can be important (Hem 1963 cited in Hem, 1985). If the sulphate activity is greater than a few hundred milligrams per liter, the $MnSO_4$(aq.) can be present (Nair and Nacollas 1959 cited in Hem, 1985). According to Hem (1985), the Mn^{2+} ion compared with Fe^{2+} in aerated water is

more stable and higher concentrations can be transported without the protection of complexation. The occurrence of Mn^{3+} species can be under conditions as stable organic complexes and in strongly acidic solutions. In natural waters, manganese with higher oxidation state than 4+ rarely occur. Theoretically, such species can occur in small amounts at very high pH (Hem, 1985).

The chemical behaviour of manganese can be predicted as a function of pH and redox potential (Eh), presented in an Eh-pH diagram (Fig. 12). The figure shows the Eh-pH relations in the system of Mn-O-H (Brookins, 1988). Under reducing conditions with low pH, the Mn^{2+} is stable, whereas with higher pH, manganese oxides like $Mn(OH)_2$, $Mn(OH)^-_3$ and Mn_3O_4 is stable. In weathering conditions near surface, various forms of MnO_2 polymorphs is stable (e.g. pyrolusite) (Brookins, 1988).

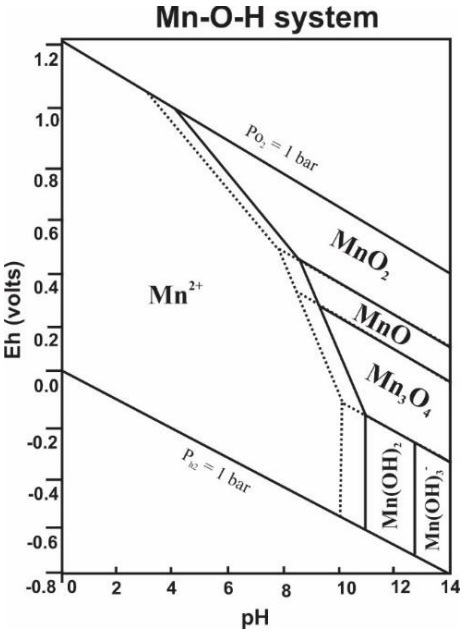

Figure 12: *Eh-pH diagram for part of the system Mn-O-H. The assumed activity of Mn is 10^{-6}. (Brookins, 1988).*

3.3.3 Heavy metals

3.3.3.1 Copper

Copper (Cu) is a chemical element of group 11 in the periodic table. It belongs to the first transition series of elements. Copper can occur as the native element (Cu^0), or as Cu^+ and Cu^{2+} cations. Commonly, copper occurs in sulphide minerals (e.g. chalcopyrite, chalcocite). In

modern society, the industrial demand for copper is large and still growing. Copper shows a very good electrical conductivity and is widely used in cables and wires (Pedersen, 2018). The extraction and use of copper may have a negative environmental impact (Hem, 1985). Elevated concentrations of copper in drinking water can be environmental harmful. Although, copper is an essential element in metabolism for plants and animals (Hem, 1985). The recommended upper limit of copper in public water supplies in Norway is 2.00 mg/L (Folkehelseinstituttet, 2018).

In solution, copper may occur as either Cu^{2+} or Cu^{+}. According to Hem (1985), cupric ions form complexes with many different ligands. The adsorption or co-precipitation with ferric oxy-hydroxides can constitute lower solubility limits for copper (Hem, 1977 cited in Hem, 1985). The concentrations of copper from acid drainage from mines may be present in concentrations up to few hundreds mg/L. If a neutralization of the acidic drainage occurs, copper is mostly precipitated. Expected levels of copper in river water are suggested to be near 10 µg/l (Turekian, 1969 cited in Hem, 1985). In river and ground waters, the concentration of copper is near or below predications based on Eh-pH diagrams (Fig. 61, Appendix A). The concentrations are explained as the results of co-precipitation by oxides or adsorption on mineral surfaces (Hem, 1985).

3.3.3.2 Arsenic

Arsenic (As) is a chemical element of group 15 in the periodic table. It belongs to the group of metalloids. According to Hem (1985), arsenic can form metal arsenides and is often present as accessory minerals in sulphides and metals. Arsenate (As^{5+}) or arsenite (As^{3+}) oxyanions commonly forms in solution. The mobility of arsenic is strongly dependent on the pH of the system (Fig. 63, Appendix A). Lower solubility of arsenates can be due to complexing with iron and other metals. Arsenic is toxic to humans and is considered to be a highly undesirable impurity in water supplies, where the upper concentration limit in Norway is 10 µg/l (Hem, 1985; Folkehelseinstituttet, 2018).

Other relevant elements Eh-pH diagrams (Cobalt and Antimony), see Appendix A.

3.3.4 Sulphur

Sulphur (S) is a chemical element of group 16 in the periodic table. It belongs to the group of non-metallic elements. According to Rose (1979), sulphur is a relatively abundant component in natural waters. The dissolved species of sulphur are sulphate (SO_4^{2-}), hydrogen sulphate (HSO_4^-), hydrogen sulphide (H_2S) and bi-sulphide (HS^-), where the form in solution varies depending on pH and Eh of the system (Fig. 13). The most economical important sulphide mineral is pyrite (FeS_2). Other minerals are e.g. sphalerite (ZnS), galena (PbS) and cinnabar (HgS). There are no health problems related to sulphur in drinking water, but high levels can cause corrosion and bad taste of water. The upper concentration limit for sulphur is 250 mg/l (Folkehelseinstituttet, 2018).

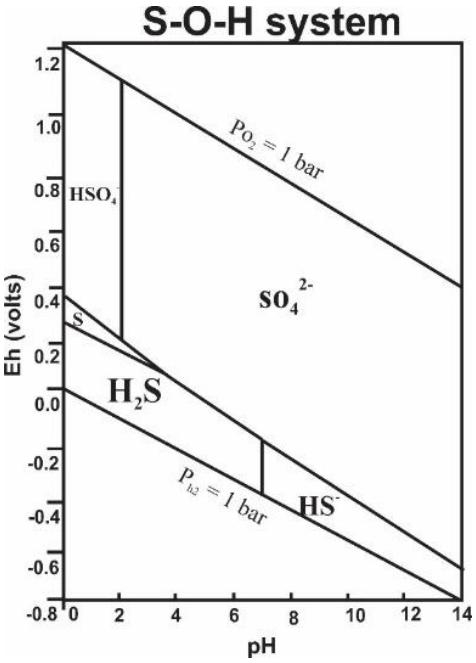

Figure 13: Eh-pH diagram for part of the S-O-H system Activity assumed of dissolved S = 10^{-3}. The importance of the boundary between sulphate (HSO_4^-, SO_4^{2-}) and sulphide (H_2S, HS^-, S^{2-}) (Brookins, 1988).

3.3.4.1 Acid Mine Drainage

Acid mine drainage (AMD) is acidic sulphur-rich wastewater produced by sulphide-bearing minerals that are exposed to oxygen and water (Johnson and Hallberg, 2005; Akcil and Koldas, 2006). When sulphide minerals are exposed to oxygen and water, the minerals can commonly oxidize, generating sulphuric acid causing the water to be acidic.

The oxidation of iron sulphide (pyrite (FeS_2)) is given by Equation 5;

$4FeS_2(s) + 15O_2(g) + 14H_2O(l) \rightarrow 4Fe(OH)_3 + 8SO_4^{2-}(aq) + 16H^+(aq)$ **(Equation 5)**

Here is the pyrite exposed to air and water, forming sulphuric acid and dissolved iron. The dissolved iron can be precipitated to form iron-hydroxide, also called yellow boy (yellow colour of the precipitation).

Even though AMD is a naturally occurring process, the mining industry can increase the exposure of sulphide minerals that can promote AMD generation (Akcil and Koldas, 2006). Therefore, it is a challenging problem for the mining industry to handle tailings that contain large amounts of sulphide minerals (Dold, 2014). AMD is an environmental pollution that can degrade streams with loss of aquatic life and restrict streams for use in recreation, as drinking water and industrial water supplies (Johnson and Hallberg, 2005; EPA and Sweeney). The acid runoff can cause heavy metals to dissolve into ground or surface water, which can have toxic consequences. Carbonates can be used to neutralize acidic conditions, that can cause a precipitation of heavy metals (Akcil and Koldas, 2006).

4 Methods of work

4.1 Fieldwork

The fieldwork took place in the Rana Gruber mine in the Dunderland Valley (Fig. 3), Nordland, Northern Norway, from the 22nd to 24th August 2018. The main purpose of the fieldwork was to collect representative samples of the ore mineralization. Samples from both the open pit and the underground mine were collected. A total of three samples were selected as representative endmembers of a hematite-, magnetite- and manganese-rich ore.

4.2 Sample preparation

A homogenized sample for each sample was prepared to use for XRD, lithogeochemistry and the kinetic column test (see description of the methods below) at the Department of Geosciences, UiT, by using a jaw crusher and a ball mill. Prior to the preparation, the samples were washed and air-dried to prevent contamination.

4.2.1 Crushing

The samples were crushed with a Retsch jaw crusher. After crushing, the size of the samples was reduced to approximately 5 mm after crushing. Between each crushing, the jaw crusher was washed with water and ethanol and blow-dried with an air compressor to avoid contamination.

4.2.2 Milling

The material of the crushed samples was milled in a Retsch Planetary ball mill PM 100, where an agate bowl of 250 ml with 10 agate balls of 3 cm in diameter were used. The samples were milled in different times (10 minutes to 30 minutes) at a speed of 475 rpm with 5 minutes intervals of milling to get the grain size to less than 20 μm. Between each milling, the bowl, balls and spoon (used to get sample in the bowl) were cleaned with water and ethanol and blow-dried with an air compressor.

4.3 Thin sections

Thin sections were made from three samples collected in the Dunderland Valley. The samples were cut into blocks (approx. 1 cm x 2 cm x 3 cm), labelled (Sample ID: BF1, BF2 and FL7), glued, cut and polished to the final products (BF1(a,b,c,d), BF2(a,b,c,d) and FL7 (a,b,c,d)) of 12 thin sections.

4.4 Kinetic column test

The kinetic column test (modified EPA method 1627) was performed with the purpose to characterize water quality of simulated tailing disposal weathering conditions, and thereby be able to determine the concentrations of possible contaminant(s) that are present in the waste and their mobility. The simulated disposal sites conditions include non-buffered on-land (i.e. columns filled with quartz), buffered on-land (i.e. columns filled with carbonates) and submarine (i.e. columns filled with marine sediments) environments. The goal of the test is to be able to evaluate weathering conditions in the different environments, and thereby predict the best disposal method for the different tailings.

EPA method 1627 kinetic test is a column test originally developed by the U.S. Environmental Protection Agency in 2011 to better predict mine drainage quality.

4.4.1 Sediment preparation

4.4.1.1 Quartz

Polished quartz pebbles were used in the kinetic column test to simulate non-buffered on-land conditions. The size of the pebbles was from approx. 1 cm up to 2.5 cm. All glassware and quartz were washed with 20% nitric acid (HNO_3), distilled water and dried before the experiments.

4.4.1.2 Carbonates

Carbonates from Evenes quarry were used to buffer the kinetic column test. The carbonate rocks were crushed by using a jaw crusher to get an approx. grain size smaller than 5 mm.

4.4.1.3 Marine sediments

The marine sediments that were used in the kinetic column test were sampled near the shore outside of Nordkjosbotn in Balsfjord, 75 km outside of Tromsø. The purpose of the sampling was to get marine sediments that are like the sediments in submarine tailings disposal settings, were the amount of organic material needs to be high enough to preserve reductive conditions. To determine if the sediments had high enough amount of organic matter, the samples were heated at 450°C for 4 hours. The sample weight was measured before and after heating of the sample.

4.4.2 Column setup

The columns used in the kinetic column test were plastic (PP) measuring cylinders of 250 ml with height of 25 cm and diameter of 4 cm. At the bottom of each column there was drilled a hole to fit a plastic tube of 0.5 cm to channel the leachates. The tube was glued together with the column. Columns were placed on a wooden bench with drilled holes for the tube to fit. An Erlenmeyer flask of 250 ml was placed at the bottom of the tube to collect leachates for further analysis. Between flushing, a clip was placed at the end of the tubes to prevent flushing/spilling of leachates (Fig. 14).

Three conditions were simulated in the kinetic column test with three different samples (BF1 (Hematite), BF2 (Manganese rich) and FL7 (Magnetite), with an additional three blanks set-up. In total there was 12 columns (Fig. 15). The column set-up for each condition is shown in Figure 14. Every column has quartz pebbles placed at the bottom 3 cm of the column with a filter of 0.2 µm pore size placed at the top. A bulk sample of 50±0.0001 g is placed between 8-10 cm, except in the blanks (no sample). At the top of the column from 20-25 cm, water (distilled water for the on-land conditions from the lab or seawater collected in the sea outside of Telegrafbukta for the marine condition) were added to the samples.

- In non-buffered on-land conditions (marked OQ), polished pebbles of quartz are placed at the top of the filer from 3-8 cm and a filter is placed before the bulk samples between 8-10 cm. The upper part of the column from 10-20 cm is added with quartz pebbles (Fig. 14a). The top of the column is left open to the atmosphere.
- In buffered on-land conditions (marked OC), fine-grained sand is placed at the top of the filter from 3-8 cm. The bulk samples are placed on the carbonate sand from 8-10 cm. Above the bulk sample, carbonate sand is placed from 10-20 cm (Fig. 14b). The top of the column is left open to the atmosphere.
- In submarine conditions (marked RM), marine sediments are placed at the top of the filter from 3-8 cm. The bulk samples are placed on the marine sediments from 8-10 cm. Above the bulk sample, the marine sediment is filled from 10-20 cm (Fig. 14c). The top of the columns was sealed with Parafilm M to get reducing conditions.

- The blanks were set-up in the same way as the conditions explained above, except without the bulk sample. In the different environments, the representative sediments of quartz, carbonates or marine sediments were filled instead from 8-10 cm.

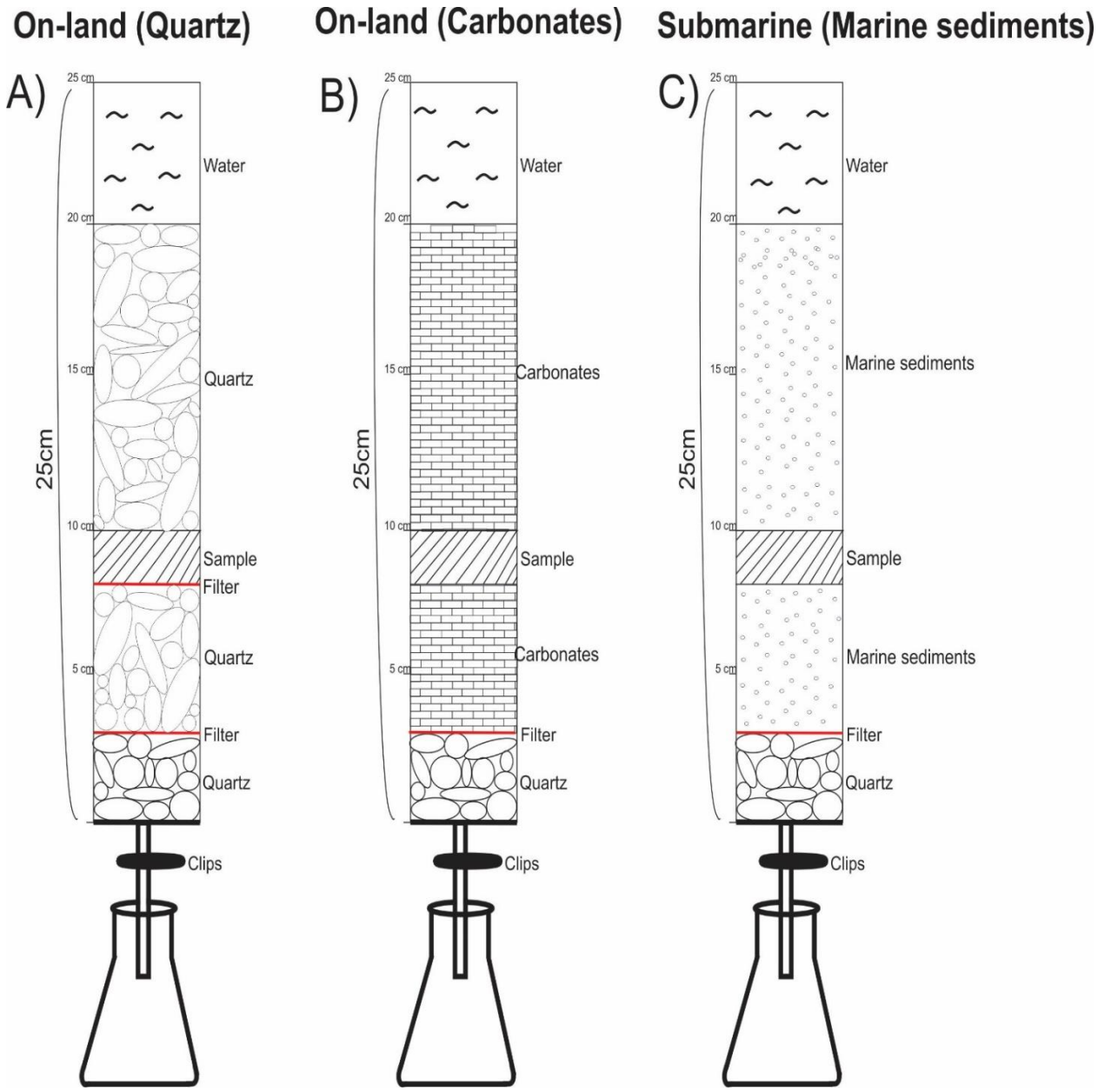

Figure 14: *Illustration of the kinetic column setup. A) Non-buffered on-land setup, B) Buffered on-land, C) Submarine.*

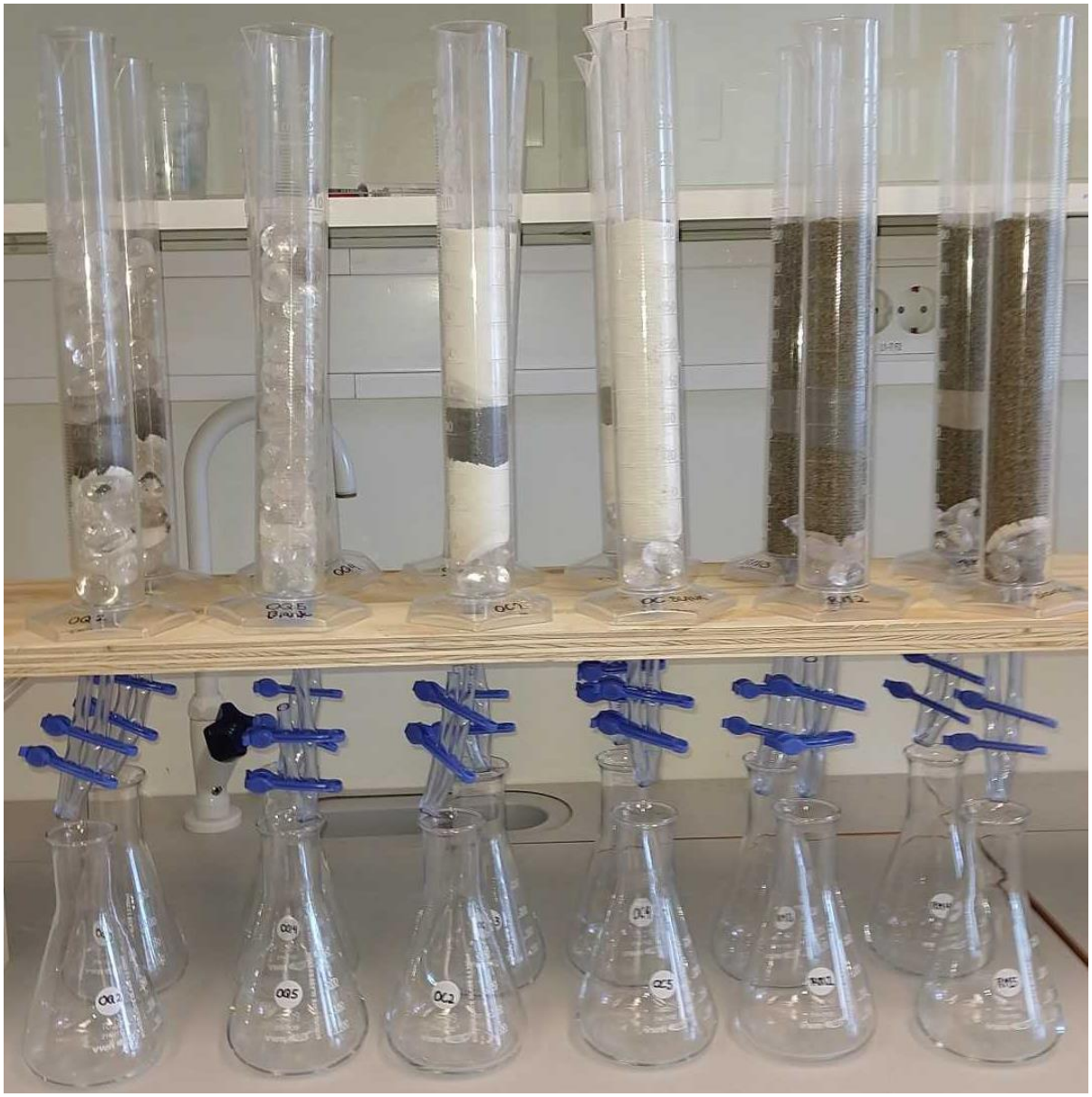

Figure 15: *Kinetic column test setup. Every column and flask marked with respective conditions OC (1, 2, 3, 4), OQ (1, 2, 3, 4) and RM (1, 2, 3, 4). Picture from the lab. 3.9.2018 by Birgitte Fagerheim.*

4.4.3 Experiment method

The kinetic column test started 4th September 2018 and lasted until 4th December 2018, a total of 12 weeks. The run time is shorter than the general recommendation of 20 weeks, but keep the recommended minimum run time for the experiment of 12 weeks according to the EPA method 1627 (EPA, 2011).

4.4.3.1 Watering of columns

The prepared columns were watered by pouring water slowly on the top of the columns to simulate rainfall (flood method). For the first watering, 150 ml of distilled water (on-land) or seawater (marine) was added to the columns. For the rest of the watering, 100 ml of water was added to the columns each time. The water was situated in the columns for 1 week, 2 weeks, 6 weeks and 12 weeks before flushing of columns and sampling of leachates.

4.4.3.2 Sampling and measurements

After the first watering of the column physicochemical measurements (pH, redox potential and conductivity) were measured at the top of the column (20-25 cm: water zone) by a multimeter after 24 and 48 hours.

The first sampling of leachates was done after one week. Erlenmeyer flasks were placed under the columns were the clips were open and tubes were placed into the flaks to collect the leachates for further analysis. To prevent contamination, the flasks were washed multiple times with 10% nitric acid (HNO_3) and dried before sampling. The analysis includes physicochemical measurements (pH, redox potential, conductivity and temperature) by using a multimeter and measurements of the approximately amounts of leachates sampled.

Multimeter HACH HQ440D multi

The multimeter used for physicochemical measurements was a HACH HQ440D Laboratory Dual Input. The multimeter is designed for water quality experiments. Electrodes connected to the multimeter were a pH meter, RedOx meter (redox potential) and conductivity meter (electrical conductivity). The multimeter had an automatic temperature compensation (ATC) probe. Before the measurements, the multimeter was calibrated. To prevent contamination the electrodes were cleaned with distilled water and paper before every use.

4.5 Thin sections exposed to weathering

Thin sections of ore samples from the Dunderland Valley were exposed to different conditions to represent the same conditions as the kinetic column test with a non-buffered on-land, buffered on-land with carbonates and submarine condition with marine sediments. The intention of this method is to observe changes in the mineralogy in the thin sections by exposure to different conditions.

Each thin section was placed in a beaker of 250 ml/400 ml with a height of 9 cm/10.5 cm and diameter of 7 cm/8.5 cm (Fig. 16). Depending on the condition being simulated, three samples were filled with distilled water, three were covered with carbonate rich sediments and filled with distilled water, and three were covered with marine sediments and filled with seawater (Fig. 17). The marine condition samples were covered with Parafilm M to seal the columns from oxygen to reach reducing conditions. The samples in on-land conditions were re-filled once a week to prevent the samples from being exposed to oxygen due to evaporation. The thin sections were sampled after 12 weeks of exposure in the conditions and carefully cleaned by distilled water and air-dried. The thin sections were then analysed by optical microscopy, SEM/EDS and Raman spectroscopy.

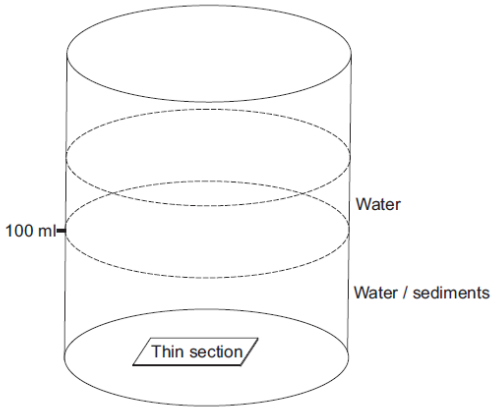

Figure 16: *Setup of the thin sections exposed to weathering. In non-buffered on-land conditions the whole beaker was filled with water (200 ml). For on-land conditions with additional carbonates and marine conditions the beakers were filled with sediments (100 ml) and water (100 ml).*

Figure 17: *Thin sections exposed to weathering. The picture is taken from the experiment in the lab.*

4.6 Optical microscopy

A study of the mineralogical characteristics of the ore samples from the Dunderland Valley were performed by using Leica DMLP polarization microscope at the Institute of Geoscience, UiT. The purpose of the study is to get a mineralogical description of the thin sections. The samples were studied by using plane polarised light (PPL) and cross polarised light (XPL) transmitted and reflected light microscopy. A Leica DFC450 camera was connected to the polarization microscope that took photomicrographs presenting the observations. CorelDraw was used to process the pictures and making figures. The minerals of specific interests were marked for further analysis by SEM/EDS and Raman.

4.7 Scanning Electron Microscopy (SEM) imaging / Energy Dispersive Spectroscopy (EDS)

Scanning Electron Microscopy (SEM) imaging / Energy Dispersive Spectroscopy (EDS) analysis was performed to analyse and obtain chemical composition of minerals by using a Hitachi TM 3030 tabletop electron microscope with an EDS detector at the Department of Geoscience, UiT. The data from the analysis were further processed in the software Quantax 70. From the analysis, element maps and high-quality images of minerals were obtained.

4.8 Raman spectroscopy

Raman spectroscopy was conducted by Sabina Strmić Palinkaš at the Department of Earth Science, The Faculty of Mathematics and Natural Sciences, University of Bergen (UiB). A JobinYvon LabRAM HR800 confocal Raman spectrometer equipped with a frequency doubled Nd-YAG laser (100 mW, 532 nm) and LMPlan FI 50× objective (Olympus) were

used to identify mineral phases in studied ore samples, as well as the degree of weathering after simulation of weathering conditions in on-land and submarine conditions. The identifications were based on Raman spectra published in the literature.

4.9 X-ray powder diffraction (XRD)

XRD analysis were performed to analyse and identify mineralogical phases by Andrea Čobić at the Department of Mineralogy and Petrography Faculty Science, University of Zagreb, on a Philips PW 3040/60 X'Pert PRO powder diffractometer (45 kV, 40 μA), with CuKα-monochromatized radiation (λ = 1.54056 Å) and θ-θ geometry. The area between 4° and 63° 2θ, with 0.02° steps, was measured with a 0.5° primary beam divergence. Compound identifications were based on a computer program X'Pert high score 1.0B and literature data.

4.10 Lithogeochemistry analysis

Bulk samples were prepared at the Department of Geosciences, UiT, by using an agate mortar and pestle to crush and grind the bulk material to powder fraction. Five grams of each samples was sent to Bureau Veritas Commodities Canada Ltd. (Vancouver, Canada) for lithogeochemical analysis. The analysis was performed by a combination of lithium borate fusion and tetraborate fusion using ICP-ED (Inductively Coupled Plasma-Emission Spectrometry) for the major elements and ICP-MS (Inductively Coupled Plasma-Mass Spectrometry) for the trace elements. Detection limits for all analysed elements are listed in Table 21 and 22 in Appendix C.

4.11 Isochon diagrams

The isochon diagrams are presented to compare samples before weathering and after weathering of the different conditions (non-buffered on-land, buffered on-land and submarine). An isochon (a line) with a slope of one (no gain or loss of elements) is shown for comparison (e.g. Fig. 35). The isochon is defined by the constant mass and by one or more immobile elements e.g. aluminium, titanium, etc. (Shervais et al., 2005). The elements that are plotted above the isochon have been enriched to the sample, whereas for elements plotted below the isochon are elements that have been leached out during the kinetic test.

4.12 Thermodynamic modelling

Visual Minteq (VM), version 3.1 (vminteq.lwr.kth.se) was used in thermodynamic modelling (Gustafsson, 2012). The VM is a freeware for simulation of chemical equilibrium models and

calculation of metal speciations, mineral solubility, sorption etc. in natural waters (Gustafsson, 2011). The modelling was used to present the speciation of iron (Fe^{2+} and Fe^{3+}) and manganese (Mn^{2+}) in submarine and non-buffered on-land and buffered on-land with carbonates conditions. For the hematite sample, Fe^{2+}, Fe^{3+} and hematite were added, whereas for the magnetite sample, Fe^{2+}, Fe^{3+} and magnetite were added. For the manganese-rich sample, Mn^{2+} and rhodochrosite (Mn-carbonate mineral) were added. The concentration of the components Fe^{2+}, $Fe^{3+}$and Mn^{2+} was set to 10^{-6} mg/l. To simulate non-buffered on-land conditions no additional components were added. For buffered on-land conditions with carbonates, calcite (CaCO3) was added as infinite phase. The components for submarine conditions chloride (Cl^{-}), sodium (Na^{+}), sulphate (SO_2^{4-}), magnesium (Mg^{2+}), calcium (Ca^{2+}) and potassium (K^{+}) were added in solution. The concentration of the components was added as the total molal composition of seawater (See Appendix B, Table 12).

5 Results

5.1 Mineral characteristics of analysed samples

Three samples from the Dunderland Valley (ID: BF1, BF2, FL7) were analysed to characterize the mineralogy of the samples.

5.1.1 Hematite sample

Sample ID: BF1

Location: The stratiform deposit in the Dunderland Valley (66.40°N, 14.54°E).

Sample BF1 is a hematite sample from the underground mine of the stratiform iron deposit in the Dunderland Valley. The hand specimen represents a folded hematite mineralization and consists of a brittle and dark coloured matrix with some lighter veins (Fig. 18). The matrix is mainly composed of flaky hematite and minor amounts of muscovite, whereas the veins consist of quartz and minor calcite (Fig. 19) (Table 1).

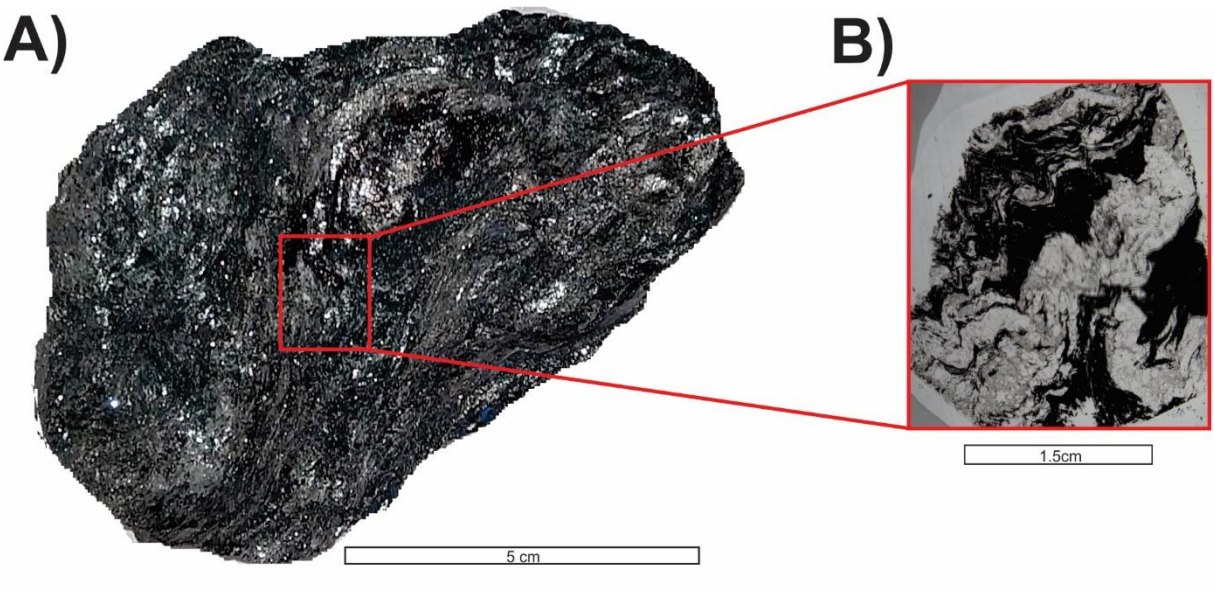

Figure 18: *A) Hand specimen of the hematite sample (BF1) from the stratiform deposit in Dunderland Valley. B) Area of thin section with overview of the thin section studied.*

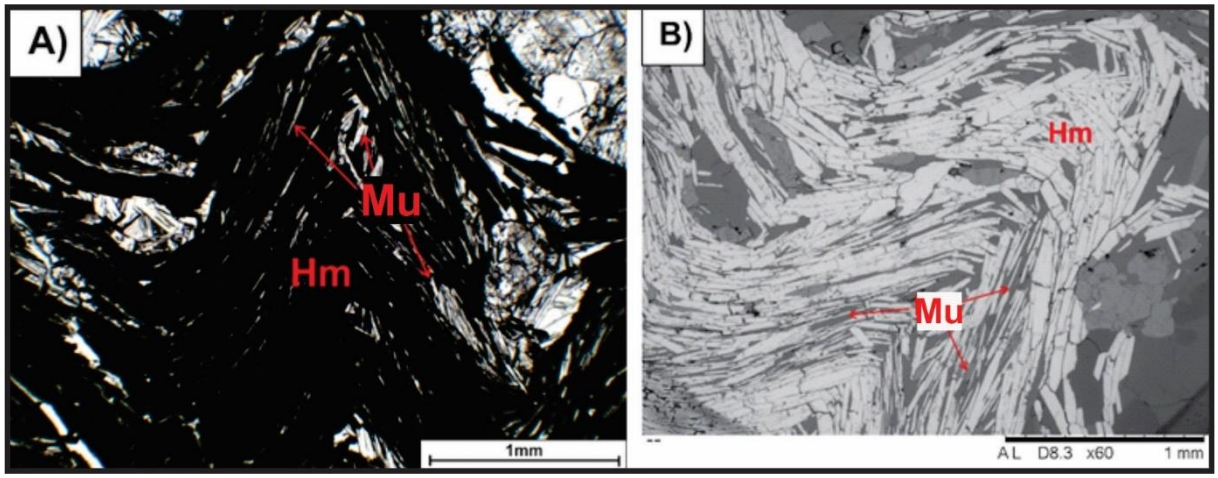

Figure 19: *A) Photomicrograph of hematite sample (BF1) in PPL reflected light microscopy (black = hematite, white/grey = muscovite). B) SEM image of hematite sample (BF1) (white = hematite, dark grey = muscovite).*

Table 1: *Table of elements for hematite from the element analysis.*

Element	[wt.%]	[norm. wt.%]	[norm. at.%]	Error in %
Iron	60,78	59,31	30,42	1,79
Oxygen	32,19	31,41	56,24	3,59
Silicon	6,60	6,44	6,57	0,29
Carbon	2,9	2,83	6,76	0,51

5.1.2 Magnetite sample

Sample ID: FL7

Location: The stratiform deposit in the Dunderland Valley (66.40ºN, 14.54ºE).

Sample FL7 is a magnetite rich sample from the underground mine of the stratiform iron deposit in the Dunderland Valley. The hand specimen represents a folded massive iron-bearing sample of dark colour layers altering with lighter colour, greenish-tined layers (Fig. 20). The sample is mainly composed of quartz and magnetite, with some epidote, biotite, muscovite, apatite and calcite, as well as rare copper sulphide (chalcocite and chalcopyrite) as an accessory mineral (Figs. 21 and 22) (Table 2). Magnetite grains are subhedral and large (>1 mm) with an elongated shape.

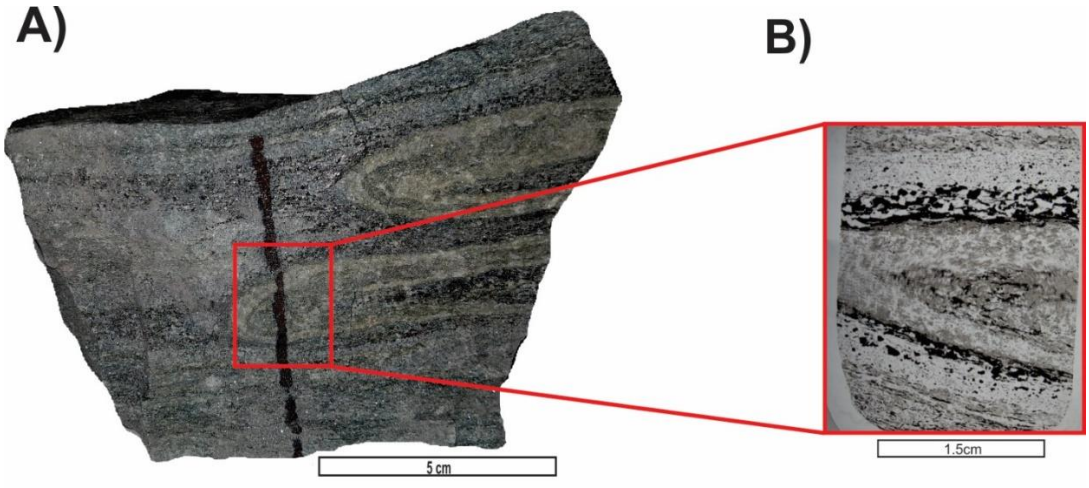

Figure 20: *A) Hand specimen of the magnetite sample (FL7) from the stratiform deposit in Dunderland Valley. B) Area of thin section with overview of the thin section studied.*

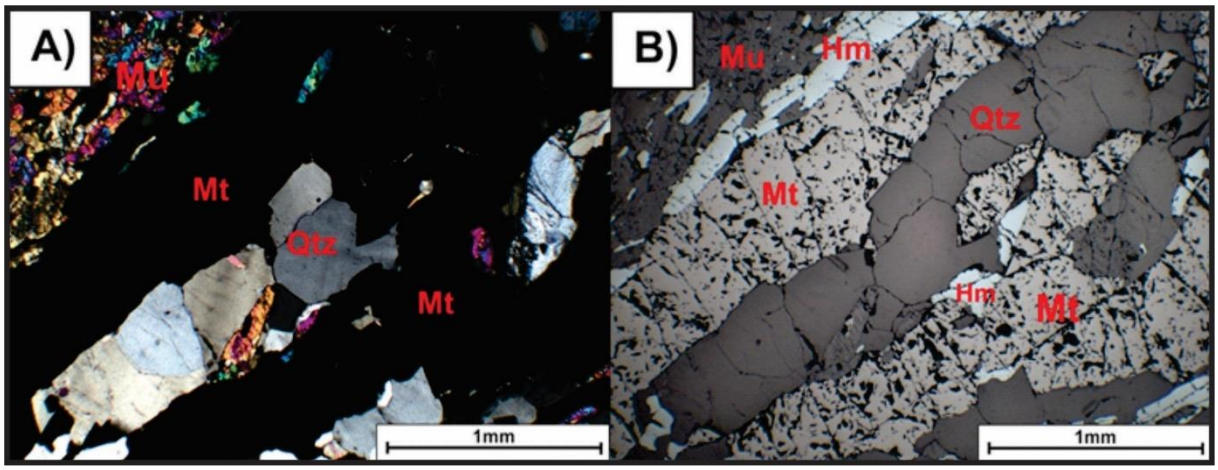

Figure 21: *Photomicrograph of magnetite sample (FL7) in A) XPL reflected light microscopy (black = magnetite or hematite, white/grey = quartz, multi-coloured = muscovite), B) transmitted light microscopy (white/grey = hematite, grey/beige = magnetite, brown/grey = quartz, brown/grey = muscovite). The magnetite grain is large (>1mm) and elongated.*

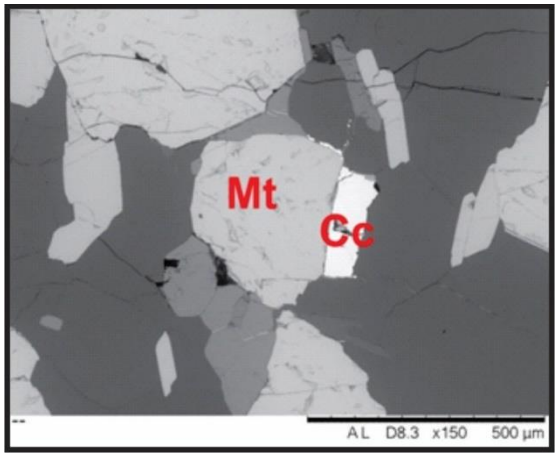

Figure 22: *BSE image showing chalcocite (Cc) as an accessory mineral of the magnetite mineralization.*

Table 2: Table of elements for magnetite from the element analysis.

Element	[wt.%]	[norm. wt.%]	[norm. at.%]	Error in %
Iron	66,77	69,58	40,41	1,97
Oxygen	26,90	28,03	56,82	3,08
Silicon	1,79	1,86	2,15	0,09
Alumnium	0,49	0,51	0,619	0,05

5.1.3 Manganese rich sample

Sample ID: BF2

Location: The stratiform iron deposit in the Dunderland Valley (open pit; 66,43ºN, 14,73ºE).

Sample BF2 represents a hand specimen of typical manganese (Mn) rich mineralization from the stratiform iron deposit in the Dunderland Valley (Fig. 23). The sample is stratified and consists of mm-cm thick brownish to yellowish Mn-bearing bands that alter with darker layers. The Mn-bearing bands are predominantly composed of fine-grained subhedral spessartine and oligonite, quartz and biotite with some small inclusions of hematite. The darker layers are composed of fine-grained subhedral hematite with quartz and some carbonates (Fig. 24) (Table 3).

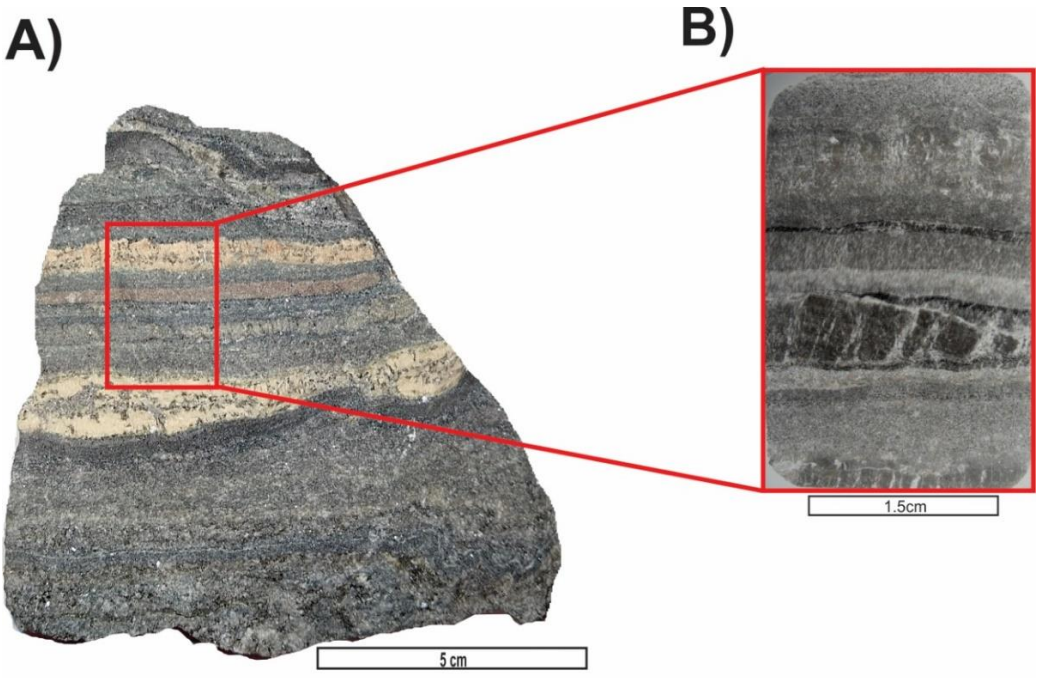

Figure 23: A) Hand specimen of the Mn rich sample (BF2) from the stratiform deposit in Dunderland Valley. B) Area of thin section with overview of the thin section studied.

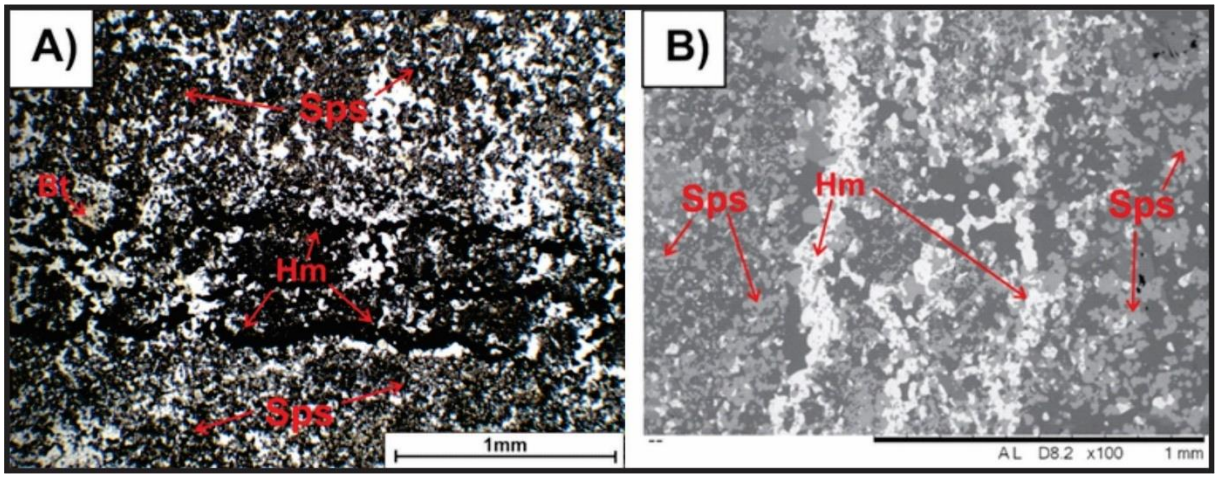

Figure 24: *A) Photomicrograph of iron ore in Mn rich sample (BF2) in PPL reflected light microscopy (black = hematite, brown = spessartine, brown/orange/yellow = biotite). B) SEM image of iron ore in Mn rich sample (BF2) (white = hematite, dark grey = spessartine).*

Table 3: *Table of elements for spessartine from element analysis.*

Element	[wt.%]	[norm. wt.%]	[norm. at.%]	Error in %
Oxygen	33,07	41,99	61,69	3,75
Manganese	20,33	25,82	11,04	0,61
Silicon	17,56	22,29	18,65	0,75
Aluminium	7,79	9,89	8,61	0,38

5.2 XRD analysis

The XRD analysis show the mineralogical content of the three samples from the Dunderland Valley.

- **Hematite sample (ID: BF1)**

  The XRD analysis of the hematite sample shows a pattern indicating a presence of hematite, quartz, muscovite (mica) and zeolite (aluminosilicate) (Fig. 25a).

- **Magnetite sample (ID: FL7)**

  The XRD analysis of the magnetite sample revealed that the sample, in addition to magnetite, contains quartz, albite (plagioclase feldspar), ankerite (carbonate mineral) and flurannite (mica) (Fig. 25b).

- **Manganese rich sample (ID: BF2)**

  XRD analysis of the manganese rich sample presents a pattern that show a composition of quartz, garnet, biotite, zeolite and hematite (Fig. 25c).

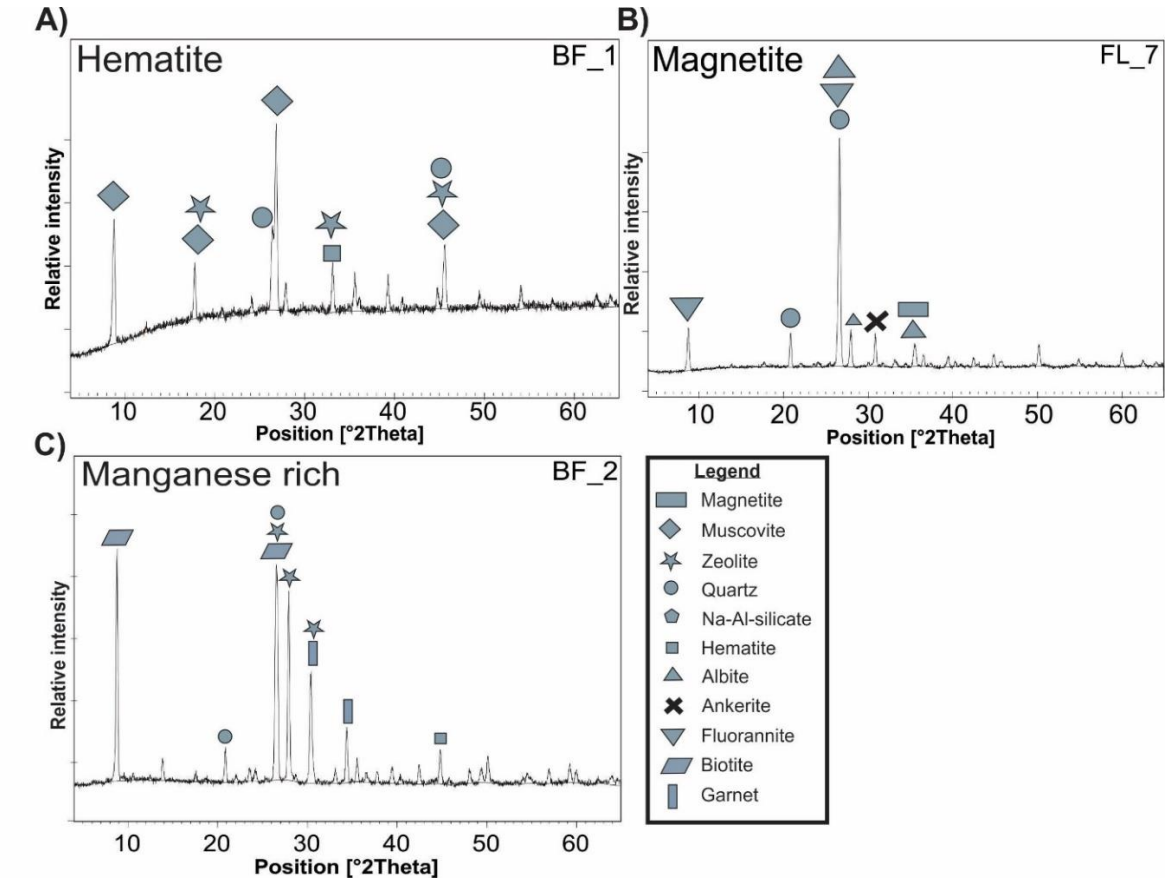

Figure 25: XRD pattern of A) Hematite sample (ID: BF1), B) magnetite sample (ID: FL7) and C) manganese rich sample (ID: BF2).

5.3 Lithogeochemistry

Lithogeochemical data are presented in Table 4 and 5 to present major oxides and trace elements of the hematite, magnetite and manganese rich sample. In this thesis, the elevated values are marked in red with bold font, set as twice value of the Clarke-values (Taylor, 1964) of the elements.

- The hematite sample (BF1) contains silica, iron, with some manganese, aluminium and calcium. Trace elements with elevated values of copper (Cu).
- The magnetite sample (FL7) contains silica, iron, with some manganese, aluminium and calcium. Trace elements with elevated values of copper (Cu).
- The manganese rich sample (BF2) contains silica, iron, manganese with some aluminium, calcium, magnesium and sodium. Trace elements with elevated values of cobalt (Co), arsenic (As) and antimony (Sb).

All samples have low values of sulphur (<0,002%).

Table 4: Lithogeochemical data presented in the table of representative samples from Dunderland Valley (FL7 = Magnetite, BF1 = Hematite and BF2 = Manganese rich sample). LOI = loss on ignition. Clarke (Taylor, 1964; Bielowicz et al., 2018).*

	BF1	FL7	BF2	Clarke*
(wt.%)				
SiO2	42,04	42,87	47,83	**60,18**
Al2O3	5,69	5,88	9,02	**15,61**
Fe2O3	**40,95**	**39,93**	**14,29**	**3,14**
MgO	1,59	1,62	3,27	**3,56**
CaO	4,92	4,79	5,49	**5,17**
Na2O	0,78	0,73	1,83	**3,91**
K2O	0,53	0,55	0,89	**3,19**
TiO2	0,44	0,39	0,6	**1,06**
P2O5	0,45	0,40	0,24	
MnO	**0,24**	**0,27**	**11,2**	**0,09**
Cr2O3	0,005	0,00	0,008	**0,01**
LOI	2,2	2,40	5,1	
Sum	99,86	99,87	99,84	
(%)				
TOT/C	0,6	0,67	1,47	
TOT/S	<0,02	<0,02	<0,02	

Table 5: Trace elements values of magnetite sample (FL7), hematite sample (BF1) and manganese rich sample (BF2) compared with Clarke values (Taylor, 1964; Robb, 2005) of the average crystal abundance in ppm (parts per million).*

	BF1	FL7	BF2	Clarke*
ppm				
Ba	140	161,00	192	**425**
Sc	10	9,00	11	**22**
Be	<1	<1	<1	**2,8**
Co	6,8	8,90	**197,9**	**25**
Cs	0,7	0,70	1,7	**3**
Ga	7,1	11,40	13,6	**15**
Hf	1,7	1,60	3,8	**3**
Nb	5,6	6,40	14,2	**20**
Rb	18,9	20,00	39,5	**90**
Sn	<1	<1	1	**2**
Sr	405,8	384,10	196,8	**375**
Ta	0,3	0,40	0,8	**2**
Th	2,4	2,20	5,8	**7,2**
U	0,7	0,70	0,2	**2,7**
V	120	91,00	38	**135**
W	<0,5	0,60	1,1	**1,5**
Zr	67,2	66,10	138,1	**165**
Y	29,5	26,20	31,9	**33**
La	15,8	13,40	30,4	**30**
Ce	30,7	27,80	56,6	**60**
Pr	3,59	3,50	6,49	**8,2**
Nd	15,6	14,90	26	**28**
Sm	3,17	3,11	5,06	**6**
Eu	0,82	0,78	1,21	**1,2**
Gd	3,52	3,42	5,58	**5,4**
Tb	0,57	0,53	0,91	**0,9**
Dy	3,88	3,42	5,48	**3**
Ho	0,83	0,79	1,11	**1,2**
Er	2,74	2,51	3,2	**2,8**
Tm	0,38	0,35	0,46	**0,48**
Yb	2,68	2,45	3,11	**3**
Lu	0,43	0,39	0,49	**0,5**
Mo	0,2	0,30	0,5	**1,5**
Cu	**133,3**	**116,80**	49,5	**55**
Pb	1	1,80	3,2	**13**
Zn	20	20,00	47	**70**
Ni	8,1	7,10	40,2	**75**
As	<0,5	1,00	**45,2**	**1,8**
Cd	<0,1	<0,1	<0,1	**0,2**
Sb	<0,1	<0,1	**1**	**0,2**
Bi	<0,1	<0,1	<0,1	**0,17**
Ag	<0,1	<0,1	<0,1	**0,07**
Au	0,0021	<0,5	0,0011	**0,004**
Hg	<0,01	<0,01	<0,01	**0,08**
Tl	0,1	0,10	0,3	**0,45**
Se	<0,5	<0,5	<0,5	**0,05**

5.3.1 Additional SEM/EDS analysis

An additional SEM/EDS analysis of the samples was done after lithogeochemical results to detect which mineral phases the elevated trace elements were located in.

The hematite sample was analysed for copper concentrations. From the analysis the copper was not detected to a specific mineral phase (Fig. 26).

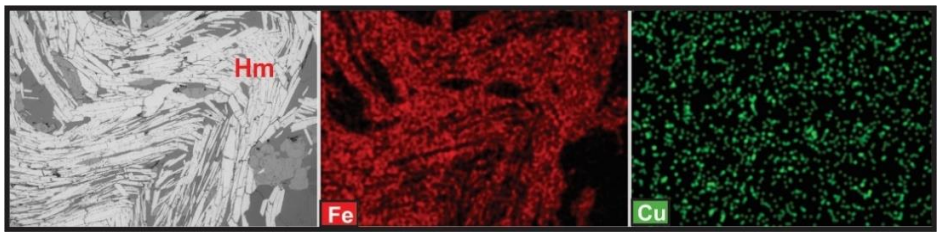

Figure 26: EDS mapping images of the hematite sample, presented for iron (Fe) and copper (Cu) concentrations.

The magnetite sample was analysed for copper concentrations. The copper was located in rare copper sulphides (chalcocite) (Fig. 27).

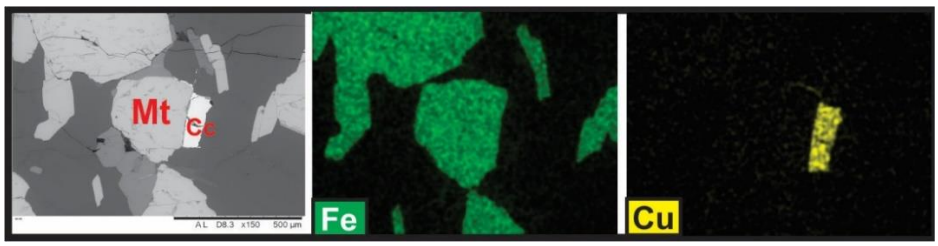

Figure 27: EDS mapping images of the magnetite sample, presented for iron (Fe) and copper (Cu) concentrations.

The manganese rich sample was analysed for cobalt, arsenic and antimony concentrations. The cobalt was mostly located in the hematite. The arsenic was located in the biotite and the antimony in the spessartine (Fig. 28).

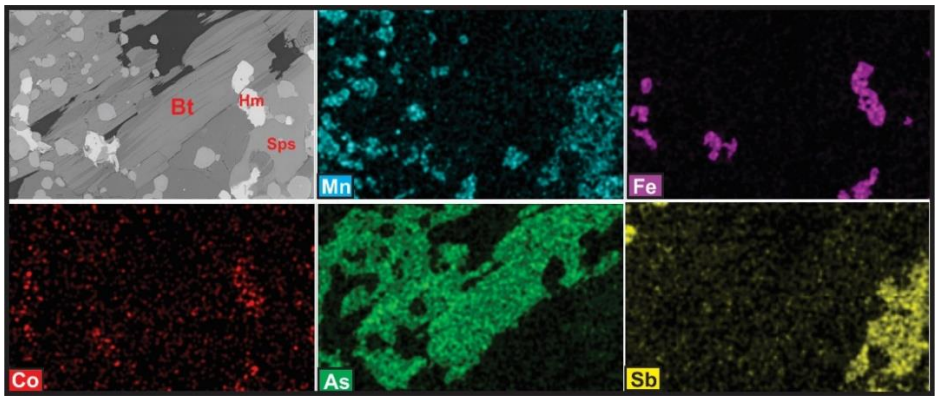

Figure 28: EDS mapping images of the manganese rich sample, presented for manganese (Mn), iron (Fe), cobalt (Co), arsenic (As) and antimony (Sb) concentrations.

5.4 Kinetic column test

5.4.1 Physicochemical measurements

5.4.1.1 PH

The behaviour of pH of the samples are presented in Figure 29. The different weathering conditions are marked with different colours. The different samples have variations of the colours, where the hematite samples have the weakest colour and the manganese rich samples have the strongest.

The non-buffered on-land condition (orange) show variations in pH during the experiment run. The maximum pH was approx. 8.5 to the lowest value of approx. 6. The highest pH values were in the beginning of the experiment after 48 hours and at the end of the experiment after six weeks, whereas the lowermost values appeared after one week and two weeks. Generally, the different samples follow the trend for the non-buffered on-land conditions. However, minor variations occur. The hematite sample has the lowermost value after one week. The magnetite sample has fewer fluctuating values than the other samples, indicating it is more stable. The manganese rich sample has the highest value of pH after 48 hours and the lowest value at the experiment stop.

The buffered on-land with carbonates condition (green) shows relatively few variations in pH during the experiment run. The pH varies between a high value of approx. 9 and a low of approx. 8, with a median of approx. 8.5. The different samples show a minimal difference of the general trend for the buffered on-land with carbonates conditions. The hematite sample has the lowest values after one week, while the manganese rich sample show a similar trend after 48 hours. All the samples have the highest values at the beginning of the experiment, after 24 hours, with pH near 9. After two weeks the pH stabilizes around 8.5.

The submarine condition (blue) show relatively constant values of pH during the experiment, with a median value of approx. 7.8. At the beginning of the experiment, the pH values were constant at approx. 8, before decreasing to approx. 7.5-7.6 the remaining time. The different samples have almost no variations compared to each other and follows the same trend, with one exception after six weeks where the magnetite sample has some higher values of pH (approx. 7.8).

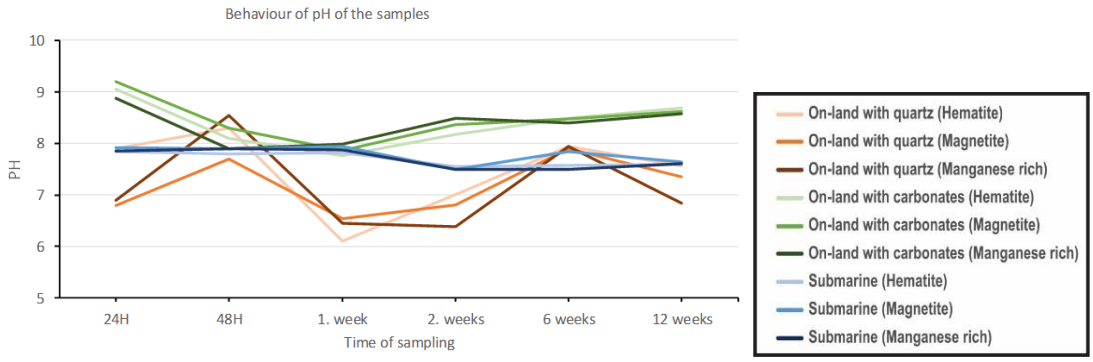

Figure 29: *Variations in pH during the kinetic column test.*

5.4.1.2 Redox potential

The behaviour of redox potential (Eh) of the samples are presented in Figure 30. The different weathering conditions are marked with different colours, where the different samples have different variations of the colours.

The non-buffered on-land condition (orange) show variations in Eh during the experiment run. The trend of the Eh variations starts relatively high at approx. 240 mV, then decreases to approx. 220 mV after 48 hours, and further increases to the highest value of approx. 260-280 mV after two weeks and to the end of the experiment. Generally, the different samples follow the same trend. However, some variations occur. The manganese rich sample variates with some lower values from the start of the experiment and higher values up to week six, before it follows the same trend as the other samples.

The buffered on-land with carbonates condition (green) presents a pattern of small variations during the experiment run. In general, the trend starts relatively low at approx. 175 mV and then increase to the end of the experiment to approx. 240 mV. The hematite and magnetite sample follow the same trend, while the manganese rich sample have some fluctuations in the start (lowest value after 24 hours of approx. 140mV and highest value after 48 hours of approx. 220 mV) of the experiment up to the first week, before following the trend.

The submarine condition (blue) show relatively constant values of Eh during the experiment, except a small decrease of Eh after one week from approx. 240 mV to 225 mV. The different samples show almost no variations compared to each other, except for the hematite sample that has some higher values in the start of the experiment up to one week, then follows the same trend.

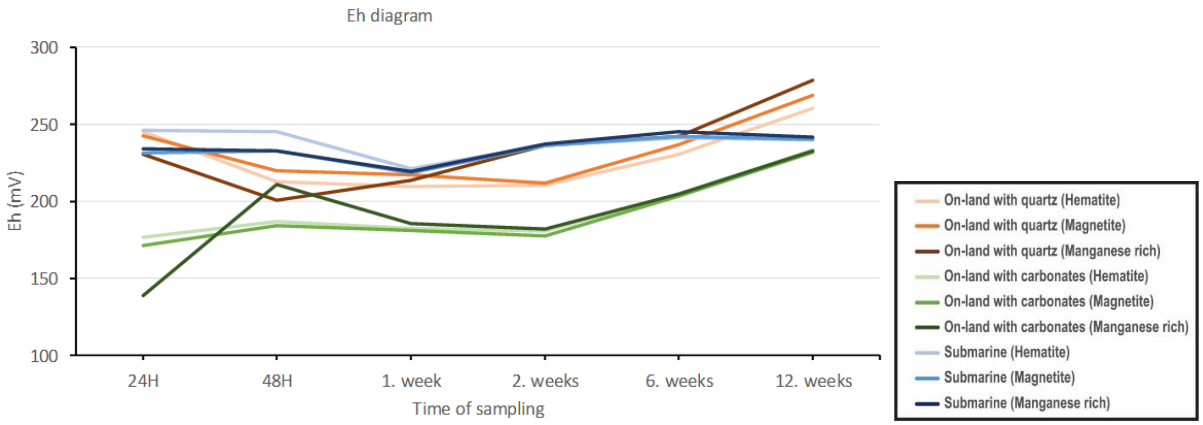

Figure 30: *Variations in redox potential (Eh) during the kinetic column test.*

5.4.1.3 Conductivity

The behaviour of conductivity of the samples are presented in Figure 31. The different weathering conditions are marked with different colours, where the different samples have different variations of the colours.

The non-buffered on-land condition (orange) show low values (mostly under 100 µS/cm) and minimal variations of conductivity during the experiment run. The hematite sample has higher values than 100 µS/cm after two weeks.

The buffered on-land with carbonates condition (green) presents a pattern of relatively low values that has some variations. The values are constant and low (approx. 150 µS/cm) before increasing values after six weeks (approx. 300 µS/cm). At the end of the experiment, the values decrease to the start values of approx. 150 µS/cm.

The submarine condition (blue) show high values above and close to 500 µS/cm that is relatively stable with some variations. The hematite sample show a decrease in conductivity after 48 hours to values under 400 µS/cm, and the manganese rich sample show the same trend at the end of the experiment with values just above 400 µS/cm.

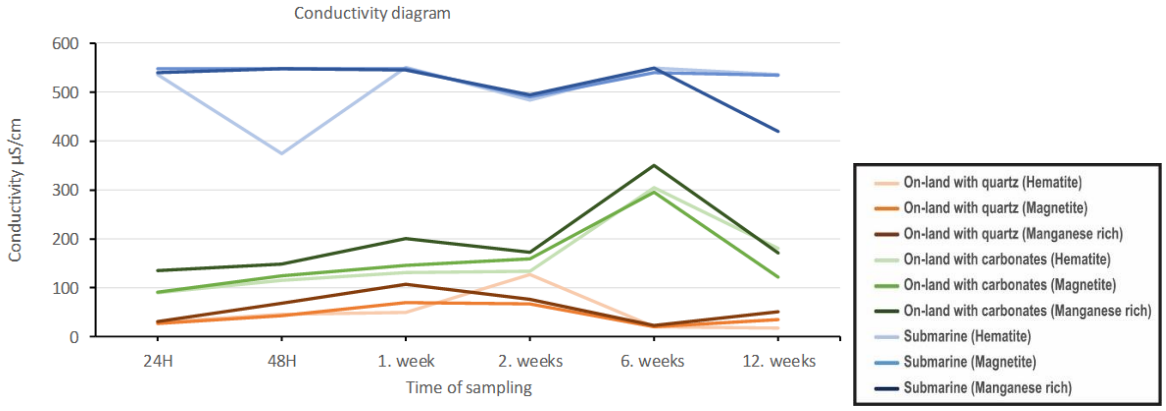

Figure 31: *Variations in conductivity during the kinetic column test.*

5.4.2 Eh-pH diagrams

Eh-pH diagrams are presented in Figures 32, 33 and 34 at standard conditions to present the stability fields of measurements for the hematite, magnetite and manganese rich samples in simulated on-land and submarine conditions in terms of the activity of pH (hydrogen ions) and the activity of electrons (Eh) of the systems. The measurements are marked as circles in the diagrams with respective colours (orange, green and blue) to represent the different conditions (respectively, non-buffered on-land (on-land with quartz), buffered on-land (on-land with carbonates) and submarine).

5.4.2.1 Hematite

The Eh-pH diagram for the hematite sample is presented in Figure 32, a Fe-O-H system. The measurements are located in the stability field of hematite, indicating that the iron is stable. Except one measurement for non-buffered on-land condition has a lower pH, resulting that the measurement are located on the boundary between stable hematite and mobile Fe^{2+}. This indicates that the iron can be mobile ferrous iron with lower pH.

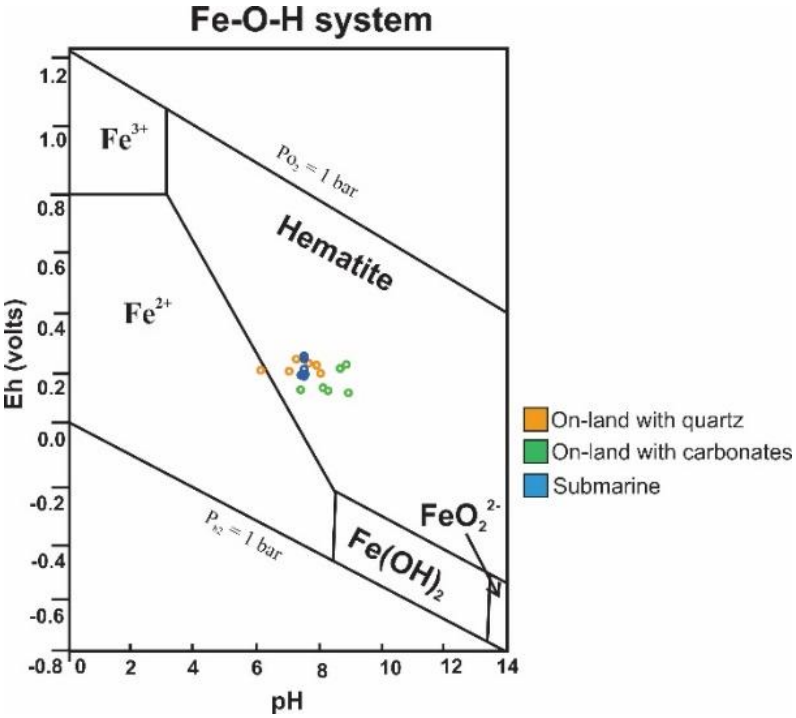

Figure 32: *Eh/pH diagram for Fe-O system, showing variations in Eh and pH values during kinetic column test in the different conditions for hematite sample. The assumed activity of dissolved Fe = 10^{-6}.*

5.4.2.2 Magnetite

The Eh-pH diagram for the magnetite sample is shown in Figure 33, a Fe-O-H-Si system. All measurements are located in the stability field of goethite (FeO*OH), meaning that the iron is stable in all conditions. This indicates that the magnetite in these conditions are not stable, and is altered to a different phase, iron(III) oxide-hydroxide (goethite).

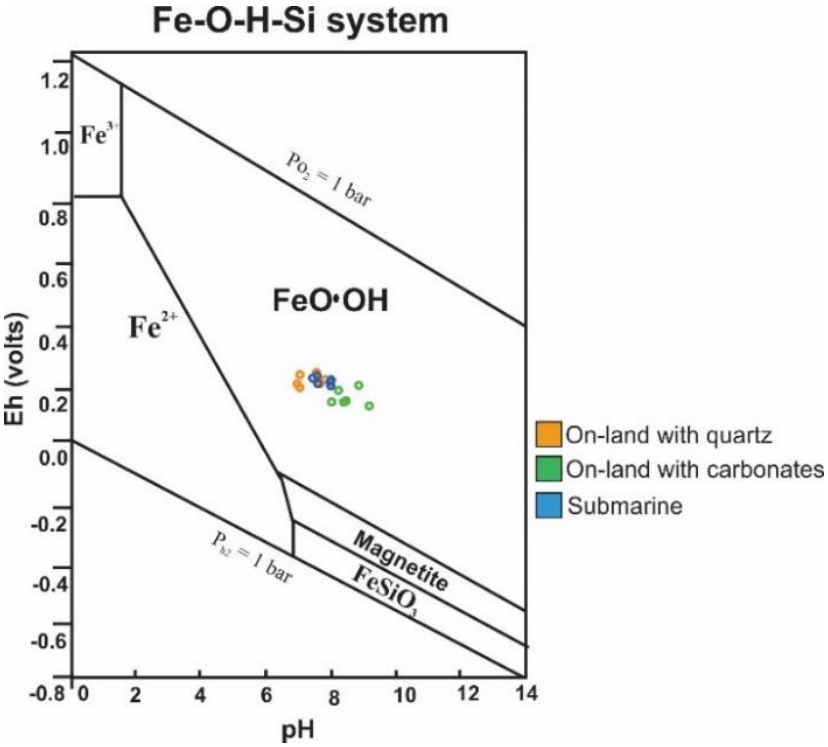

Figure 33: *Eh/pH diagram for Fe-O-H-Si system, showing variations in Eh and pH values during kinetic column test in the different conditions for the magnetite sample. The assumed activities for dissolved species are for Fe = 10^{-6}, Si = 10^{-3}, Fe(III) is assumed to be present in both magnetite and goethite (FeO*OH).*

5.4.2.3 Manganese rich

The Eh-pH diagram for the manganese rich sample is shown in Figure 34 (Mn-O-H (A) and Mn-C-S-O-H (B) system). All measurements are located in the stability field of Mn^{2+}, indicating that manganese is mobile in all conditions.

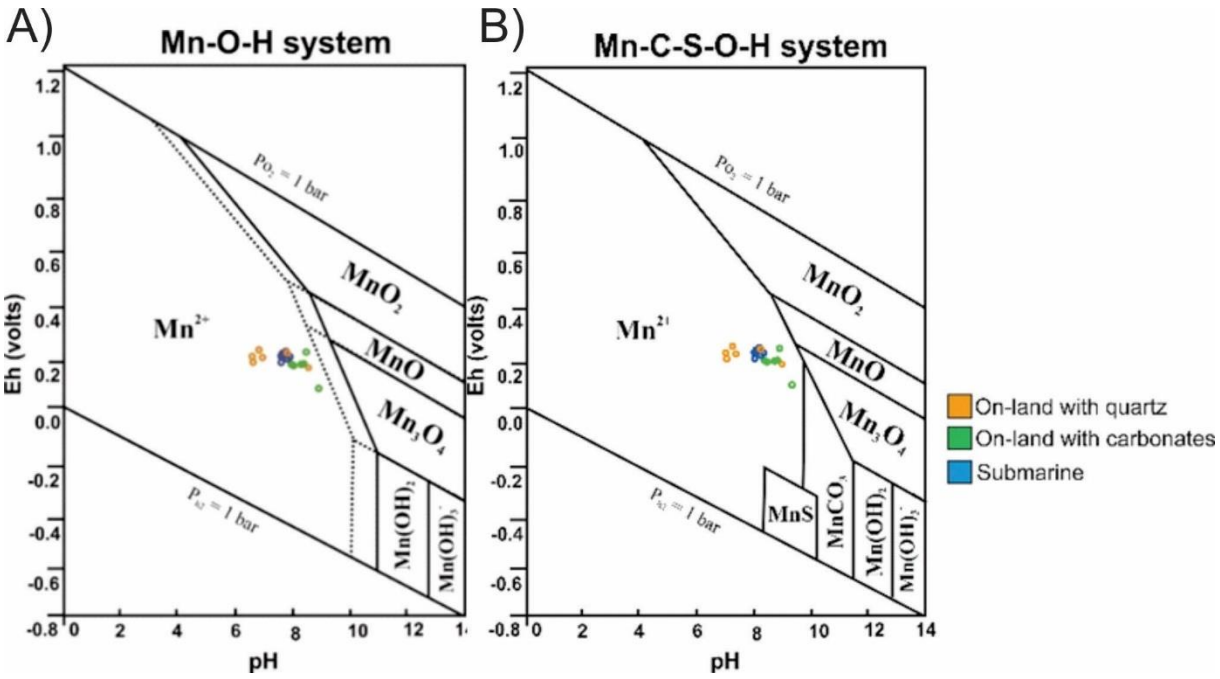

Figure 34: *Eh/pH diagram for A) Mn-O-H system, showing variations in Eh and pH values during kinetic column test in the different conditions for the Mn rich sample. The assumed activity for Mn = 10^{-6}. B) Mn-C-S-O-H system, showing variations in Eh and pH values during kinetic column test in the different conditions for the Mn rich sample. The assumed activity for Mn = 10^{-6}, C =10^{-3}, S = 10^{-3}.*

5.4.3 Lithogeochemistry

Results from lithogeochemical analyses of the samples before and after kinetic tests are listed in Table 6 for the major elements and Table 7 for the trace elements. The different samples (Hm = BF1, Mt = FL7, Mn = BF2) are presented before weathering, in non-buffered on-land (+Q), buffered on-land with carbonates (+C) and submarine (+SM) conditions. The sulphur content was low in all analysed samples and in all simulated conditions.

The hematite sample in the weathering conditions show minimal changes of the content in major oxides and trace elements compared to each other, whereas to the sample before weathering there is observed some changes. The content of silica has decreased to half of the amount as the original (Table 6). Trace element values of copper has decreased compared with the sample before weathering. The copper concentration has decreased from 133 ppm to approximately 6 ppm in all conditions (Table 7).

The magnetite sample before weathering and in the different weathering conditions show similar content of the major oxides and trace elements compared to each other. The most distinctive changes are higher content of calcium in buffered on-land conditions and higher values of sodium in submarine conditions (Table 6). The trace element concentrations show remaining high values of copper in all samples. By comparing the different conditions to each other, the non-buffered on-land has the lowermost value of copper with 89 ppm compared with the highest value of 146 ppm in the buffered on-land with carbonates conditions (Table 7).

The manganese-rich sample has relatively similar content of the major oxides and trace elements compared to each other. Trace element values of cobalt, arsenic and antimony are remaining high (Table 7).

Table 6: Lithogeochemistry results of major oxides of the samples in the different conditions.

Major oxide	Hm	Hm + Q	Hm + C	Hm + SM	FL7	Mt + Q	Mt + C	Mt + SM	Mn	Mn + Q	Mn + C	Mn + SM	Clarke*
(wt.%)													
SiO2	42,04	22,30	22,29	22,26	42,87	41,56	41,22	42,24	47,83	48,60	44,64	47,71	**60,18**
Al2O3	5,69	9,15	9,08	9,09	5,88	5,97	5,92	6,01	9,02	9,63	8,89	9,40	**15,61**
Fe2O3	**40,95**	**56,99**	**53,12**	**56,40**	**39,93**	**41,33**	**40,55**	**39,97**	**14,29**	**13,34**	**12,37**	**14,08**	**3,14**
MgO	1,59	2,25	3,26	2,41	1,62	1,63	1,87	1,65	3,27	3,20	4,64	3,20	**3,56**
CaO	4,92	2,36	3,57	2,31	4,79	4,83	5,19	4,96	5,49	5,36	7,39	5,45	**5,17**
Na2O	0,78	0,68	0,66	0,83	0,73	0,74	0,73	0,83	1,83	1,94	1,87	1,84	**3,91**
K2O	0,53	2,49	2,55	2,61	0,55	0,58	0,57	0,57	0,89	0,91	0,84	0,88	**3,19**
TiO2	0,44	0,79	0,72	0,77	0,39	0,41	0,42	0,42	0,6	0,59	0,55	0,59	**1,06**
P2O5	0,45	0,76	0,74	0,76	0,40	0,42	0,42	0,44	0,24	0,23	0,22	0,22	
MnO	0,24	0,09	0,12	0,09	0,27	0,23	0,24	0,23	**11,2**	**10,92**	**10,11**	**11,07**	**0,09**
Cr2O3	0,005	0,01	0,01	0,01	0,00	0,00	0,00	0,00	0,008	0,01	0,01	0,01	**0,01**
LOI	2,2	1,90	3,60	2,20	2,40	2,10	2,70	2,50	5,1	5,10	8,30	5,40	
Sum	99,86	99,83	99,82	99,84	99,87	99,87	99,85	99,86	99,84	99,84	99,82	99,85	
(%)													
TOT/C	0,6	0,13	0,67	0,12	0,67	0,64	0,80	0,67	1,47	1,50	2,42	1,48	
TOT/S	<0,02	<0,02	<0,02	<0,02	<0,02	<0,02	<0,02	<0,02	<0,02	<0,02	<0,02	<0,02	

Table 7: Lithogeochemistry results of trace elements of the samples in the different conditions.

Trace elements	Hm	Hm + Q	Hm + C	Hm + SM	Mt	Mt + Q	Mt + C	Mt + SM	Mn	Mn + Q	Mn + C	Mn + SM	Clarke*
ppm													
Ba	140	648,00	661,00	676,00	161,00	168,00	166,00	167,00	192	217,00	197,00	207,00	**425**
Sc	10	17,00	15,00	16,00	9,00	10,00	10,00	10,00	11	11,00	10,00	11,00	**22**
Be	<1	3,00	2,00	4,00	<1	<1	<1	1,00	<1	1,00	1,00	<1	**2,8**
Co	6,8	34,60	37,80	36,30	8,90	7,20	7,70	7,10	**197,9**	**197,10**	**178,10**	**186,70**	**25**
Cs	0,7	2,50	2,80	2,90	0,70	0,70	0,80	0,70	1,7	1,90	1,60	1,80	**3**
Ga	7,1	9,20	12,40	11,00	11,40	7,10	8,60	8,20	13,6	19,20	18,50	19,20	**15**
Hf	1,7	3,60	3,40	3,60	1,60	1,70	1,80	1,80	3,8	3,60	3,60	3,60	**3**
Nb	5,6	8,00	8,20	8,80	6,40	6,70	7,30	6,20	14,2	15,40	15,00	13,60	**20**
Rb	18,9	82,70	86,00	85,60	20,00	20,50	21,70	20,40	39,5	40,80	37,00	38,40	**90**
Sn	<1	<1	<1	<1	<1	<1	<1	<1	1	<1	<1	<1	**2**
Sr	405,8	329,60	322,90	293,80	384,10	405,60	422,90	420,00	196,8	190,20	187,20	193,60	**375**
Ta	0,3	0,40	0,50	0,40	0,40	0,30	0,40	0,30	0,8	0,80	0,90	0,70	**2**
Th	2,4	5,60	5,00	5,10	2,20	2,30	2,20	2,40	5,8	5,40	5,00	5,20	**7,2**
U	0,7	0,60	0,50	0,60	0,70	0,70	0,60	0,70	0,2	0,20	0,10	0,20	**2,7**
V	120	118,00	109,00	113,00	91,00	94,00	98,00	93,00	38	36,00	34,00	34,00	**135**
W	<0,5	0,80	0,70	0,70	0,60	0,60	<0,5	0,60	1,1	1,50	1,30	1,10	**1,5**
Zr	67,2	125,40	119,70	129,40	66,10	67,20	68,70	67,10	138,1	141,40	134,40	136,20	**165**
Y	29,5	40,00	36,10	35,60	26,20	27,00	27,90	28,50	31,9	33,50	28,90	32,60	**33**
La	15,8	21,80	19,70	18,60	13,40	13,90	13,90	13,90	30,4	25,40	21,70	21,90	**30**
Ce	30,7	45,60	41,90	39,20	27,80	28,00	30,00	29,40	56,6	49,00	45,10	44,80	**60**
Pr	3,59	5,84	5,36	5,12	3,50	3,53	3,62	3,66	6,49	6,04	5,33	5,48	**8,2**
Nd	15,6	24,00	21,50	20,10	14,90	15,10	15,40	15,20	26	23,90	20,80	22,30	**28**
Sm	3,17	5,08	4,54	4,57	3,11	3,01	3,07	3,13	5,06	4,88	4,52	4,64	**6**
Eu	0,82	1,19	1,13	1,01	0,78	0,81	0,80	0,77	1,21	1,19	1,06	1,16	**1,2**
Gd	3,52	5,67	5,22	5,16	3,42	3,55	3,64	3,48	5,58	5,82	5,31	5,66	**5,4**
Tb	0,57	0,93	0,85	0,87	0,53	0,56	0,56	0,57	0,91	0,96	0,86	0,92	**0,9**
Dy	3,88	**6,09**	5,66	5,75	3,42	3,61	3,57	3,70	5,48	5,76	5,24	5,57	**3**
Ho	0,83	1,38	1,28	1,24	0,79	0,85	0,88	0,86	1,11	1,21	1,07	1,11	**1,2**
Er	2,74	4,17	3,79	3,85	2,51	2,62	2,71	2,64	3,2	3,48	3,13	3,38	**2,8**
Tm	0,38	0,59	0,52	0,54	0,35	0,37	0,37	0,39	0,46	0,47	0,44	0,47	**0,48**
Yb	2,68	3,86	3,43	3,64	2,45	2,57	2,57	2,57	3,11	3,22	2,96	3,06	**3**
Lu	0,43	0,62	0,56	0,60	0,39	0,42	0,41	0,42	0,49	0,50	0,47	0,48	**0,5**
Mo	0,2	0,10	<0,1	<0,1	0,30	0,20	0,20	0,20	0,5	0,40	0,40	0,30	**1,5**
Cu	**133,3**	5,60	6,40	5,60	**116,80**	89,70	**146,20**	**122,80**	49,5	53,10	45,20	44,60	**55**
Pb	1	1,40	1,20	1,30	1,80	1,60	1,50	1,80	3,2	3,50	3,10	3,30	**13**
Zn	20	43,00	44,00	47,00	20,00	20,00	21,00	20,00	47	50,00	43,00	47,00	**70**
Ni	8,1	15,90	16,10	16,20	7,10	6,60	6,70	6,80	40,2	37,20	33,10	36,40	**75**
As	<0,5	2,30	2,60	2,30	1,00	0,70	0,70	0,60	**45,2**	**42,70**	**41,10**	**41,50**	**1,8**
Cd	<0,1	<0,1	<0,1	<0,1	<0,1	<0,1	<0,1	<0,1	<0,1	<0,1	<0,1	<0,1	**0,2**
Sb	<0,1	<0,1	<0,1	<0,1	<0,1	<0,1	<0,1	<0,1	1	0,90	0,90	0,80	**0,2**
Bi	<0,1	<0,1	<0,1	<0,1	<0,1	<0,1	<0,1	<0,1	<0,1	<0,1	<0,1	<0,1	**0,17**
Ag	**<0,1**	<0,1	<0,1	<0,1	**<0,1**	**<0,1**	**<0,1**	**<0,1**	**<0,1**	**0,60**	**<0,1**	**<0,1**	**0,07**
Au	**2,1**	<0,5	<0,5	<0,5	**<0,5**	**<0,5**	**<0,5**	**<0,5**	**1,1**	**<0,5**	**<0,5**	**0,80**	**0,004**
Hg	<0,01	<0,01	0,01	0,01	<0,01	<0,01	<0,01	<0,01	<0,01	<0,01	<0,01	<0,01	**0,08**
Tl	0,1	0,20	0,30	0,20	0,10	0,10	0,10	0,10	0,3	0,30	0,30	0,30	**0,45**
Se	<0,5	<0,5	<0,5	<0,5	<0,5	<0,5	<0,5	<0,5	<0,5	<0,5	<0,5	<0,5	**0,05**

5.4.3.1 Isochon diagrams

Isochon diagrams are presented in Figures 35-43 and 67-69 in Appendix B by comparing the content of elements in the samples before and after weathering (non-buffered on-land, buffered on-land with carbonates and submarine conditions).

Hematite sample

The hematite sample of the different conditions are presented in isochon diagrams (Figs. 35-38). In general, the diagrams comparing the samples before and after weathering (Figs. 35-37) show a slightly enrichment of potassium oxide (K_2O), barium (Ba) and cobalt (Co), and a depletion of copper (Cu), molybdenum (Mo) and manganese (Mn). Whereas for the diagrams comparing the weathering conditions (Figs. 67-69, Appendix B) to each other, presents no variations. The included species in the diagrams are: Ba, Co, Cs, Ga, Ta, Th, U, V, Zr, Mo, Cu, Pb, Zn, Ni, Tl, SiO2, Al2O3, Fe2O3, MgO, CaO, Na2O, K2O, TiO2, P2O5, MnO, Cr2O3.

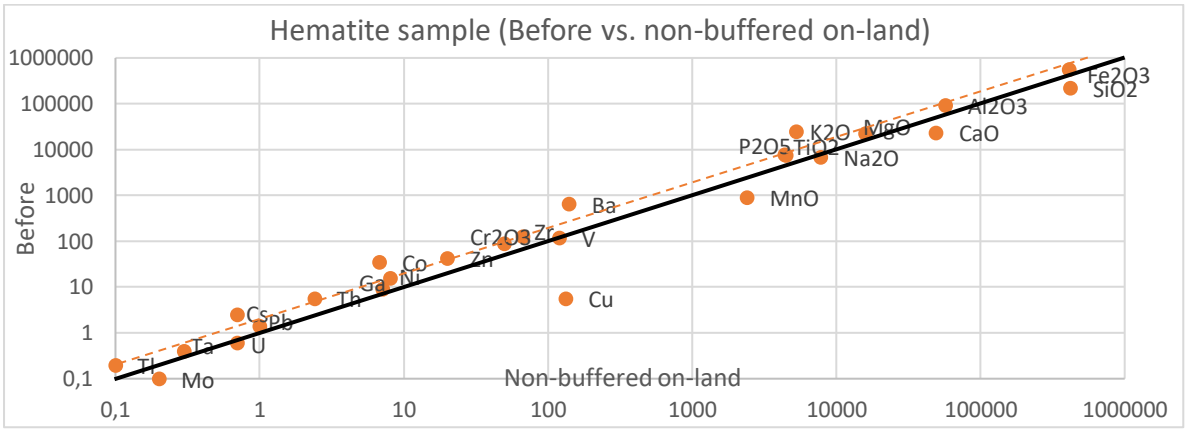

Figure 35: Isochon diagram of the hematite sample before vs. non-buffered on-land condition.

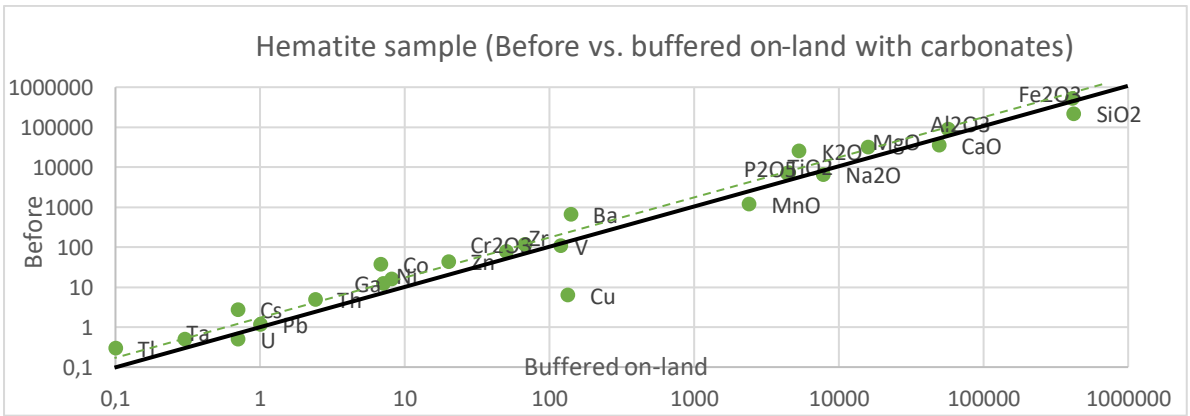

Figure 36: Isochon diagram of the hematite sample, the content before vs. on-land with carbonates condition.

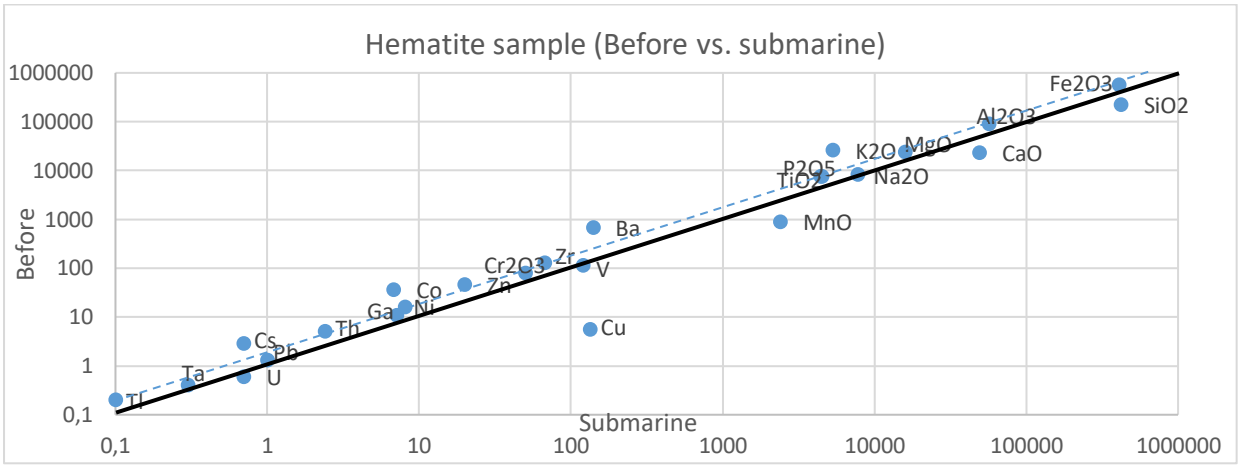

Figure 37: Isochon diagram of the hematite sample, the content before vs. submarine condition.

Magnetite sample

The magnetite sample of the different conditions are presented in isochon diagrams (Figs. 38-41). In general, the diagrams show almost no changes. There are no representative variations of the different conditions. The included species in the diagrams are: Ba, Co, Cs, Ga, Ta, Th, U, V, Zr, Mo, Cu, Pb, Zn, Ni, As, Tl, SiO2, Al2O3, Fe2O3, MgO, CaO, Na2O, K2O, TiO2, P2O5, MnO, Cr2O3.

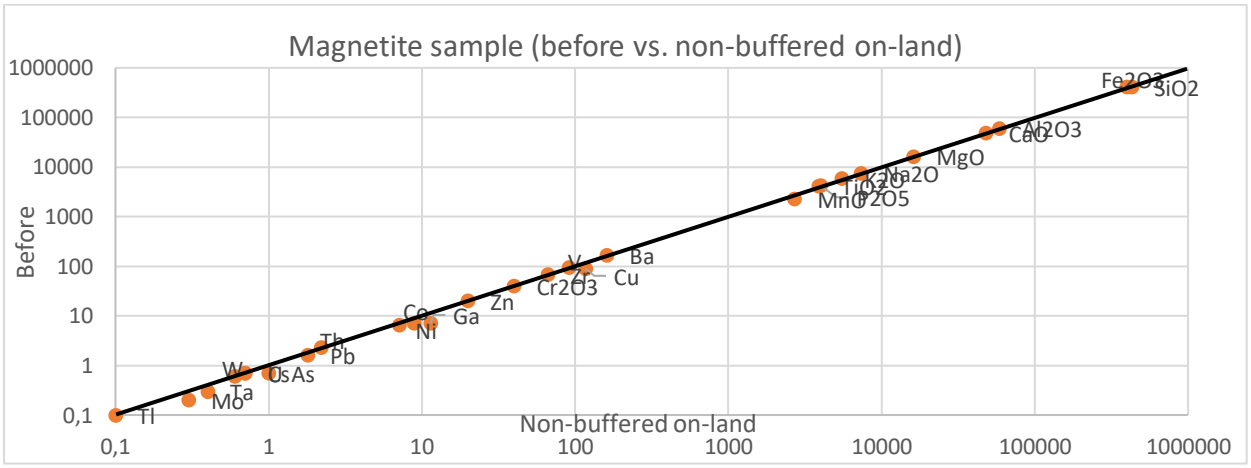

Figure 38: Isochon diagram of the magnetite sample, the content before vs. on-land with quartz condition.

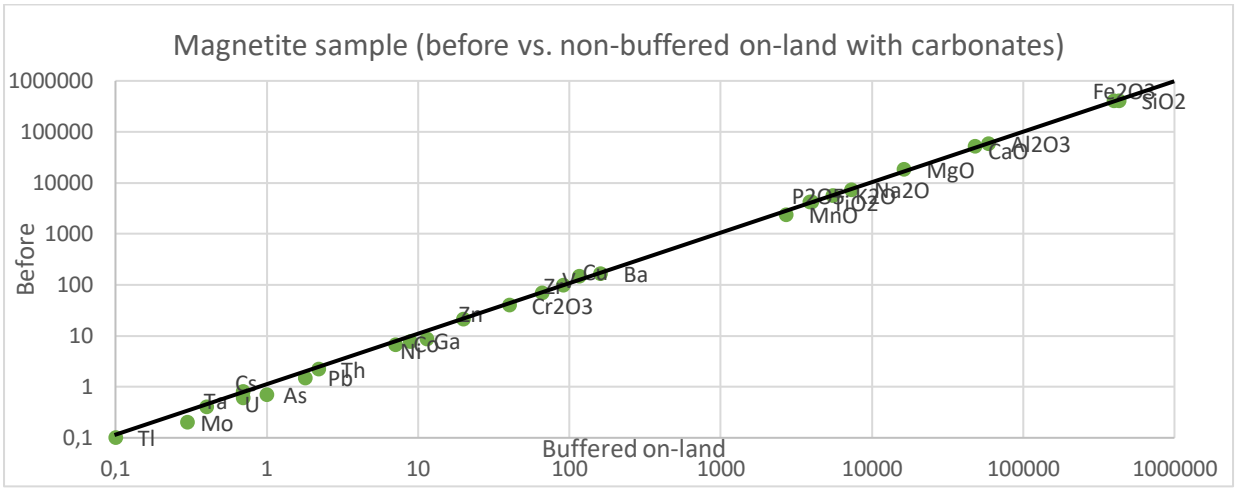

Figure 39: Isochon diagram of the magnetite sample, the content before vs. on-land with carbonate condition.

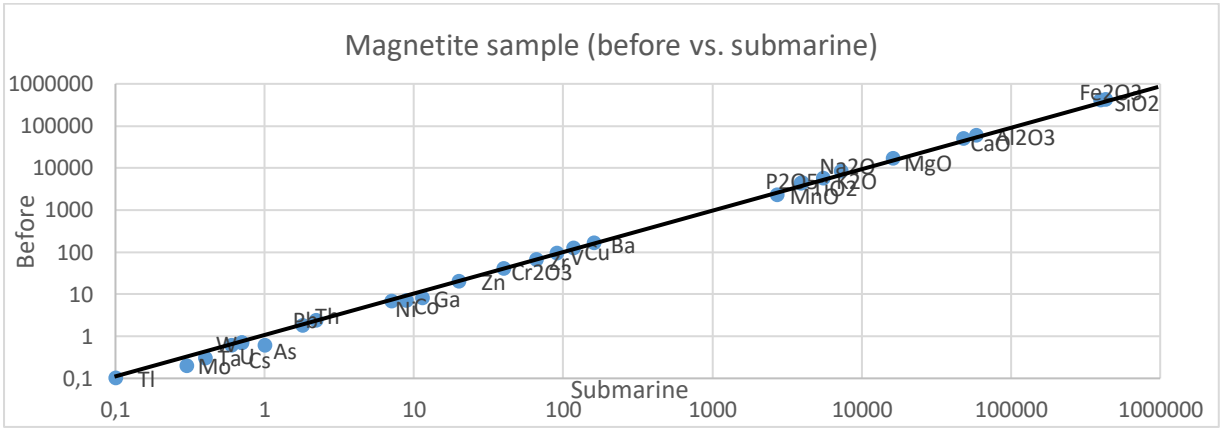

Figure 40: Isochon diagram of the magnetite sample, the content before vs. submarine condition.

Manganese rich sample

The manganese rich sample for the different conditions are presented in the isochon diagrams in Figures 41-43. The diagrams show minimal changes, with no representative variations of the different conditions. The included species in the diagrams are: Ba, Co, Cs, Ga, Ta, Th, U, V, Zr, Mo, Cu, Pb, Zn, Ni, As, Sb, Tl, SiO2, Al2O3, Fe2O3, MgO, CaO, Na2O, K2O, TiO2, P2O5, MnO, Cr2O3.

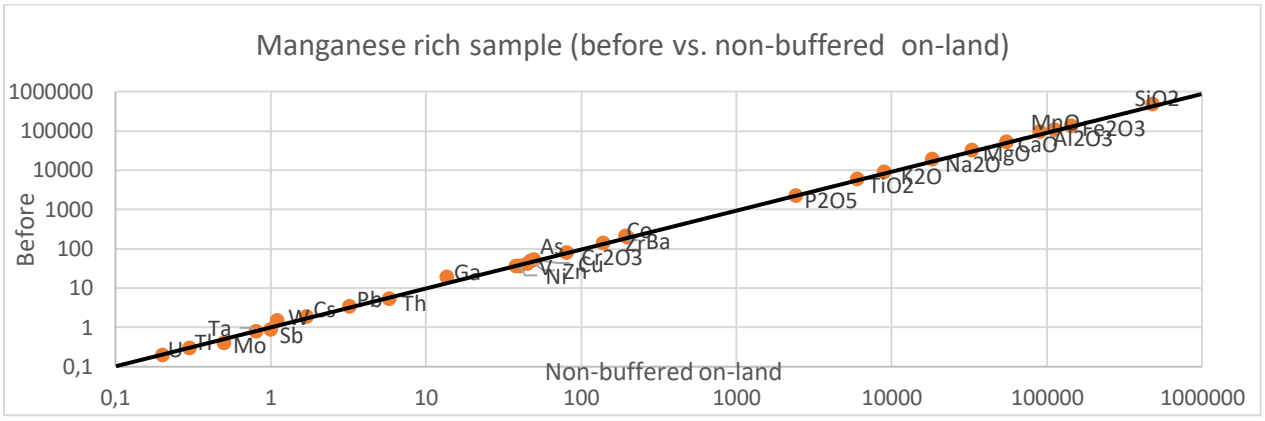

Figure 41: Isochon diagram of the manganese rich sample, the content before vs. on-land with quartz condition.

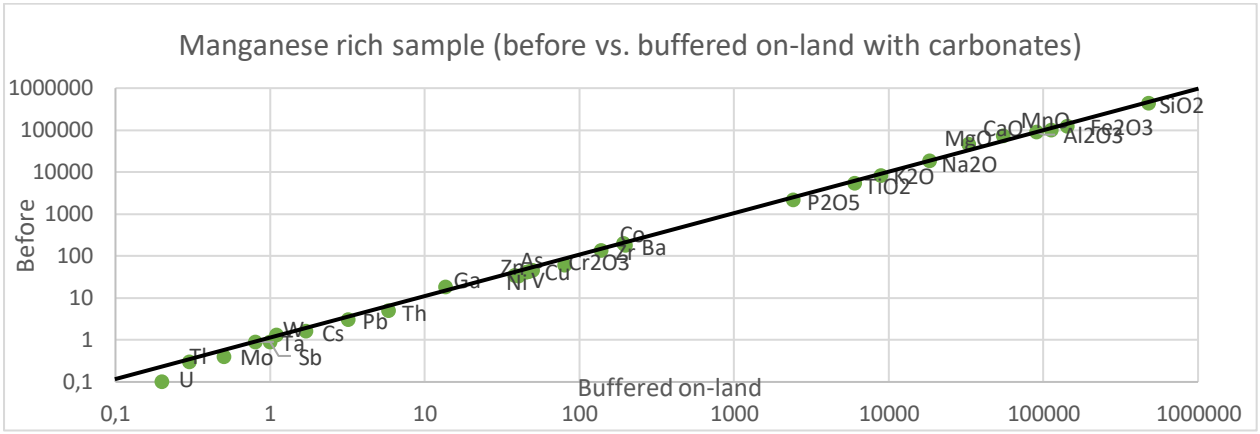

Figure 42: Isochon diagram of the manganese rich sample, the content before vs. on-land with carbonates condition.

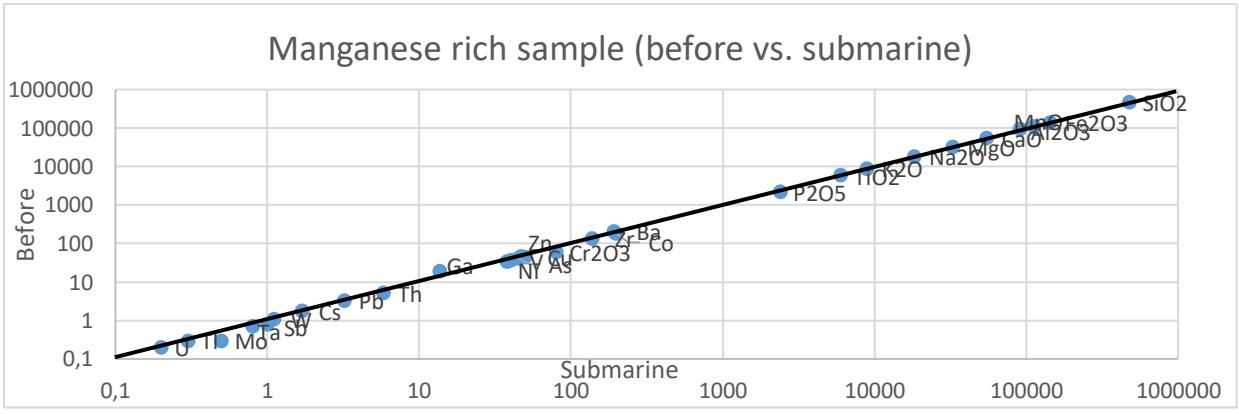

Figure 43: Isochon diagram of the manganese rich sample, the content before vs. submarine condition.

5.5 Thin sections exposed to weathering

The polished thin sections of three representative samples from the Dunderland Valley (BF1, FL7 and BF2) were analysed before and after exposure of the three conditions (non-buffered on-land, buffered on-land and submarine). They were analysed by optical microscopy, SEM/EDS and Raman spectroscopy to observe eventual changes in the mineralogy. The results are presented in the chapters below.

5.5.1 Description of samples

Hematite sample: Thin sections of the hematite samples before and after exposure of the weathering conditions are shown in Figure 44. In general, the samples are composed of hematite, muscovite, quartz and some calcite. In the samples before weathering, in buffered on-land and submarine conditions there is no observed changes in the mineralogy of the samples. The non-buffered on-land conditions has visible changes of the colour of calcite grains, it has a brown-yellow colour.

Magnetite sample: Thin sections of the magnetite sample before and after exposure of the conditions are shown in Figure 45. In general, the samples are composed of hematite, quartz, muscovite and minor calcite. As in the hematite sample, the calcite grains in non-buffered on-land conditions has a change in colour to brown-yellow. The samples before weathering, in buffered on-land and submarine conditions has no observed changes in the mineralogy of the samples.

Manganese rich sample: Thin sections of the manganese rich sample before and after exposure of the conditions are shown in Figure 46. In general, the samples are composed of spessartine, hematite, quartz, minor muscovite and calcite. Like the hematite and magnetite samples in non-buffered on-land conditions, the manganese rich sample in the same condition has an altered calcite grain. The grain has a brown-beige colour. The outer boundary and the lamellas of the grain has a dark colour and an altered rim. The other samples before weathering and in buffered on-land and submarine conditions has no observed changes in the mineralogy of the samples.

5.5.1.1 Hematite sample

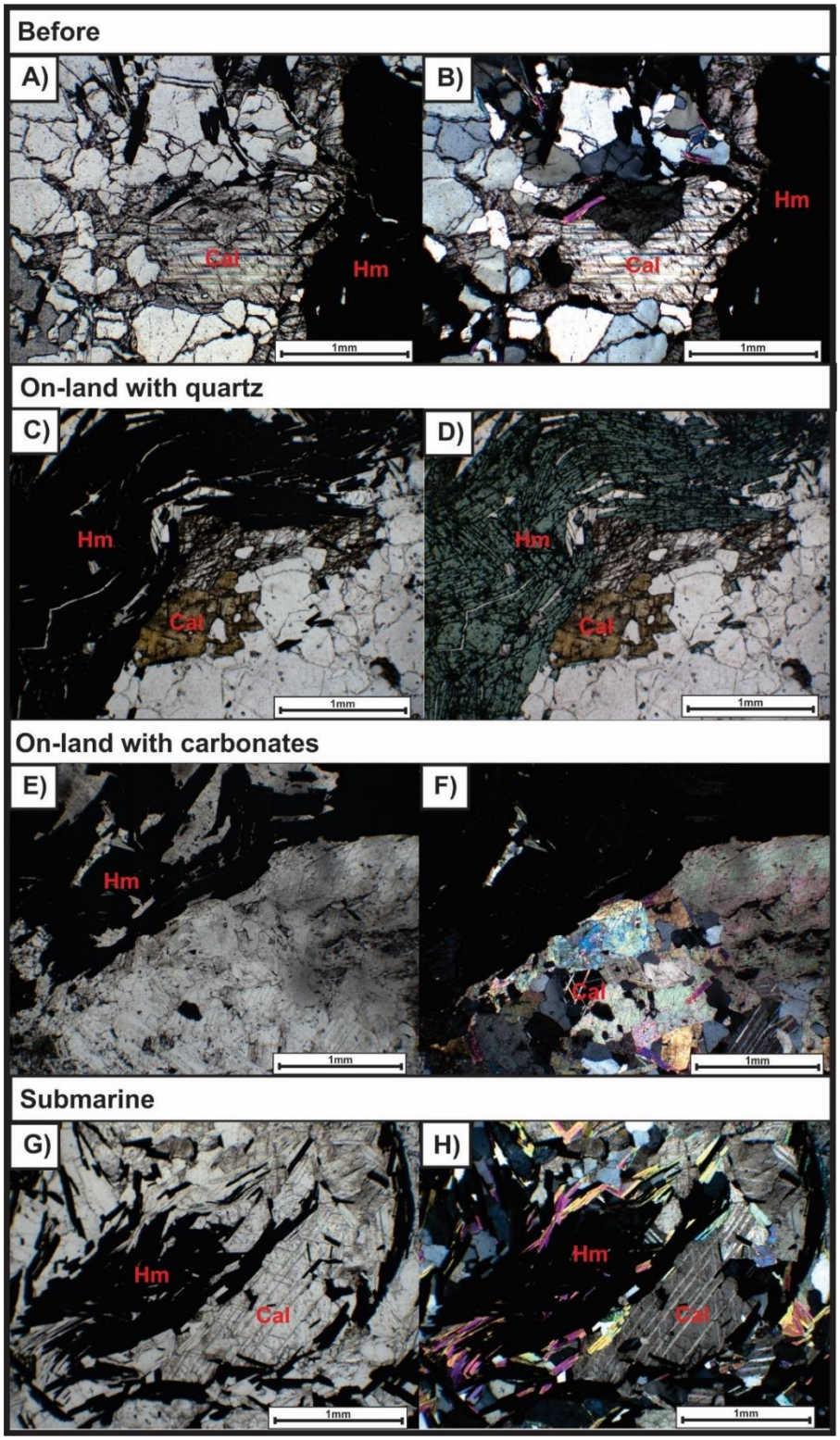

Figure 44: *Thin sections of hematite sample (BF1). A) and B) before, C) and D) exposed to on-land conditions with quartz, E) and F) exposed to on-land conditions with carbonates and G) and H) exposed to submarine conditions.*

5.5.1.2 Magnetite sample

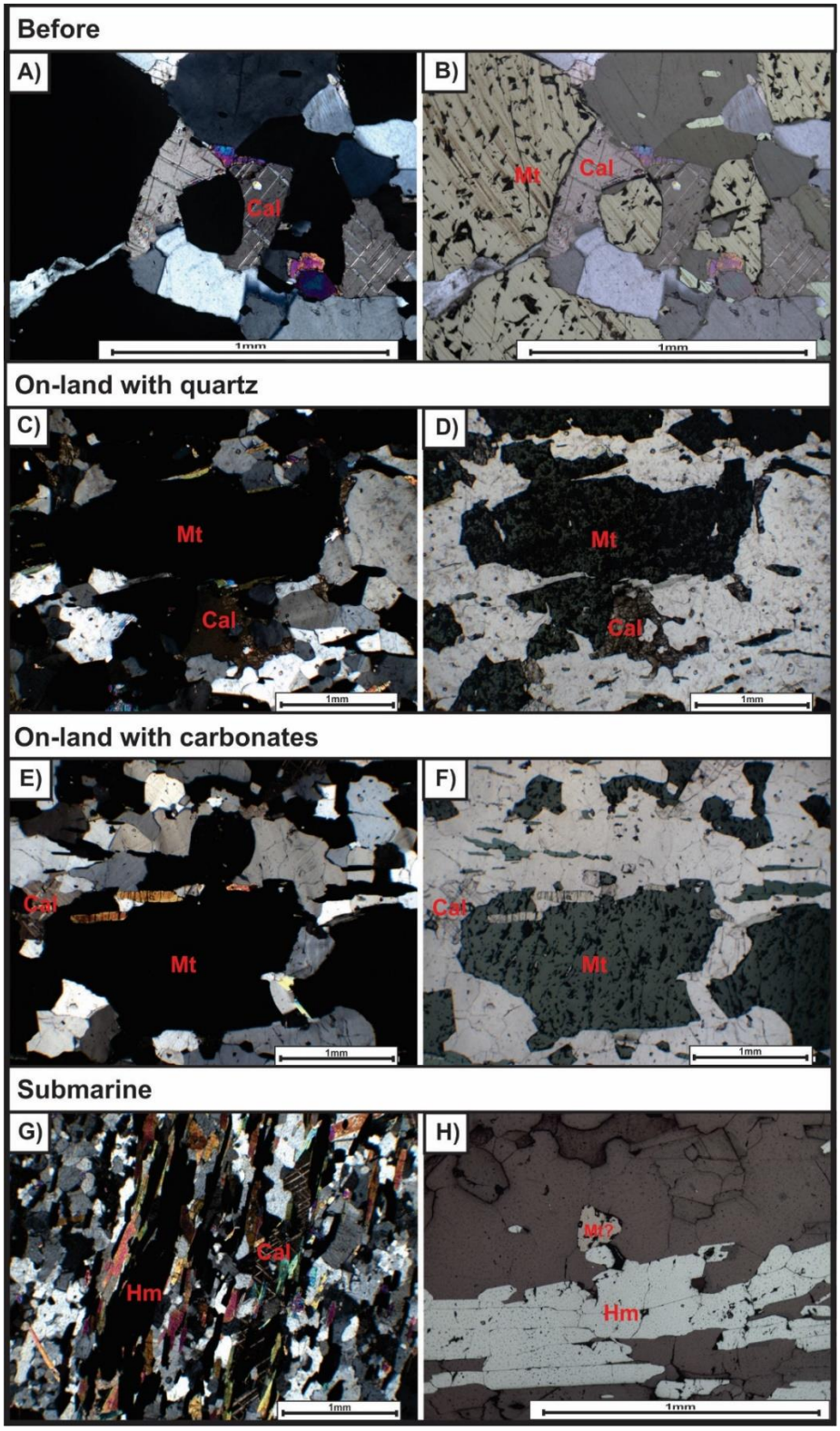

Figure 45: *Thin sections of magnetite sample (FL7). A) and B) before, C) and D) exposed to on-land conditions with quartz, E) and F) exposed to on-land conditions with carbonates and G) and H) exposed to submarine conditions.*

5.5.1.3 Manganese rich sample

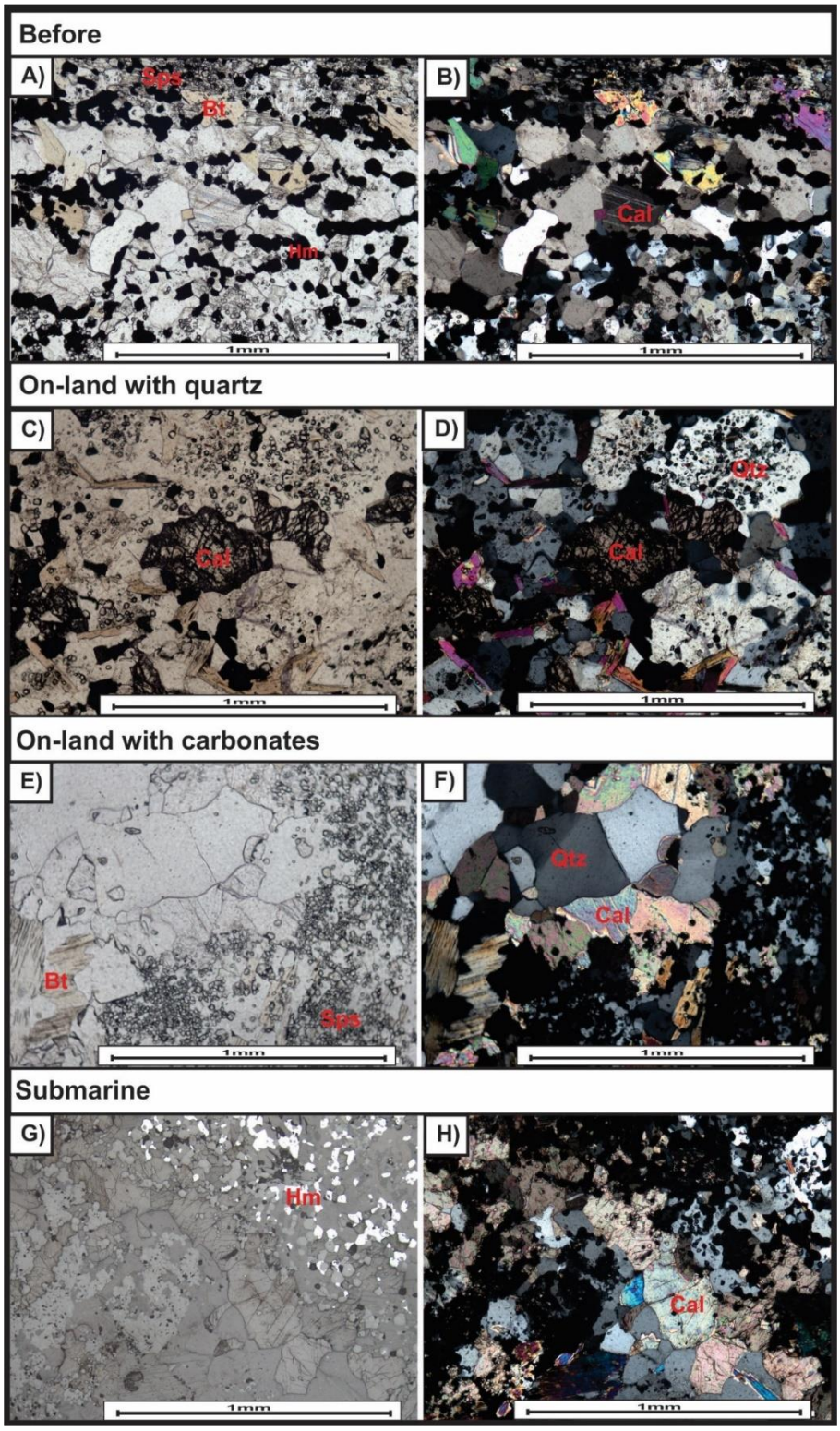

Figure 46: *Thin sections of manganese rich sample (BF2). A) and B) before, C) and D) exposed to on-land conditions with quartz, E) and F) exposed to on-land conditions with carbonates and G) and H) exposed to submarine conditions.*

5.5.2 Additional SEM/EDS analysis of the magnetite samples

The analysis of the thin section exposed to weathering showed a magnetite sample (FL7) in submarine condition with no confirmed magnetite content. Therefore, an additional SEM/EDS analysis of the magnetite samples were done to analyse the supposed magnetite grains in the different conditions.

The magnetite grains before and after weathering in the three conditions were analysed for their ratio of iron and oxygen content (Fig. 47). Since the samples contain quartz (SiO_2 (silicon and oxygen)), the values needed to be subtracted from the value of the oxygen to get a more precise value of the iron related to the oxygen. The ratio of iron related to oxygen were calculated using Equation 6 (Table 8, 9, 10 and 11). The ratio was compared with the ratio for magnetite ($Ratio_{Fe3O4\ (Magnetite)} = 0.75$). See Appendix B for complete calculations.

$Ratio_{FeO}$ = Fe / O **(Equation 6)**

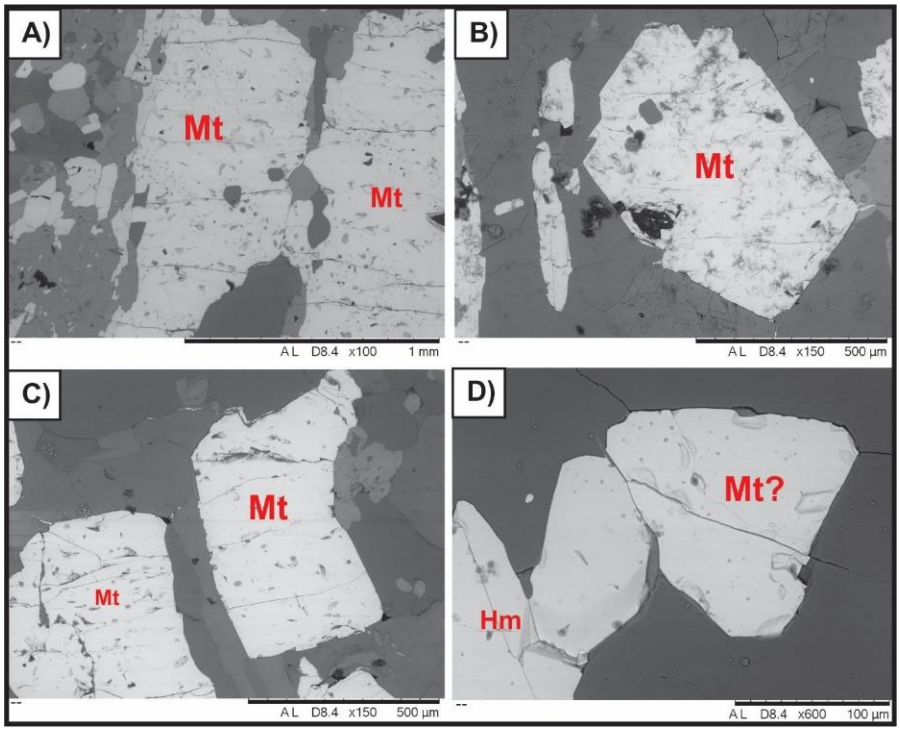

Figure 47: *SEM image of magnetite sample A) before, B) on-land with quartz condition, C) on-land with carbonates condition, D) submarine conditions (Mt = magnetite, Hm = hematite).*

- **Before**

Table 8: Table of elements for magnetite grain before weathering from element analysis of iron, oxygen and silicon content.

Element	[wt.%]	[norm. wt.%]	[norm. at.%]	Error in %
Iron	66,90	70,01	40,74	1,97
Oxygen	26,85	28,10	57,08	3,08
Silicon	1,79	1,88	2,18	0,09
	95,54	~100	~100	

$Ratio_{FeO}$ = 0.77

- **Non-buffered on-land**

Table 9: Table of elements for magnetite grain in non-buffered on-land conditions from element analysis of iron, oxygen and silicon content.

Element	[wt.%]	[norm. wt.%]	[norm. at.%]	Error in %
Iron	66,05	67,82	38,86	1,95
Oxygen	27,69	28,44	56,88	3,26
Silicon	3,64	3,74	4,26	0,17
	97,39	~100	~100	

$Ratio_{FeO}$ = 0.80

- **Buffered on-land**

Table 10: Table of elements for magnetite grain in buffered on-land with carbonates condition from element analysis of iron, oxygen and silicon content.

Element	[wt.%]	[norm. wt.%]	[norm. at.%]	Error in %
Iron	63,75	67,29	38,29	1,88
Oxygen	27,35	28,87	57,36	3,30
Silicon	3,63	3,83	4,34	0,17
	94,73	100	100	

$Ratio_{FeO}$ = 0.78

- **Submarine**

Table 11: Table of elements for magnetite grain in submarine conditions from element analysis of iron, oxygen and silicon content.

Element	[wt.%]	[norm. wt.%]	[norm. at.%]	Error in %
Iron	57,84	59,23	31,74	1,71
Oxygen	30,09	30,82	57,65	3,40
Silicon	9,72	9,95	10,61	0,43
	97,65	100	100	

$Ratio_{FeO}$ = 0.87

5.5.3 Raman spectroscopy

A Raman study of a hematite, magnetite and spessartine (manganese rich) sample have been performed to study changes in mineralogical characteristics of the samples before and after exposure to the conditions like the conditions in the kinetic column test.

5.5.3.1 Hematite sample

The patterns in Figure 48 are identified as a spectrum of hematite by published literature of Raman analysis. From literature ((De Faria et al., 1997b)[1](De Faria and Lopes, 2007)[2]), the expected Raman spectrum has seven bands (Table 12). The strongest bands before weathering are at approx. 224, 291, 410 and 1328 cm^{-1}.

Table 12: *Band positions and relative intensities (in parenthesis: w = weak, m = medium, s = strong) for the hematite samples from literature, before weathering and in the three conditions. ("-"= absent band).*

$Hematite_{Literature}$[1,2]	226[1], 227(s)[2]	292[1], 293(w)[2]	410[1], 412(s)[2]	497[1], 498(w)[2]	611[1], 610(m)[2]	-	1330[1], 1322(s)[2]
$Hematite_{Before}$	224(m)	291(s)	410(s)	502(w)	615(w)	667(w)	1328(s)
$Hematite_{Non\text{-}buffered\ on\text{-}land}$	224 (s)	290(s)	411(s)	-	617(w)	665(w)	1333(s)
$Hematite_{Buffered\ on\text{-}land}$	224(m)	290(s)	411(s)	508(w)	617(w)	668(w)	1324(s)
$Hematite_{Submarine}$	224(s)	292(s)	413(m)	495(w)	620(w)	669(m-w)	1328(s)

The Raman spectrum for the samples of hematite before, in non-buffered on-land conditions, buffered on-land with carbonates and in submarine conditions show clearly a similar spectrum, with some spectral variations (Fig. 48) (Table 12), with a difference in peak positions of maximum ±13 cm^{-1}. The most prominent variations are the intensity of the 410 cm^{-1} peak and the 1320 cm^{-1} shoulder.

- The spectrum for non-buffered on-land conditions compared with the original sample show similar bands at approx. 224, 290, 411 and 1333 cm^{-1} that are sharp and strong. The broad shoulder at 1333 cm^{-1} show a lower intensity. The band at approx. 500 cm^{-1} are absent.

- The spectrum for buffered on-land conditions compared with the original sample appear similar to the original. The bands have similar intensity and positions (Fig. 48).
- The spectrum for submarine conditions compared with the original sample show a lower intensity of the peak at 413 and 1328 cm^{-1}. The bands at 620 and 669 cm^{-1} are displaced.

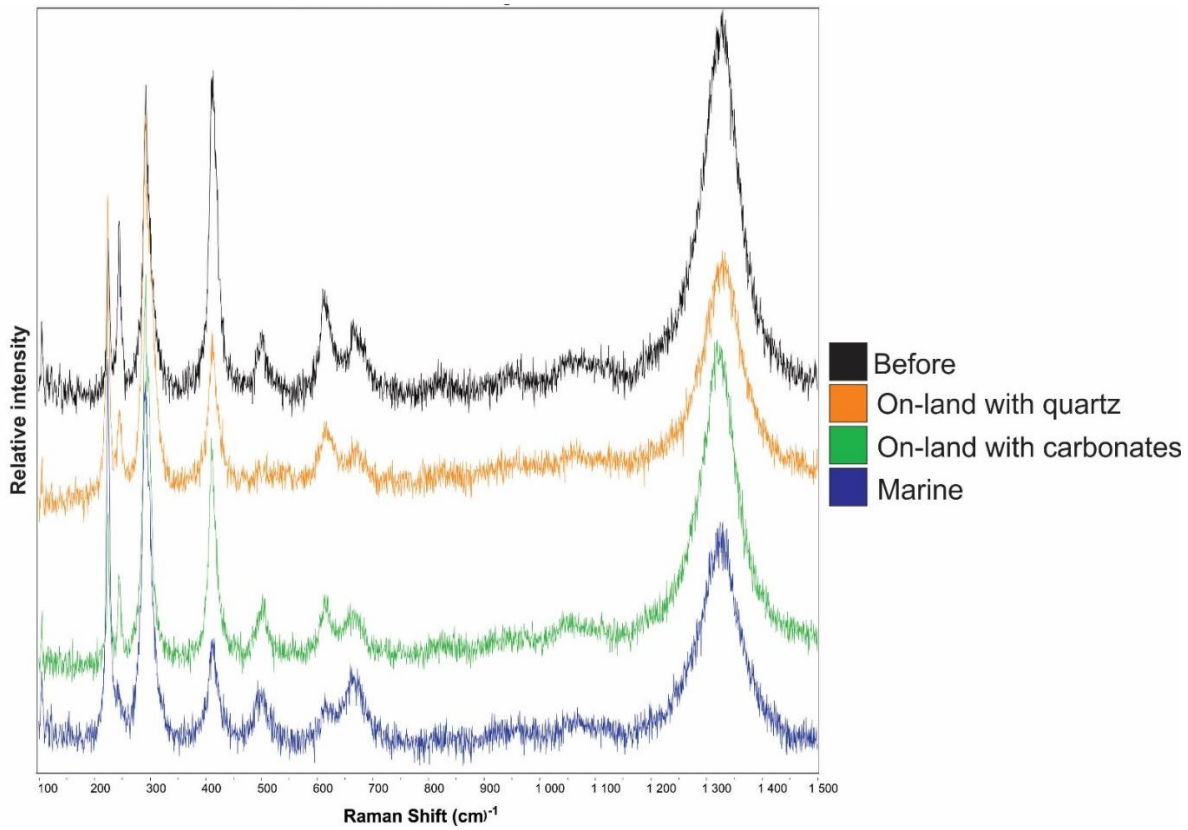

Figure 48: *Raman spectrum of the hematite sample before (black), non-buffered on-land with quartz (orange), buffered on-land with carbonates (green) and submarine environments (blue).*

5.5.3.2 Magnetite sample

The patterns in Figure 49 are identified as a spectrum of magnetite by published literature of Raman analysis. Previously published Raman studies on magnetite includes the strongest bands at approx. 306, 538 and 666 cm^{-1} (Table 13) (De Faria et al., 1997a)[1]. The original magnetite sample ($Magnetite_{Before}$) is not the sample from the Dunderland Valley, due to a misunderstanding of bringing the sample to Raman analysis. The original sample in Table 13 and Figure 49 is a sample from literature taken from RRuff.info (ID: R060656) from Jacupiranga, Brazil, by Michael Scott that represents a typical magnetite spectrum (Scott).

The magnetite sample in submarine conditions are not present because the thin section did not contain any magnetite as thought before weathering. This was a source of error in the thin section preparation, that could have been solved if the thin sections were studied before weathering. A pre-study of the thin sections before weathering are recommended for future work.

Table 13: *Band positions and relative intensities (in parenthesis: w = weak, m = medium, s = strong) for the magnetite samples from literature, before weathering and in the three conditions. ("-"= absent band). Additional bands marked in red.*

$Magnetite_{Literature}$[1]	306(w)[1]	538(w)[1]	666(s)[1]	-
$Magnetite_{Before}$	306(w)	558(w)	671(s)	-
$Magnetite_{Non\text{-}buffered\ on\text{-}land}$	303(w)	544(w)	669(s)	-
$Magnetite_{Buffered\ on\text{-}land}$	307(w)	546(w)	670(s)	462(w) 1040(m) 1397(w)

The Raman spectrum for the samples of magnetite before, in non-buffered on-land conditions, buffered on-land with carbonates and in submarine conditions show clearly a similar spectrum, with bands at approx. 305, 545 and 669 cm^{-1} (Fig. 49) (Table 13), with a small change in peak positions of maximum ±4 cm^{-1}. Some variations appear in the buffered on-land conditions, where additional bands occur at 462, 1040 and 1397 cm^{-1}.

- The spectrum for non-buffered on-land conditions compared with the original sample show almost identical bands at approx. 303, 544 and 669 cm^{-1} that are relatively sharp with weak to strong intensity. The spectrum is generally flat with no other bands than expected for a magnetite spectrum.
- The spectrum for buffered on-land conditions compared with the original sample appear in relatively similar positions, except that additional bands occur at 462, 1040 and 1397 cm^{-1}. The spectrum is broad and the additionally bands have weak to medium intensity (Fig. 49).

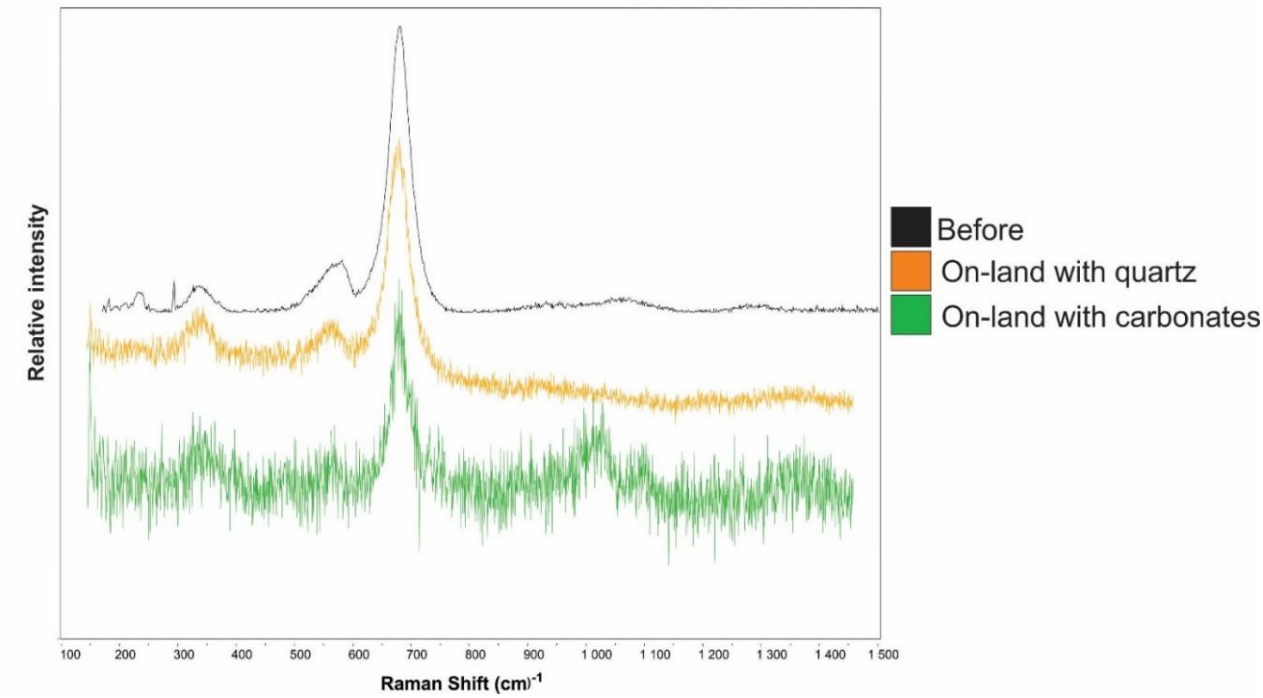

Figure 49: *Raman spectrum of the magnetite sample before (black), non-buffered on-land (orange) and buffered on-land with carbonates (green).*

5.5.3.3 Spessartine (manganese rich) sample

The patterns in Figure 50 are identified as a spectrum of spessartine by published literature of Raman analysis. From literature (Kolesov and Geiger, 1998), studies on spessartine includes the strongest bands at approx. 350, 552 and 905 cm^{-1} (Table 14).

Table 14: *Band position and relative intensities (in parenthesis: w = weak, m = medium, s = strong) for the spessartine samples from literature, before weathering and in the three conditions ("-"= absent band). Additional bands marked in red.*

$Spessartine_{Literature}$	221	350	552	849	905	1029	-	-
$Spessartine_{Before}$	224(w-m)	353(m)	549(w)	846(w)	904(s)	1024(w)	1320(w)	-
$Spessartine_{Non\text{-}buffered\ en\text{-}land}$	224(w)	354(m)	549(w-m)	846(w)	904(s)	1024(w)	-	-
$Spessartine_{Buffered\ on\text{-}land\ with\ carbonates}$	224(s)	352(m)	549(w-m)	848(w)	906(s)	1024(w)	1320(m)	288(s) 409(m) 609(m)
$Spessartine_{Submarine}$	224(m)	353(m)	550(w-m)	846(w)	904(s)	1027(w)	1318(w-m)	294(m)

The Raman spectrum for the samples of spessartine before, in non-buffered on-land conditions, buffered on-land and in marine conditions show clearly a similar spectrum with bands at approx. 224, 353, 549, 846, 904 and 1024 cm^{-1} (Fig. 50) (Table 14), with small difference in peak positions of maximum ±3 cm^{-1}. Variations are shown in on-land conditions with quartz and carbonates, where bands in on-land conditions with quartz are less prominent and out of shift and for carbonates additional bands occur at 288, 409 and 609 cm^{-1}.

- The spectrum for non-buffered on-land conditions compared with the original sample show a variation of bands with a weak intensity of the peak at 224 cm^{-1}, bands out of shift from the peak at 354 cm^{-1} to a drop at approx. 600 cm^{-1} position and a missing peak at 1320 cm^{-1} position.
- The spectrum for buffered on-land conditions compared with the original sample show additional bands occurring at 288, 409 and 609 cm^{-1} of strong to medium intensity (Fig. 50). The broad peak at 609 cm^{-1} position have a higher intensity compared with the original.
- The spectrum for marine conditions compared with the original sample appear at relatively similar positions, except higher intensity of the 224 cm^{-1} position band and an additional band occurring at 294 cm^{-1}.

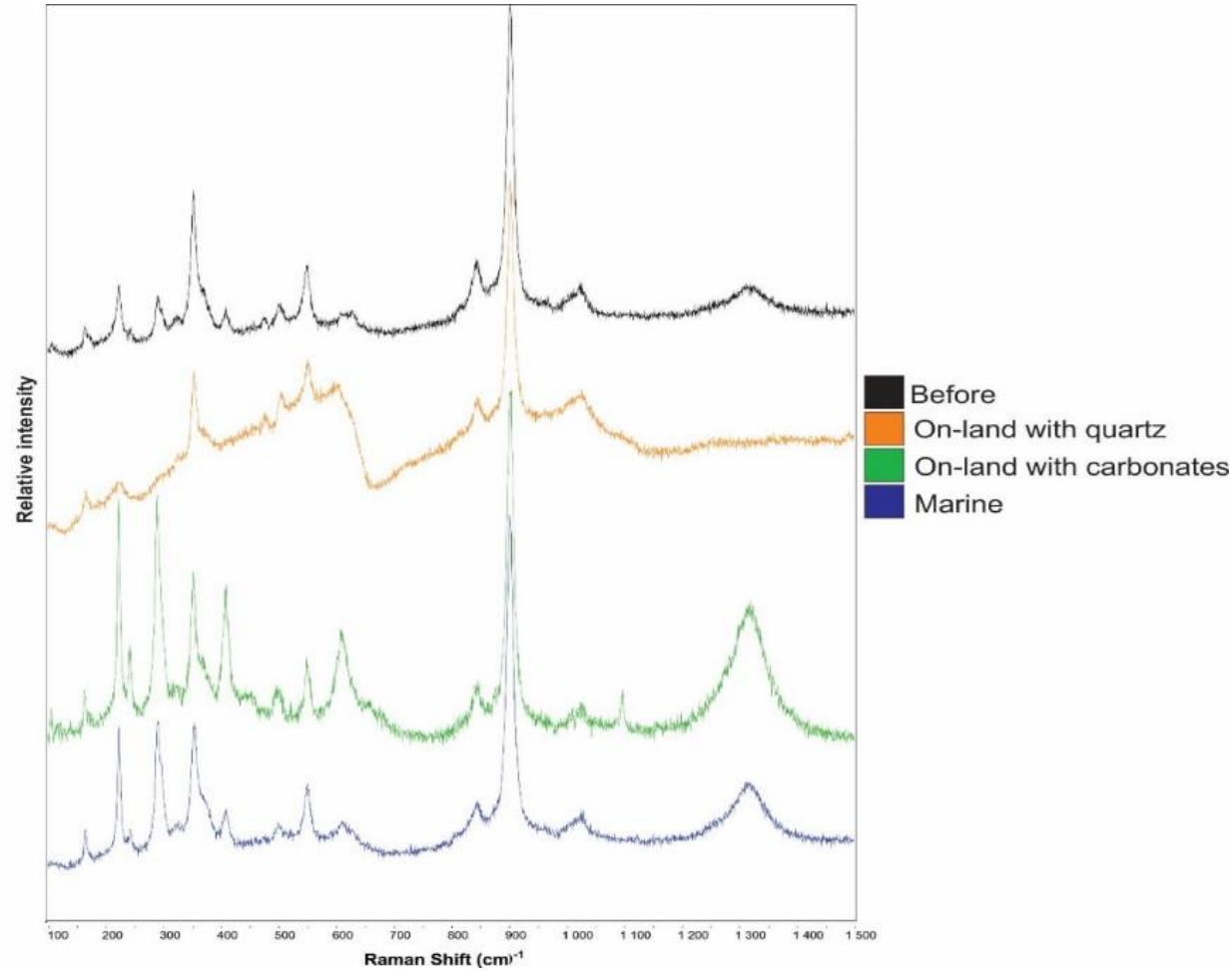

Figure 50: *Raman spectrum of the spessartine samples before (black), non-buffered on-land with quartz (orange), buffered on-land with carbonates (green) and submarine environments (blue).*

5.6 Thermodynamic modelling

Thermodynamic modelling was conducted to estimate the speciation of iron and manganese in the simulated on-land and submarine conditions.

Hematite sample

The hematite sample for non-buffered on-land condition (Fig. 51) presents a speciation in reductive conditions as ferrous iron (Fe^{2+}) and in oxidative conditions as ferric iron (Fe^{3+}). In the reductive condition (Fig. 51a), the dominant species at low pH is Fe^{2+}. At neutral pH (7), the abundance of Fe^{2+} decreases with some addition of $FeOH^{+}$ and $Fe(OH)_2$(aq.). At pH 11, $Fe(OH)_3^{-}$ is the most abundant species. In the oxidative condition (Fig.51b), the dominant species under low pH are Fe^{3+} up to a pH of 2, where a shift to $FeOH^{+}$ occur. At pH 4, the most dominant species shifts to $Fe(OH)_2^{+}$ that dominates at neutral pH up to pH 8, where $Fe(OH)_4^{-}$ is the most dominant species at high pH. For buffered on-land condition in reductive conditions (Fig. 52a), the dominant species at low pH is Fe^{2+} with some abundance of $FeHCO_3^{+}$. At neutral pH, the abundance of Fe^{2+} decreases. At high pH, some abundance of $FeOH^{+}$ and $Fe(OH)_2$(aq.) occur and the most dominant specie at pH 11 is $Fe(OH)_3^{-}$. In oxidative conditions (Fig. 52b), the most dominant species at low pH is $FeOH^{2+}$ and Fe^{3+}, with an increasing abundance of $Fe(OH)_2^{+}$ that is the most dominant species after pH 3. The abundance of $Fe(OH)_2^{+}$ decreases after neutral pH, where a shift to $Fe(OH)_4^{-}$ occur at high pH. For submarine conditions in reducing conditions (Fig. 53a), the most dominant species is Fe^{2+}, with some abundance of iron sulphate, $FeSO_4$(aq.), and iron chloride, $FeCl^{+}$. At pH 9, the abundance of Fe^{2+} decreases, where a shift to $Fe(OH)_3^{-}$ as the dominant species occur at high pH. In oxidative conditions (Fig. 53b), the most dominant species is $FeCl^{2+}$, $FeSO_4^{+}$ and Fe^{3+}. A shift to $Fe(OH)_2^{+}$, as the dominant species occur at pH of 3.5 up to pH of 8, where $Fe(OH)_4^{-}$ dominates at high pH.

Magnetite sample

The magnetite sample for non-buffered on-land conditions (Fig. 54) presents a speciation in reductive conditions as ferrous iron (Fe^{2+}) and in oxidative conditions as ferric iron (Fe^{3+}). In the reductive condition (Fig. 54a), the dominant species at low pH up to pH 10 is ferrous iron. At neutral pH, some introduction of $FeOH^{+}$ and $Fe(OH)_2$(aq.) occur. At high pH>11, the most

dominant species is $Fe(OH)_3^-$. In oxidative condition (Fig. 54b), the dominant species under low pH are Fe^{3+} up to pH of 3, $FeOH^{2+}$ up to pH 4, where a shift to $Fe(OH)_2^+$ occur. At neutral pH and up to pH 8, $Fe(OH)_2^+$ is the dominant species. After pH 8, $Fe(OH)_4^-$ is the dominant species. For buffered on-land with carbonates condition in reductive condition (Fig. 55a), Fe^{2+} is the most dominant species at low pH, with some abundance of $FeHCO_3^+$. At neutral pH, the abundance of Fe^{2+} decreases. At high pH, some abundance of $FeOH^+$ and $Fe(OH)_2$(aq.) occur and the most dominant species (pH>11) is $Fe(OH)_3^-$. In oxidative conditions (Fig. 55b), the most dominant species are $FeOH^{2+}$ and Fe^{3+}. At pH 3, $Fe(OH)_2^+$ dominates up to pH 7 where it decrease. At high pH 8 a shift to the most dominant species of $Fe(OH)_4^-$ occur. For the submarine condition in reductive condition (Fig. 56a), the dominant species at low pH up to pH 11 is Fe^{2+}. Some abundance of SO_4(aq.) and $FeCl^+$ occurs around pH 3 to 9. At high pH, some $FeOH^+$ and $Fe(OH)_2$(aq.) occurs, with a decreased abundance of Fe^{2+} that shift to $Fe(OH)_3^-$ as dominant species after pH 11. In oxidative condition (Fig. 56b), the abundance of species are $Fe(OH)^{2+}$, $FeSO_4^+$, $FeCl^{2+}$ and Fe^{3+}. At pH 3.5, the most dominant species are $Fe(OH)_2^+$ that decreases after neutral pH and shifts to $Fe(OH)_4^-$ at pH 8.

Manganese rich sample

The manganese rich sample for non-buffered on-land conditions (Fig. 57) presents a speciation where the dominant species at low and neutral pH is Mn^{2+} as the only dominant species. Around pH 9, a decrease of Mn^{2+} occur. A shift of the most dominant species from Mn^{2+} to $Mn_2(OH)_3^+$ occur at pH around 10. In buffered on-land with carbonates condition (Fig. 58) at low pH, Mn^{2+} dominates with some abundance of $MnHCO_3^+$. At neutral pH, Mn^{2+} dominates that decreases after neutral pH. At high pH around 10, the most dominant species shift from Mn^{2+} to $Mn_2(OH)_3^+$. Some abundance of $MnCO_3$(aq.) occur from pH 8 to 10. In submarine conditions (Fig. 59) at low pH, Mn^{2+} dominates, with some abundance of $MnCl^+$ and $MnSO_4$(aq.) up to pH of 9. At pH 10, the dominant species shifts from Mn^{2+} to $Mn_2(OH)_3^+$.

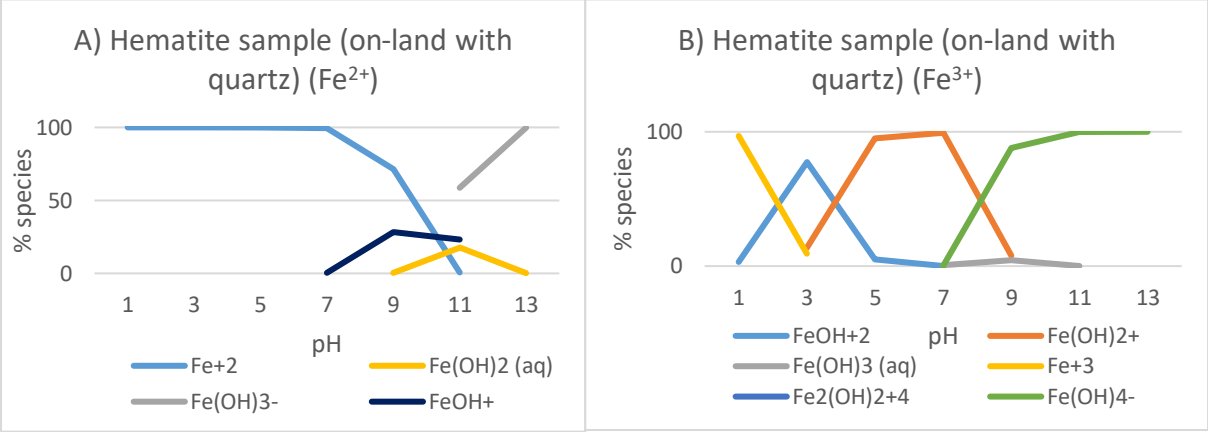

Figure 51: Speciation of hematite sample in on-land with quartz conditions associated with A) Fe^{2+} or B) Fe^{3+} with hematite as infinite phase.

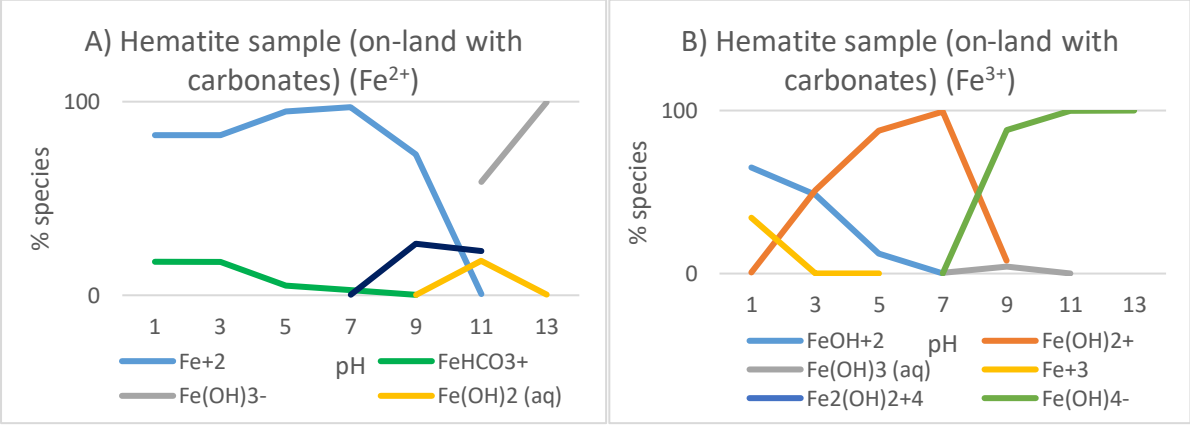

Figure 51: Speciation of hematite sample in on-land with carbonates condition associated with A) Fe^{2+} or B) Fe^{3+} with hematite and calcite as infinite phase.

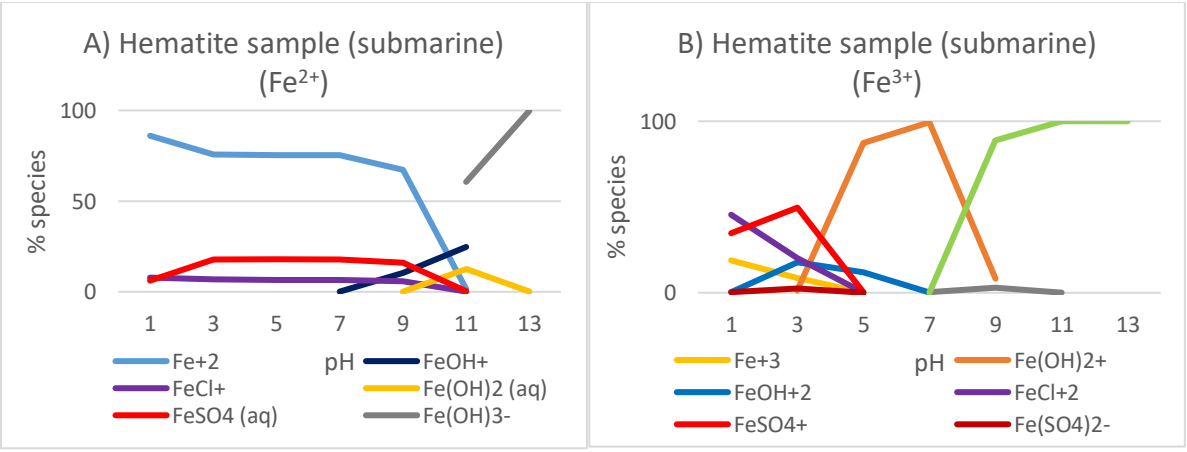

Figure 52: Speciation of hematite sample in submarine condition associated with A) Fe^{2+} or B) Fe^{3+}, additionally Cl^-, Na^+, SO_2^{4-}, Mg^{2+}, Ca^{2+} and K^+ in solution with hematite as infinite phase.

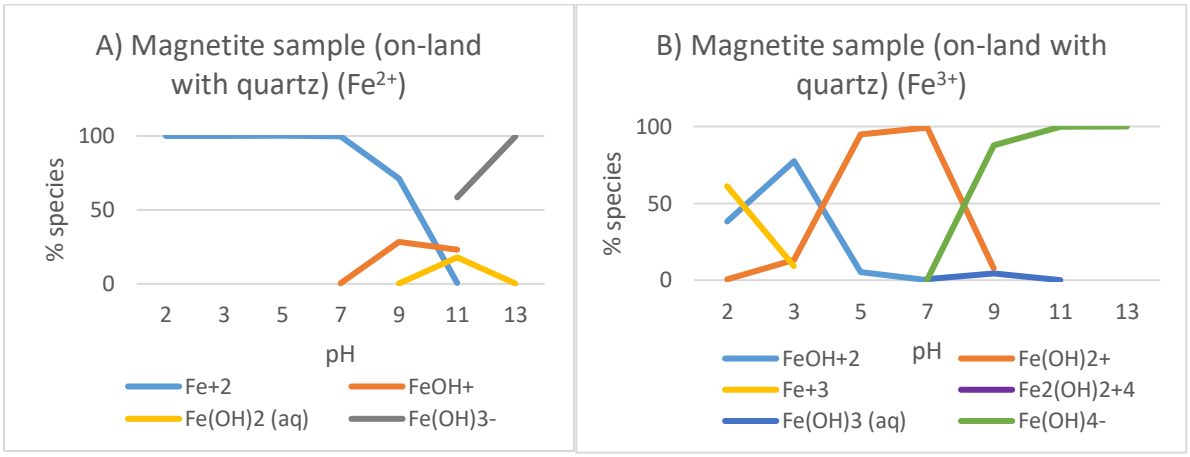

Figure 53: Speciation of magnetite sample in on-land with quartz conditions associated with A) Fe^{2+} or B) Fe^{3+} with magnetite as infinite phase.

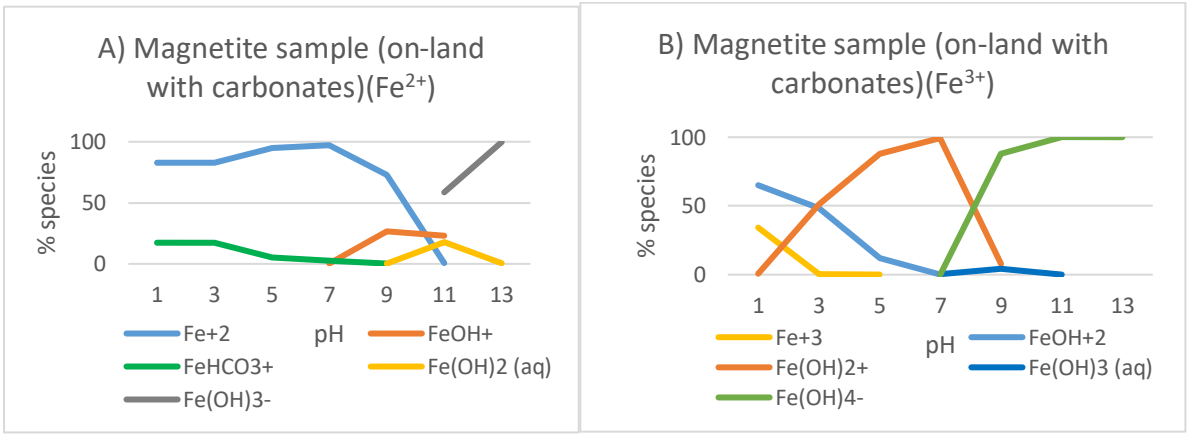

Figure 54: Speciation of magnetite sample in submarine conditions associated with A) Fe^{2+} or B) Fe^{3+}, additionally Cl^-, Na^+, SO_2^{4-}, Mg^{2+}, Ca^{2+} and K^+ in solution with magnetite as infinite phase.

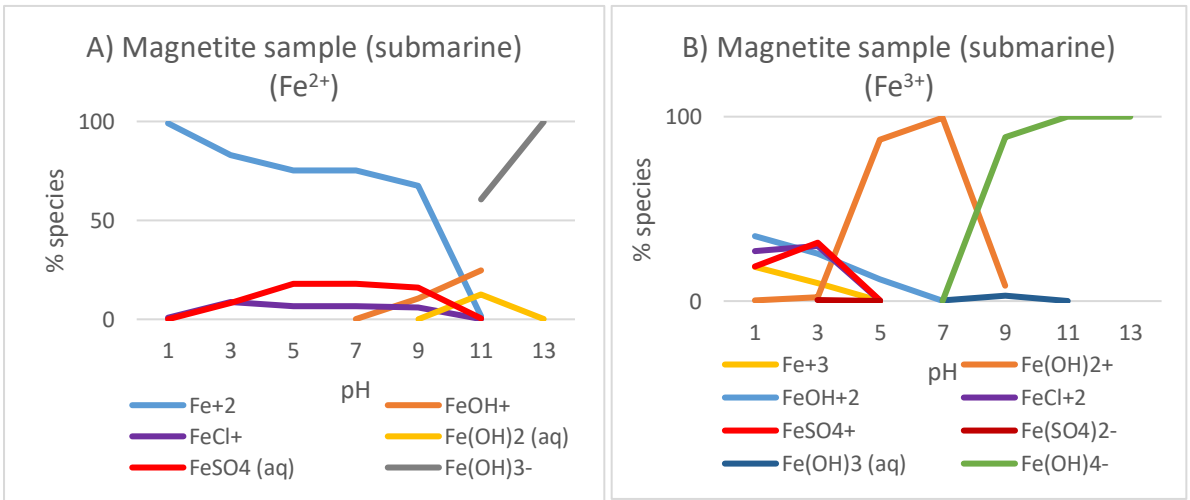

Figure 55: Speciation of magnetite sample in on-land with carbonate conditions associated with A) Fe^{2+} or B) Fe^{3+} with magnetite and calcite as infinite phase.

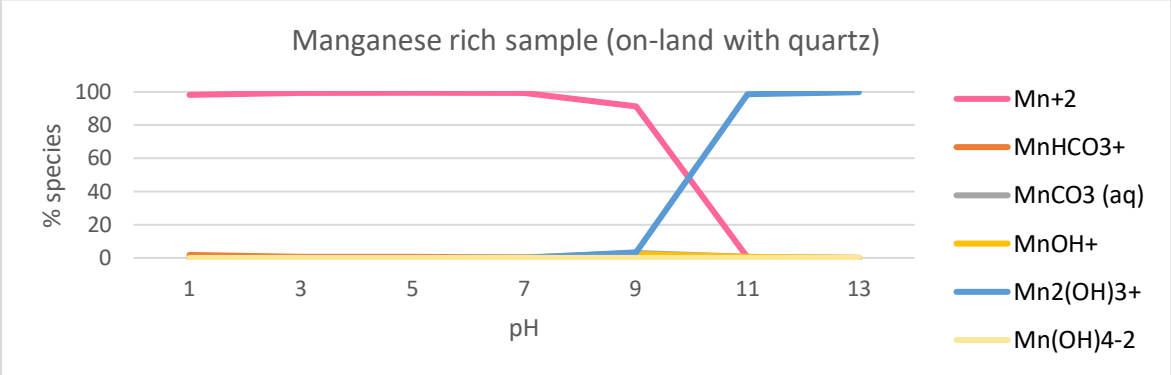

Figure 56: Speciation of manganese rich sample in on-land with quartz condition associated with Mn^{2+} with rhodochrosite ($MnCO_3$) as infinite phase.

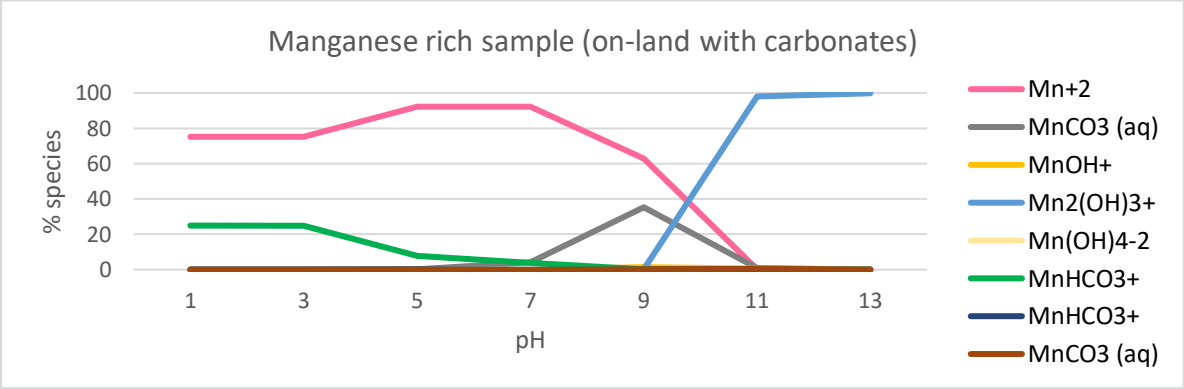

Figure 57; Speciation of manganese rich sample in on-land with carbonates condition associated with Mn^{2+} with rhodochrosite ($MnCO_3$) and calcite as infinite phases.

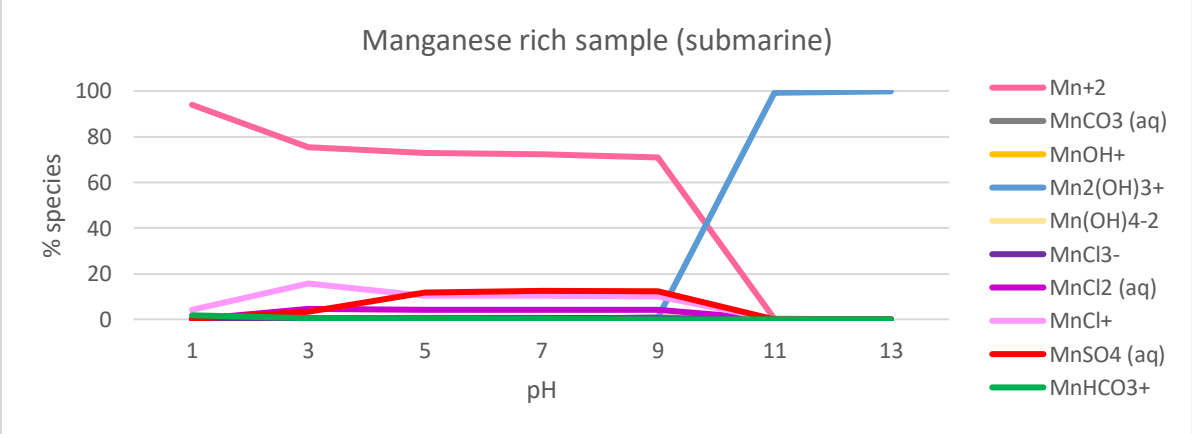

Figure 58: Speciation of manganese rich sample in submarine conditions associated with Mn^{2+}, additionally Cl^-, Na^+, SO_2^{4-}, Mg^{2+}, Ca^{2+} and K^+ in solution with rhodochrosite ($MnCO_3$) as infinite phase.

6 Discussion

In this chapter, the obtained results are discussed with the aim to assess the potential environmental impact of tailings from the stratiform iron mineralization in on-land and submarine disposal conditions. The case study was conducted on samples from the stratiform iron mineralization in the Dunderland Valley.

6.1 Mineral and geochemical characteristics of the ore mineralization

The analysed samples of the stratiform iron mineralization from the Dunderland Valley were selected as typical representatives of three main types of the ore mineralization in the area. They include a hematite-, magnetite- and manganese-rich mineralization. The environmental impact related to disposal of tailings strongly depends on the mineral and geochemical characteristics of the mineralization and its host rocks (Dold, 2014).

1) The hematite sample is mainly composed of hematite, quartz, muscovite and calcite. By XRD analysis an additional component of zeolite is present as well. Supported by lithogeochemical analysis, the major oxides are enriched in silica and iron, with some aluminium and calcium. Comparing to the crustal average values (Clarke), an elevated content of copper was recorded. The SEM/EDS analyses have not revealed the mineral phase that brings copper. All other metals and matalloids were within ranges typical for upper continental crust.
2) According to the results of the optical microscopy, the magnetite sample was composed of quartz, magnetite, epidote, biotite, muscovite, apatite, calcite and rare copper sulphides, mostly chalcocite. In addition, the XRD analysis revealed a presence of albite, ankerite and fluorannite. According to the lithogeochemical analysis, the major oxides are oxides of iron and silica, with some aluminium and calcium oxides. An enrichment in copper has been recorded as well, comparing to Clarke values. In this sample, copper is predominantly sitting within the crystal lattice of sulphide minerals.
3) The manganese rich sample represents a sample mainly composed of spessartine, quartz, biotite and minor amounts of hematite and calcite. The XRD analysis suggests a presence of zeolite as well. The lithogeochemical analysis shows the predomination

of silica, iron and manganese with some aluminium, calcium, magnesium and sodium. Comparing to the Clarke values, cobalt, arsenic and antimony are present in the concentration above the average crustal values. The SEM/EDS analyses indicate that cobalt is hosted by hematite, arsenic is located in biotite, while antimony is sitting in the crystal lattice of spessartine.

The lithogeochemical analyses revealed that all of three analysed samples are enriched in Fe, Si, Mn, Al and Ca. The mineralogical analyses indicate that Fe, Si, Mn and Al are mostly bonded in mineral phases resistant to weathering (hematite, magnetite, quartz, garnets and micas). In contrast, Ca is bonded mostly in carbonates, but this element belongs to the group of essential elements and does not show any environmental threat.

Magnetite ore contains minor amounts of chalcopyrite that may be affected by a process of oxidation when they are exposed to the oxygen-rich environment (Equation 6). Consequently, the pH value of the system may be decreased and Cu^{2+} may be released in the environment.

$$4CuFeS_2 + 17O_2 + 4H_2O \rightarrow 2Fe_2O_3 + 4Cu^{2+} + 8SO_4^{2-}(aq.) + 8H^+(aq.) \quad \textbf{(Equation 6)}$$

Anyhow, abundant amounts of carbonate minerals in this type of the mineralization prevent generation of acid mining drainages (Equation 7) and buffer the aqueous solutions to near-neutral conditions.

$$CaCO_3 + 2H^+ \rightarrow Ca^{2+} + CO_2(g) + H_2O \quad \textbf{(Equation 7)}$$

According to the presented Eh-pH diagrams, the most of transitional metals, including copper, are immobile and therefore not bioavailable under the near-neutral pH conditions.

In the manganese rich sample an elevated content of cobalt, arsenic and antimony compared to the crustal average values (Clarke) are present. However, all three elements are bonded within mineral phases resistant to weathering. Cobalt is an element that has similar physical properties as iron (Barceloux and Barceloux, 1999). In low amounts cobalt is an essential element for human metabolism (B-12 vitamin), as well as for metabolic processes of many lower organisms including blue-green algae (Holm-Hansen et al., 1954). Anyhow, high concentrations of cobalt can be harmful for the environment. According to the Eh-pH diagram, the Co-O-H system (Fig. 62, Appendix A), cobalt is mobilized under acidic

conditions (low pH). Arsenic is considered to be a very toxic elements when it is bioavailable and it is highly undesirable component in natural waters (Hem, 1985; Berg et al., 2001). The mobility of arsenic is strongly dependent on pH and redox potential of the system (Fig. 63, Appendix A). Antimony is a non-essential toxic metalloid that can cause environmental problems (Zeng et al., 2015). The mobility of antimony depends on the chemical speciation (He et al., 2018) and it is dependent on the pH and Eh of the system (Fig. 64, Appendix A). Weathering and biological activity can cause release of antimony to the environment, that can give toxic effects on the ecosystem (He et al., 2018).

All samples contain low concentrations of sulphur. As presented in section 3.3.4 (**Sulphur**), sulphur is a relatively abundant component in natural waters (Rose et al., 1979). The form of sulphur depends on pH and Eh of the system (Figure 13). The abundance of sulphide-minerals in mineralization can cause AMD, described in section 3.3.4.1 (**Acid mine drainage**), as acidic sulphur-rich wastewater produced by sulphide-bearing minerals that are exposed to oxygen and water (Johnson and Hallberg, 2005; Akcil and Koldas, 2006). A consequence of AMD is acidity of water that can cause heavy metals (e.g. lead, zinc and arsenic) to dissolve into ground or surface water, that can have toxic consequences. The acidic conditions can be treated by supply of carbonates to neutralize the acid and precipitate heavy metals (Akcil and Koldas, 2006). Since the samples are characterized by high Fe^{3+}/Fe^{2+} ratios, contain negligible amounts of sulphur and are rich in carbonates, their capability to generate AMD is extremely low, classifying the stratiform iron deposits in the Dunderland Valley as ore deposits of a low environmental risk.

6.2 Kinetic column test

The kinetic column analysis was conducted to test the stability of ore and associated gangue minerals to physical conditions characteristics for on-land and submarine tailing disposal sites.

6.2.1 Physicochemical measurements

Figure 29 shows variations in pH values for the different samples in different simulated conditions. The leachates released from columns simulating the non-buffered on-land conditions show variable, but generally neutral pH values. The on-land set-up buffered with carbonates resulted with generation of alkaline leachates. Whereas, the submarine conditions had the most constant and relatively high pH values.

The variations in measured Eh values of the released leachates are presented in Figure 30. The leachates for the on-land conditions show the most fluctuating values, whereas the submarine condition had more constant values of Eh. For submarine conditions with presence of organic matter it is expected low values of Eh. The measurements showed relatively high values, indicating the reducing conditions for the submarine condition may not have been achieved.

Measurements of conductivity was analysed as a proxy for total amount of ions present in the leachates (Fig. 31). Whereas the columns that simulated submarine conditions were flooded with seawater, the solutions leached from this type of columns had expectedly high conductivity due to the high content of various cations (Na^+, Ca^{2+}, Mg^{2+}) and anions (Cl^-, SO_4^{2-}, HCO_3^-) in seawater (Fred T. Mackenzie, 2018). The on-land buffered with carbonates had some higher values of conductivity than the non-buffered on-land conditions, plausibly indicating dissolution of carbonates (Equation 8).

$$CaCO_3 + H_2O + CO_2 \rightarrow Ca^{2+} + 2HCO_3^- \quad \textbf{(Equation 8)}$$

The difference between the samples (hematite, magnetite and manganese rich) in the conditions show minimal changes, suggesting similar solubility of all three types of ore-bearing samples.

6.2.2 Eh-pH diagrams

The recorded Eh and pH measurements are presented in Eh-pH diagrams to show stability fields of relevant mineral phases in the simulated conditions.

The hematite sample was presented in a Fe-O-H system. Most of the measurements were in the stability field of hematite, except one measurement in non-buffered on-land conditions that was on the boundary to mobile ferrous iron (Fe^{2+}) (Fig. 11). This indicates that iron could possibly be mobile in the on-land tailings disposal site if they are not buffered with carbonates. However, the diagram shows that a decrease in pH or relatively low pH together with low Eh (reducing acidic conditions (Fig. 60)) can cause mobilization of iron (Fig. 32).

The magnetite sample was presented in a Fe-O-H-Si system. All the measurements were in the stability field of FeO*OH (goethite) (Fig. 11). This indicates that the iron is immobile in all conditions, but not in form of magnetite. According to the obtained results, magnetite will start to weather in all simulated conditions, but iron will precipitate as $Fe(OH)_3$ that will diagenetically results in formation of goethite (Equation 9 and Equation 10) (Fig. 33).

Fe_3O_4 (*magnetite*) + OH^- + H_2O = γ-Fe_2O_3 + $Fe(OH)_3^-$ **(Equation 9)**

$2Fe(OH)_3^- + 1/2O_2 + 2H^+ = 2\alpha\text{-}FeOOH$ (*goethite*) + $3H_2O$ **(Equation 10)**

The manganese rich sample was presented in Mn-O-H and Mn-C-S-O-H systems and all measurements indicated that under all simulated tailing conditions, manganese shall be mobile as Mn^{2+} (Fig. 34).

By comparing the plotted conditions located in the Eh-pH diagrams (Figs. 32, 33 and 34), the measurements show a general trend for all samples. The non-buffered on-land conditions are located to more neutral-acidic conditions (to the centre-left) in the diagrams, whereas the buffered on-land conditions are located more to alkaline conditions (to the right) and the submarine conditions are in the centre. Expected variations of the conditions in the Eh-pH diagrams are presented in Figure 60. On-land conditions are expected to have oxygen available (section 3.2.1.1(**On-land**)) and will therefore be located with high Eh, an oxidizing system. Marine conditions are associated with less oxygen available (section 3.2.1.2 (**Marine**)) and will therefore be located with low Eh values, a reducing system. According to our measurements, there was minimal variations in Eh of the different conditions (on-land vs.

submarine). This indicates that the submarine conditions did not reach reducing conditions as tried to simulate. This can possibly be according to the set-up and/or the abundance of organic material. The set-up could have caused oxygen to enter the system (sealing), with addition of oxygen in the water or when sampled leachates (flooding of columns). As presented in section 3.2.1.2 (**Marine**), the amount of organic material can cause a decrease of redox potential (low Eh). If the amount of organic material in the natural marine sediments were too low, it can affect the ability to get reducing conditions. The addition of carbonates to on-land conditions (oxidizing) would affect the pH to be more alkaline as confirmed by our measurements, where the measurements were generally located more to alkaline conditions in all samples. Generally, acidic conditions associated with tailing disposal are related to AMD as presented in section 3.3.4.1 (**Acid mine drainage**). The measurements for non-buffered on-land condition showed some lower pH, around neutral (pH 6-8), compared with the other conditions. The lower values of pH do not need to indicate that there is generation of AMD, only that the expected pH is a bit lower for on-land conditions without any addition of carbonates.

The dissemination of the measurements within the conditions showed that the non-buffered on-land and buffered on-land conditions measurements were more scattered, whereas the submarine measurements were more concentrated. The spreading of the measurements indicates that the submarine conditions are more stable than the other conditions.

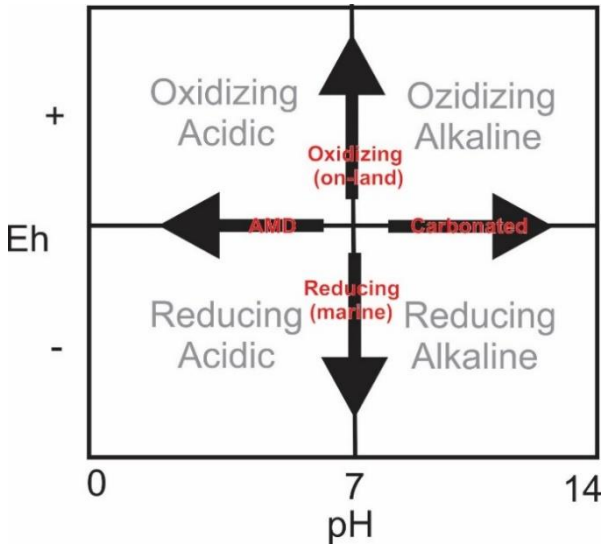

Figure 60: Basic regions in Eh-pH diagram with additional arrows with conditions commonly associated. Four regions are presented as oxidizing (acidic), oxidizing (alkaline), reducing (acidic) and reducing (alkaline)(Modified figure from Natarajan and Bangalore).

6.2.3 Lithogeochemistry

The samples used in the columns in the kinetic test were performed lithogeochemical analysis before and after the experiment (before and after weathering). The results are presented in Table 6 and 7, Figs. 35-43, 67-69.

The hematite sample presented minimal changes of major oxides and trace element content after weathering by comparing the different conditions to each other. There was some depletion of copper by comparing the samples before and after weathering, indicating leaching of copper.

The magnetite sample showed similar contents of both major oxides and trace elements before and after kinetic tests. Some minimal changes occurred, with an increased value of calcium in buffered on-land conditions and sodium in submarine conditions. This can be due to the content in sediments and water used in the kinetic test.

The manganese rich sample presented a relatively similar content of major oxides and trace elements by comparing the conditions to each other, indicating a stable sample in all conditions.

The content of sulphur in all samples are maintained low in all conditions, indicating low concentrations of sulphide minerals (e.g. pyrite, chalcopyrite). As presented in the previous section, the low levels of sulphide minerals prevent generation of AMD, that is good for the environmental aspects of mining in the area.

6.2.4 Sources of error kinetic column test

As presented is section 4.4 (**Kinetic column test**), the EPA method 1627 is a kinetic test procedure to predict mine site drainage quality. The method requires some standardization of the column test procedure, but also gives a flexibility for the test to be adjusted (Jacobs et al., 2014) to represent the actual site conditions (e.g. sample size, mass, water flow and degree of oxygenation)(Walder, 2012). In this study the method was used to simulate on-land and submarine disposal conditions for materials characteristics for sediment-hosted iron stratiform deposits. The original purpose was to use the leachates collected from the columns to analyse for dissolved metals, but due to the extent of the study it was removed from this master

project. Even though, the leachate analysis would have been useful to determine the release of metals and metalloids over time.

The modifications done were mostly related to the kinetic set-up and the masses used in the columns. The kinetic set-up was smaller and the sample masses used in the columns were 50 grams, compared to the original method 1800-2000 grams should have been used (EPA, 2011). There was used less sample material since the original plan of this study was to follow PhD student Yulia Mun for the experiment. She only had a small amount of material, so a decision to scale down the columns and sample from the original method was done. The original method saturates the columns with oxygen, a CO_2-air mixture, to maintain the expected field conditions (on-land). This is especially important for sulphide mineralization studies, since the oxidation in the kinetic test will not be as high that expected for actual on-land conditions. For the submarine condition, to get the conditions in the column more like the real-life situation, the oxygen saturation in the fjord could have been simulated. Like a study in Repparfjord, Norway, it was used 4,4 mg/L of dissolved oxygen to flow through the columns to simulate fjord conditions (Embile et al., 2018). The temperature of the submarine conditions can be adjusted for to get more like actual conditions, but a decrease in temperature give effects on the dissolution that is commonly decreased and will therefore slow down the experiment. Other modifications that could have been done to better simulate real-life situation is the simulation of flow in submarine conditions. A slow upward movement of deoxygenated water through the column could have been used for submarine conditions (Jacobs et al., 2014).

To ensure the validation of the measurements, the experiment needs to be done multiple times. Since the sampling and measurements of the leachates were cyclic, all changes may not have been detected. To make the measurements more precise, the sampling should have been done more often. Duplicate samples (identical sample and set-up) could have been run to get better quality results, that also will give an indicator of the precision of the measurements according to procedure and set-up.

6.3 Thin sections exposed to weathering

Thin sections that were exposed to weathering conditions were analysed to detect eventual changes of the mineralogy in the thin sections.

In all thin section samples there was only observed changes of the colour of the calcite grains in non-buffered on-land conditions. An unaltered calcite grain is commonly colourless with lamellar twinning that can be observed in plane polarized light (Pichler and Schmitt-Riegraf, 2012). The calcite grains in our samples in all conditions, except the non-buffered on-land condition, had these distinguishing features. In the non-buffered on-land conditions, calcite grains were yellow-brown in colour with an altered rim and weak to invisible twinning. The colour change in the calcite grain indicates partial replacement of Ca^{2+} with Fe^{2+} during the weathering processes. Other elements that commonly replace Ca are Mn, Mg and Sr. Since there were only some visible changes in non-buffered on-land condition, the condition is considered to be favourable for eventual remobilization of deposited metals. In contrast, simulated conditions of the buffered on-land sites, as well of the submarine disposal has not affected the exposed mineral phases.

The additional SEM/EDS analysis of magnetite (or similar to magnetite) grains in non-buffered on-land and submarine conditions indicates some variations in the iron-oxygen ratio. The variations can indicate an alteration of the magnetite grain that may have been altered to a form of iron hydroxides e.g. FeO(OH) or $Fe(OH)_3$.

6.3.1 Raman spectroscopy

Additional Raman study of the thin sections were performed to study eventual changes in the hematite, magnetite and spessartine grains before and after weathering that were not observed by optical microscopy and SEM/EDS.

The hematite sample showed a hematite spectrum with many similarities, indicating that the crystal structure of hematite was preserved. Some differences in the structure were in non-buffered on-land and submarine conditions that can be due to some disorder in the crystal structure. The most likely factor affecting is weathering. The cause of changes in non-buffered on-land conditions can be because of lowering of pH and for submarine conditions

because of reductive conditions, that may have caused ferric iron to be reduced to ferrous iron ($Fe^{3+} \rightarrow Fe^{2+}$).

The magnetite sample showed spectrum for buffered and non-buffered on-land conditions, where the spectrum had clearly similarities with the magnetite spectrum from literature that indicates a preserved crystal structure of magnetite.

The manganese rich sample presented spectrum of spessartine with the largest variations for the non-buffered on-land conditions, with bands less prominent and out of shift and buffered on-land conditions, with additional bands occurring. The differences may indicate a possible disorder in the crystal structure of spessartine, where the most likely factor affecting is weathering.

6.3.2 Sources of error thin section exposed to weathering

Since this method do not have been conducted before, the reliability of the method needs to be evaluated. The uncertainty of the method is connected to whether the method can detect mineralogical changes expected for the different conditions. The results from our study showed minimal changes, that were expected of weathering of oxides. A similar study conducted by PhD student Yulia Mun at UiT on copper sulphide-rich samples showed distinctive changes, that were expected of weathering of sulphides. This can indicate a reliability of the method.

For future study, each of the specific thin sections need to be analysed for mineralogical content before exposed to weathering. The original idea was to use one thin section of the sample to characterize the sample from before weathering, but after the experiment an unexpected variation in some of the thin section were observed. Therefore, the mineralogical changes cannot be stated as changed from weathering, it can be mineralogical variations in the samples before the experiment. Therefore, to ensure the results are valid, the experiment needs to be repeated.

The type of Raman analysis conducted was a point analysis, due to limited time for analysis. For future work a Raman mapping is recommended to get an overview of the components and possible weathering of the minerals.

6.4 Thermodynamic modelling

Thermodynamic modelling was performed to predict the speciation of iron and manganese in non-buffered on-land, buffered on-land with carbonates and submarine conditions (Figs. 51-59).

The speciations in the hematite saturated system and magnetite saturated system show almost no variation to each other. In general, for the iron samples in reductive conditions, the dominant species under low to neutral pH is ferrous iron, and for high pH, iron hydroxide. In oxidative conditions, the dominant species under very low pH are ferric iron, at neutral-high pH as iron hydroxide: $Fe(OH)_2^+$ at neutral pH and $Fe(OH)_4^-$ at high pH. The addition of carbonates in on-land conditions makes some content of iron carbonates ($FeHCO_3^+$) under low pH for reducing conditions. For submarine conditions, some abundance of iron sulphate and iron chlorite occur at low pH for oxidative conditions and for pH in the range from 3 to 9 for reducing conditions.

The speciation for manganese rich sample presented relatively similar abundance for all conditions with some exceptions. In general, there was abundance of Mn^{2+} from low up to pH of 9. At high pH, manganese hydroxide dominates. For on-land with carbonates condition there was an addition of manganese carbonates at low pH, whereas for submarine conditions there was some abundance of manganese sulphates and chlorides around neutral pH. For the manganese speciation only Mn^{2+} was included. The speciation of Mn^{3+} and Mn^{4+} was not included since there was no indication of occurrence of these oxidation states of manganese in our system (e.g. manganese is in the +2-oxidation state in spessartine and rhodochrosite).

Generally, the addition of carbonates to the systems do not give a significant effect to bind the iron and manganese, only some occurrence at low pH. This indicates that the carbonates added to the system will not contribute to mobilize iron and manganese. The effects connected to the submarine conditions only give some changes at low-neutral pH, were sulphate and chlorite complexes can occur. The abundance is low and will not affect the mobility significantly.

6.5 Summary of discussion

The potential environmental impact related to disposal of tailings from the Dunderland Valley in on-land and submarine conditions has been evaluated.

By the characterization of ore samples, their composition has been determined. The hematite and magnetite sample contain mostly of iron and silica, with some abundance of carbonates and elevated trace values of copper compared with crustal average values (Clarke). These elements are in stable mineral forms that are not susceptible to weathering (magnetite, hematite, quartz, micas). Consequently, these types of ore mineralization do not represent an environmental threat from a geochemical point of view. The manganese rich sample contain mostly of manganese and silica, with some content of iron and carbonates. These elements are in stable mineral phases that are resistant to weathering (garnets, quartz, hematite). There is also some content of elevated trace values of cobalt, arsenic and antimony in the sample. These elements can be considered environmental harmful elements when they are mobile. In the sample, these elements occur in stable mineral forms that makes them immobile and is therefore not considered environmentally harmful. By studying Eh-pH diagrams of the elements content in the samples, a mobilization of these elements can occur by changes in Eh and pH, especially due to lowering of pH conditions. A lowering of pH often occurs by high sulphide minerals content in the ores, by generation of acidic mine drainage (AMD). Since the samples are characterized by high Fe^{3+}/Fe^{2+} ratios, contain negligible amounts of sulphide minerals and are rich in carbonates, their capability to generate AMD is extremely low. This classify the stratiform iron deposits in the Dunderland Valley as ore deposits of a low environmental risk.

The kinetic column test presented the physicochemical properties of the different conditions according to pH, Eh and conductivity. The results showed that the non-buffered on-land conditions would be the least favourable condition with fluctuating and the lowest pH values compared to the other conditions. The on-land buffered with carbonates were relatively protective, whereas the submarine condition was the most preserving and therefore the favourable for the deposition of sediment-hosted stratiform iron deposits according to our measurements. The difference between the samples (hematite, magnetite and manganese rich)

in the conditions show minimal changes, suggesting similar solubility of all three types of ore-bearing samples.

The Eh-pH diagrams presented for the hematite sample indicted that iron could possibly be mobile in on-land disposal sites if they are not buffered with carbonates. The magnetite sample showed that magnetite would be weathered in all simulated conditions to goethite and/or be mobilized from its crystal lattice under low pH conditions. The manganese rich sample indicated that manganese shall be mobile as Mn^{2+} in all simulated conditions.

The lithogeochemical results evaluated the samples before and after the kinetic test. In general, there were only small changes in the content of the sample before and after weathering, that indicates a stable sample for all conditions. Except it was some changes in the hematite sample with occurrence of a depletion of copper in all conditions compared with the sample before. This may indicate that some copper has been mobilized and leached.

Thin section exposed to weathering showed visible changes for non-buffered on-land conditions with visible weathering of calcite grains. Since there were only visible changes in the non-buffered on-land conditions, the buffered on-land and submarine condition are considered to be more favourable for stability of deposited metals. The additional SED/EDS analyses of magnetite grains indicates that the magnetite content in the non-buffered on-land and submarine condition were not magnetite, but an altered form of iron hydroxides. The Raman analyses confirmed a preserved crystal structures of hematite, magnetite and spessartine (manganese rich sample) with some disorder in the structures, where the most likely factor affecting is weathering.

The speciation of iron and manganese in the weathering conditions indicates that the addition of carbonates to the system do not give a significant effect to bind the iron and manganese, only some occurrence at low pH conditions. The effects connected to marine systems only give some changes at low-neutral pH, were sulphate and chlorite complexes occur. Since these abundances are low, it will not affect the mobility of iron and manganese significantly.

6.6 Compared to previous work in Dunderland Valley

The obtained results are in accordance with previously published data (e.g. Molab AS and NIVA (2011), and Johansen et al. (2004) and Walday et al. (2004) (Ramirez-Llodra et al., 2015) presented in section 3.2.3. These studies indicate that there was no pollution and effects on biota by disposal of tailings from the Dunderland Valley. Some additional knowledge of the characterization of the ore samples and their behaviour in the simulated conditions has been presented from our study.

7 Conclusions

This study has estimated the potential environmental impact related to disposal of tailings from the sediment-hosted stratiform iron deposits in the Dunderland Valley in on-land and submarine conditions, the following conclusions are:

- The studied ore samples are characterized by high Fe^{3+}/Fe^{2+} ratios, high carbonate contents and negligible amounts of sulphide minerals, that results in an extremely low capability to generate AMD and mobilization of heavy metals. This classify the stratiform iron deposits in the Dunderland Valley as ore deposits with a low environmental risk.
- The studied ore samples contain low amount of heavy metals.
- There was detected some elevated trace values of copper, cobalt, arsenic and antimony that were in stable mineral forms, therefore not considered environmentally harmful.
- The simulated disposal conditions indicate that the carbonate-buffered on-land and submarine conditions are considered to be the best method for deposition of tailings from the sediment-hosted stratiform iron deposits.

8 Appendix

8.1 Appendix A - Eh-pH diagrams

8.1.1 Eh-pH diagrams

Copper

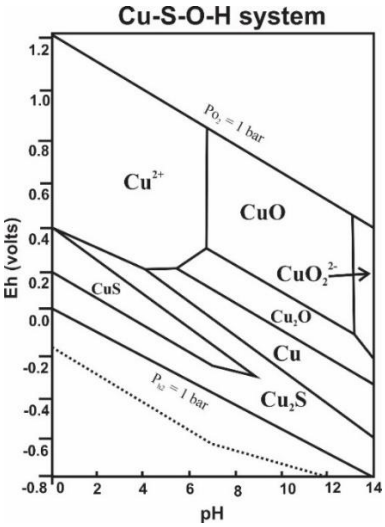

Figure 61: Eh-pH diagram for part of the system Cu-S-O-H. The assumed activities for dissolved species are Cu = 10^{-6}, S = 10^{-3} (Brookins, 1988).

Cobolt

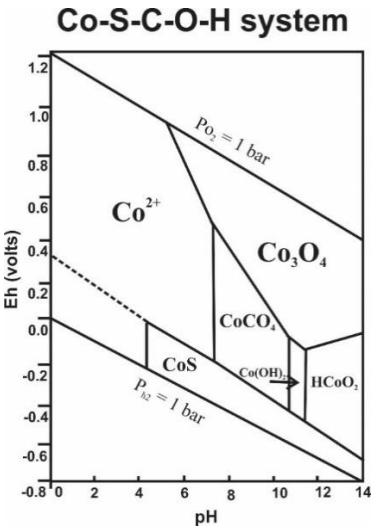

Figure 62: Eh-pH diagram for part of the Co-S-C-O-H system. Activity assumed of dissolved Co = 10^{-6}, C = 10^{-3}, S = 10^{-3}(Brookins, 1988).

Arsenic

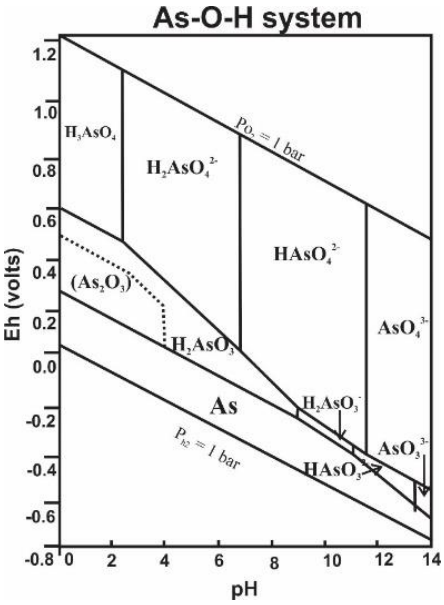

Figure 63: Eh-pH diagram for part of the system As-O-H. Assumed acitivities are As = 10^{-6}, S = 10^{-3} (Brookins, 1988).

Antimony

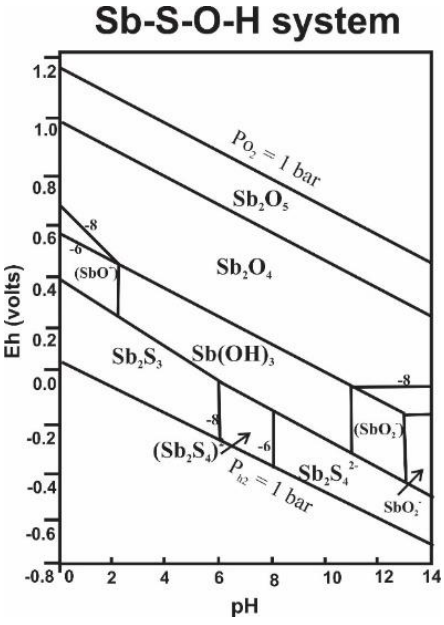

Figure 64: Eh-pH diagram for part of the Sb-S-O-H system. Activity assumed of dissolved Sb = $10^{-6,-8}$, and S = 10^{-3}. Aqueous oxyions of antimony is SbO^+ for low pH conditions, and SbO_2^- at high pH conditions (Brookins, 1988).

8.2 Appendix B - Kinetic column test analysis

8.2.1 Organic matter measurement of marine sediments

Table 15: Organic matter measurement of marine sediments and calculation.

Sample weight before	1,0002
After HCl treatment and drying	0,9931
After heating	0,99
Difference	0,0031
Total organic matter content (wt.%)	0,31

8.2.2 Volumes of collected leachates

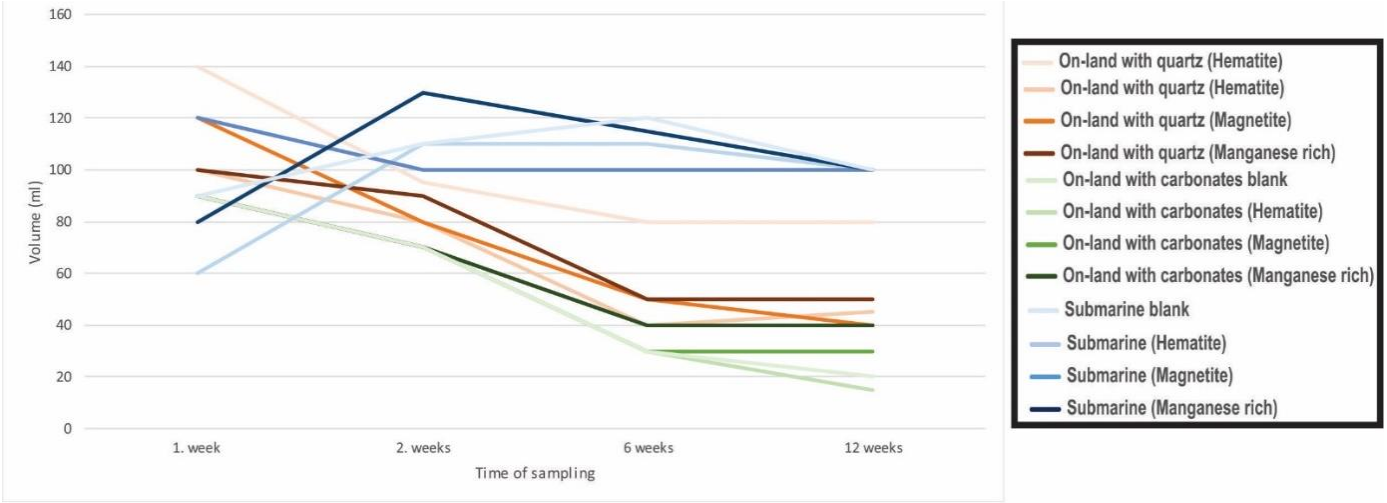

Figure 65: The volumes of the leachates from the kinetic column test.

8.2.3 Temperature variations in the columns

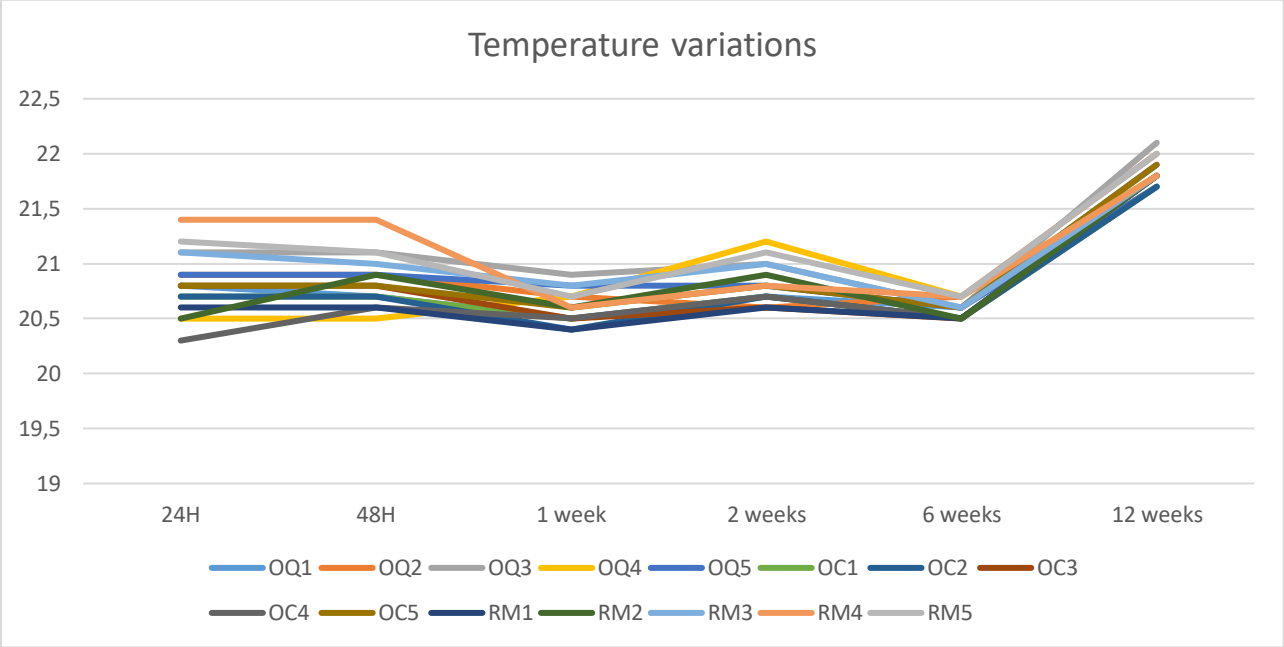

Figure 66: Temperature variations in the columns measured by the multimeter.

8.2.4 Additional SEM/EDS analysis of the magnetite samples

The ratio of silica is for each silica, there is two oxygen (SiO_2 = ratio 1:2).

Table 16: Calculation of magnetite ratio before weathering. (Silcon = silicon).

Before		Si * 2	O - (Si*2)	Ratio FeO
Element	[norm. at.%]			0,77
Iron	40,74			
Oxygen	57,08	4,36	52,72	
Silcon	2,18			

Table 17: Calculation of magnetite ratio after weathering (non-buffered on-land = on-land with quartz). (Silcon = silicon).

On-land with quartz		Si * 2	O - (Si*2)	Ratio FeO
Element	[norm. at.%]			0,80
Iron	38,86			
Oxygen	56,88	8,52	48,36	
Silcon	4,26			

Table 18: Calculation of magnetite ratio after weathering (buffered on-land = on-land with carbonates). (Silcon = silicon).

On-land with carbonates		Si * 2	O - (Si*2)	Ratio FeO
Element	[norm. at.%]			0,79
Iron	38,29			
Oxygen	57,36	8,68	48,68	
Silcon	4,34			

Table 19: Calculation of magnetite ratio after weathering (submarine).

Submarine		Si*2	O-(Si*2)	Ratio FeO
Element	[norm.at.%]			0,87
Iron	31,74			
Oxygen	57,65	21,22	36,43	
Silicon	10,61			

8.2.5 Seawater composition

Table 20: The composition of seawater with a salinity of 35. Data taken from (SOEST, 2010).

Component	Concentration (mol*kg^{-1}) = molal
Cl^-	0,546
Na^+	0,469
SO_2^{4-}	0,0283
Mg^{2+}	0,0528
Ca^{2+}	0,0103
K^+	0,0102

8.2.6 Isochon diagrams of hematite sample

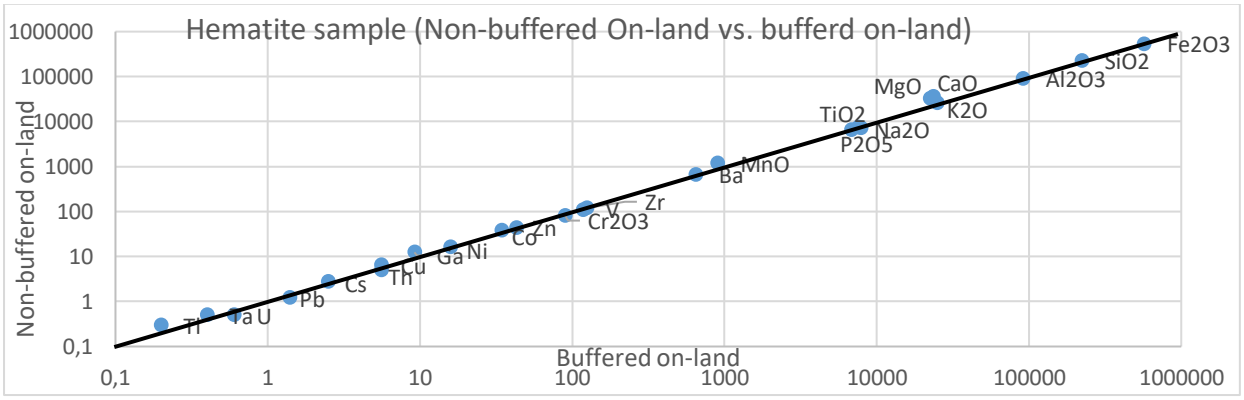

Figure 67: Isochon diagram of the hematite sample, the content on-land with quartz vs. on-land with carbonates condition.

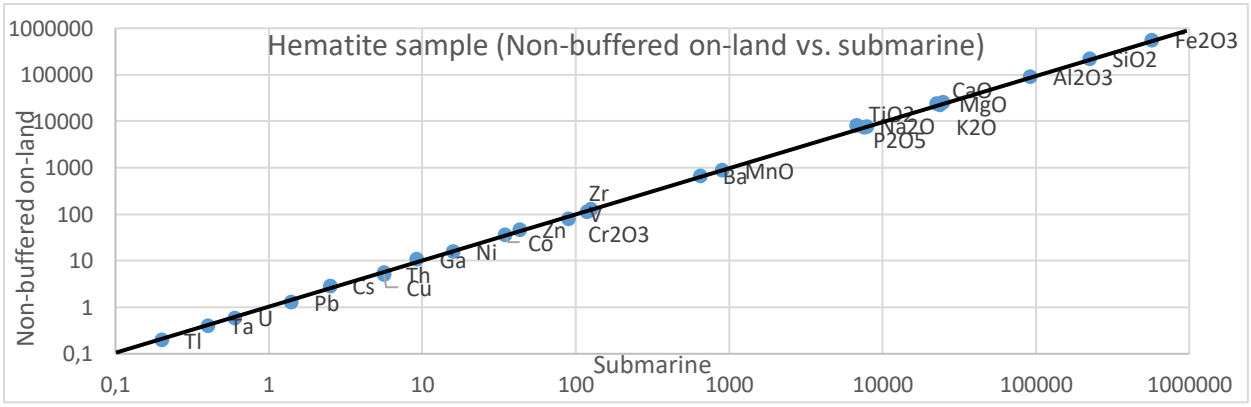

Figure 68: Isochon diagram of the hematite sample, the content on-land with quartz vs. submarine condition.

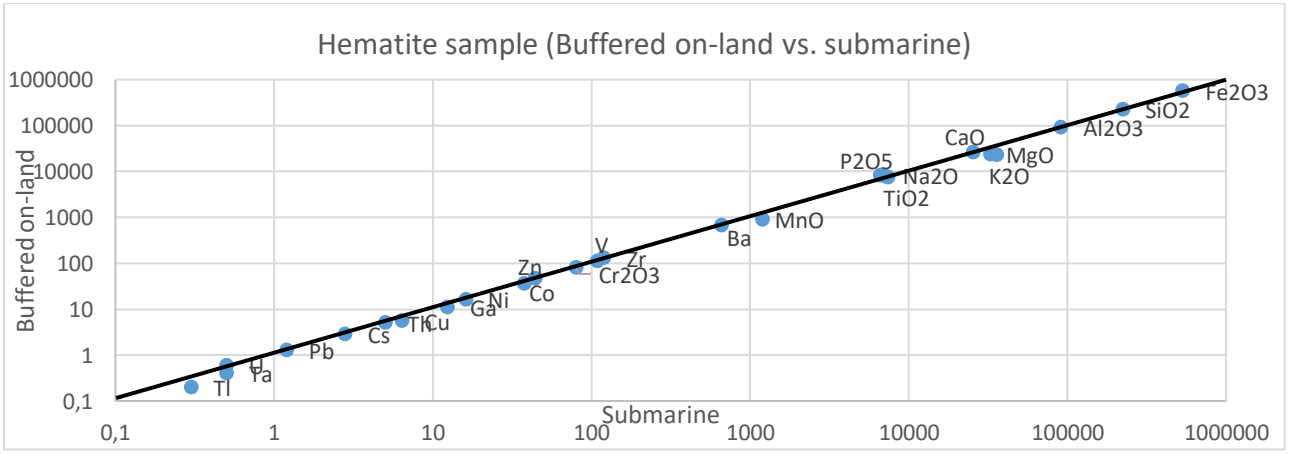

Figure 69: Isochon diagram of the hematite sample, the content on-land with carbonates vs. submarine condition.

8.3 Appendix C - Lithogeochemistry detection limits (MDL) for analysed elements

Table 21: Detection limit for major element analysis.

Analyte	Unit	MDL
SiO2	%	0,01
Al2O3	%	0,01
Fe2O3	%	0,04
MgO	%	0,01
Na2O	%	0,01
K2O	%	0,01
TiO2	%	0,01
P2O5	%	0,01
MnO	%	0,01
Cr2O3	%	0,002
LOI	%	-5,1
TOT/C	%	0,02
TOT/S	%	0,02

Table 22: Detection limit for trace element analysis.

Analyte	Unit	MDL	Analyte	Unit	MDL	Analyte	Unit	MDL
Ba	ppm	1	**V**	ppm	8	**Yb**	ppm	0,05
Ni	ppm	20	**W**	ppm	0,5	**Lu**	ppm	0,01
Sc	ppm	1	**Zr**	ppm	0,1	**Mo**	ppm	0,1
Be	ppm	1	**Y**	ppm	0,1	**Cu**	ppm	0,1
Co	ppm	0,2	**La**	ppm	0,1	**Pb**	ppm	0,1
Cs	ppm	0,1	**Ce**	ppm	0,1	**Zn**	ppm	1
Ga	ppm	0,5	**Pr**	ppm	0,02	**Ni**	ppm	0,1
Hf	ppm	0,1	**Nd**	ppm	0,3	**As**	ppm	0,5
Nb	ppm	0,1	**Sm**	ppm	0,05	**Cd**	ppm	0,1
Rb	ppm	0,1	**Eu**	ppm	0,02	**Sb**	ppm	0,1
Sn	ppm	1	**Gd**	ppm	0,05	**Bi**	ppm	0,1
Sr	ppm	0,5	**Tb**	ppm	0,01	**Ag**	ppm	0,1
Ta	ppm	0,1	**Dy**	ppm	0,05	**Au**	ppb	0,5
Th	ppm	0,2	**Ho**	ppm	0,02	**Hg**	ppm	0,01
U	ppm	0,1	**Er**	ppm	0,03	**Tl**	ppm	0,1
V	ppm	8	**Tm**	ppm	0,01	**Se**	ppm	0,5

9 References

Abdel-Shafy HI and Mansour MSM. (2016) A review on polycyclic aromatic hydrocarbons: Source, environmental impact, effect on human health and remediation. *Egyptian Journal of Petroleum* 25: 107-123.

Akcil A and Koldas S. (2006) Acid mine drainage (AMD): causes, treatment and case studies. *Journal of cleaner production* 14: 1139-1145.

Barceloux DG and Barceloux D. (1999) Cobalt. *Journal of Toxicology: Clinical Toxicology* 37: 201-216.

Bekker A and Kaufman AJ. (2007) Oxidative forcing of global climate change: a biogeochemical record across the oldest Paleoproterozoic ice age in North America. *Earth Planetary Science Letters* 258: 486-499.

Bekker A, Slack JF, Planavsky N, et al. (2010) Iron Formation: The Sedimentary Product of a Complex Interplay among Mantle, Tectonic, Oceanic, and Biospheric Processes*. *Economic Geology* 105: 467-508.

Berg M, Tran HC, Nguyen TC, et al. (2001) Arsenic Contamination of Groundwater and Drinking Water in Vietnam: A Human Health Threat. *Environmental Science & Technology* 35: 2621-2626.

Bielowicz B, Botor D, Misiak J, et al. (2018) Critical Elements in Fly Ash from the Combustion of Bituminous Coal in Major Polish Power Plants. *E3S Web of Conferences*. EDP Sciences, 02003.

Britannica. (2018) *Marine ecosystem*. Available at: https://www.britannica.com/science/marine-ecosystem.

Brookins DG. (1988) *Eh-pH diagrams for geochemistry*: Springer Science & Business Media.

Bugge JAW. (1948) *Rana gruber: Geologisk beskrivelse av jernmalmfeltene i Dunderlandsdalen*: I kommisjon hos H. Aschehoug.

Cairns-Smith AG. (1978) Precambrian solution photochemistry, inverse segregation, and banded iron formations. *Nature* 276: 807.

Canavan F. (1973) Notes on the terms ‘stratiform’,‘stratabound’and ‘stratigraphic control’as applied to mineral deposits. *Journal of the Geological Society of Australia* 19: 543-546.

Canfield DE. (1998) A new model for Proterozoic ocean chemistry. *Nature* 396: 450.

Cloud P. (1973) Paleoecological significance of the banded iron-formation. *Economic Geology* 68: 1135-1143.

Corfu F, Gasser D and Chew DM. (2014) New perspectives on the Caledonides of Scandinavia and related areas: introduction. 390: 1-8.

Cornwall N. (2013) Submarine tailings disposal in Norway's fjords: Is it the best option?

Cox GM, Halverson GP, Minarik WG, et al. (2013) Neoproterozoic iron formation: An evaluation of its temporal, environmental and tectonic significance. *Chemical Geology* 362.

De Faria D and Lopes F. (2007) Heated goethite and natural hematite: can Raman spectroscopy be used to differentiate them? *Vibrational Spectroscopy* 45: 117-121.

De Faria D, Venâncio Silva S and De Oliveira M. (1997a) Raman microspectroscopy of some iron oxides and oxyhydroxides. *Journal of Raman spectroscopy* 28: 873-878.

De Faria D, Venâncio Silva S and De Oliveira M. (1997b) Raman microspectroscopy of some iron oxides and oxyhydroxides. *Journal of Raman spectroscopy* 28: 873-878.

Deb M and Goodfellow WD. (2004) *Sediment Hosted Lead-Zinc Sulphide Deposits*: CRC Press.

Dold B. (2014) Submarine tailings disposal (STD)—A review. *Minerals* 4: 642-666.

Ehrenreich A and Widdel F. (1994) Anaerobic oxidation of ferrous iron by purple bacteria, a new type of phototrophic metabolism. *Applied environmental microbiology* 60: 4517-4526.

Embile RF, Walder IF, Schuh C, et al. (2018) Cu, Pb and Fe release from sulfide-containing tailings in seawater: Results from laboratory simulation of submarine tailings disposal. *Marine Pollution Bulletin* 137: 582-592.

Emsbo P, Seal RR, Breit GN, et al. (2016) Sedimentary exhalative (sedex) zinc-lead-silver deposit model. *Scientific Investigations Report.* Reston, VA, 72.
EPA. (2011) Method 1627: Kinetic Test Method for the Prediction of Mine Drainage Quality. In: Water (ed). United States: Environmental Protection Agency.
EPA and Sweeney D. *What is Acid Mine Drainage* Available at: http://www.sosbluewaters.org/epa-what-is-acid-mine-drainage%5B1%5D.pdf.
Figenschau N. (2018) Interaction of submarine tailings with natural sediments in three northern Norwegian coastal areas. Sedimentological, mineralogical and geochemical constraints. UiT Norges arktiske universitet.
Folkehelseinstituttet. (2018) *Kjemiske og fysiske stoffer i drikkevann* Available at: https://www.fhi.no/nettpub/stoffer-i-drikkevann/kjemiske-og-fysiske-stoffer-i-drikkevann/kjemiske-og-fysiske-stoffer-i-drikkevann.
Fred T. Mackenzie ACDaO. (2018) *Seawater*. Available at: https://www.britannica.com/science/seawater.
Gee DG, Juhlin C, Pascal C, et al. (2010) Collisional Orogeny in the Scandinavian Caledonides (COSC). *GFF* 132: 29-44.
GeologicalSurvey US, Udall SL and Nolan TB. (1962) Chemistry of iron in natural water. Washington: U.S. Govt. .
González SA, Stotz W and Lancellotti D. (2014) Effects of the discharge of iron ore tailings on subtidal rocky-bottom communities in northern Chile. *Journal of Coastal Research* 30: 500-514.
Grenne T, Ihlen P and Vokes FJMD. (1999) Scandinavian Caledonide metallogeny in a plate tectonic perspective. 34: 422-471.
Gross GA. (1996) Stratiform iron; in Geology of Canadian Mineral Deposit Types (ed.). *Geology of Canada*: 41-54.
Gustafsson J. (2012) Visual MINTEQ 3.1. *Department of land water resources engineering, Royal Institute of Technology, Stockholm*

Gustafsson JP. (2011) Visual MINTEQ 3.0 user guide. *KTH, Department of Land Water Recources, Stockholm, Sweden*.
Haldar SK. (2013) Chapter 2 - Economic Mineral Deposits and Host Rocks. *Mineral Exploration.* Boston: Elsevier, 23-39.
Hammer A-E. (2011) *Dilemmas of mining*. Available at: http://sciencenordic.com/dilemmas-mining.
Haugen AE. (2018) Distribution, deposition and impact of tailing disposal on the seafloor in Ranfjorden, northern Norway. UiT Norges arktiske universitet.
He M, Wang N, Long X, et al. (2018) Antimony speciation in the environment: Recent advances in understanding the biogeochemical processes and ecological effects. *Journal of Environmental Sciences*.
Hem JD. (1985) *Study and interpretation of the chemical characteristics of natural water*: Department of the Interior, US Geological Survey.
Hoffman PF, Kaufman AJ, Halverson GP, et al. (1998) A Neoproterozoic snowball earth. *Science* 281: 1342-1346.
Holland HD. (1973) The oceans; a possible source of iron in iron-formations. *Economic Geology* 68: 1169-1172.
Holm-Hansen O, Gerloff GC and Skoog F. (1954) Cobalt as an essential element for blue-green algae. *Physiologia Plantarum* 7: 665-675.
Jacobs JA, Lehr JH and Testa SM. (2014) *Acid mine drainage, rock drainage, and acid sulfate soils: causes, assessment, prediction, prevention, and remediation*: John Wiley & Sons.
James HL. (1954) Sedimentary facies of iron-formation. *Economic Geology* 49: 235-293.
Johnson DB and Hallberg KB. (2005) Acid mine drainage remediation options: a review. *Science of The Total Environment* 338: 3-14.

Kartverket. (2013) *Norgeskart*. Available at: https://norgeskart.no/#!?project=norgeskart&layers=1002&zoom=4&lat=7197864.00&lon=396722.00.
Kirschvink JL. (1992) Late Proterozoic low-latitude global glaciation: the snowball Earth.
Klein C. (2005) Some Precambrian banded iron-formations (BIFs) from around the world: Their age, geologic setting, mineralogy, metamorphism, geochemistry, and origins. *American Mineralogist* 90: 1473-1499.
Klein C and Beukes NJ. (1989) Geochemistry and sedimentology of a facies transition from limestone to iron-formation deposition in the early Proterozoic Transvaal Supergroup, South Africa. *Economic Geology* 84: 1733-1774.
Kolesov B and Geiger C. (1998) Raman spectra of silicate garnets. *PhysicsChemistry of Minerals* 25: 142-151.

Konhauser KO, Amskold L, Lalonde SV, et al. (2007) Decoupling photochemical Fe (II) oxidation from shallow-water BIF deposition. *Earth Planetary Science Letters* 258: 87-100.
Konhauser KO, Planavsky NJ, Hardisty DS, et al. (2017) Iron formations: A global record of Neoarchaean to Palaeoproterozoic environmental history. *Earth-Science Reviews* 172: 140-177.
Kvassnes AJS and Iversen E. (2013) Waste sites from mines in Norwegian Fjords. *Mineralproduksjon* 3: A27-A38.
Leach DL, Bradley DC, Huston D, et al. (2010) Sediment-hosted lead-zinc deposits in Earth history. 105: 593-625.
Lenntech. *Heavy Metals*. Available at: https://www.lenntech.com/processes/heavy/heavy-metals/heavy-metals.htm.
Loe T and Aagaard P. (2013) Deponering av avgangsmasser fra gruveindustrien – på land eller i vann? *Mineralproduksjon, norsk bergforening*.
McGoldrick P and Large R. (1998) Proterozoic stratiform sediment-hosted Zn-Pb-Ag deposits. *Journal of Australian Geology Geophysics* 17: 189-196.
Melezhik VA, Ihlen PM, Kuznetsov AB, et al. (2015) Pre-Sturtian (800–730Ma) depositional age of carbonates in sedimentary sequences hosting stratiform iron ores in the Uppermost Allochthon of the Norwegian Caledonides: A chemostratigraphic approach. *Precambrian Research* 261: 272-299.
Miljødirektoratet. (2012) *Strenge krav til økt produksjon ved Rana Gruber*. Available at: http://www.miljodirektoratet.no/no/Nyheter/Nyheter/Old-klif/2012/Desember_2012/Strenge_krav_til_okt_produksjon_ved_Rana_Gruber/.
Miljødirektoratet. (2015) Deponering av syredannende bergarter. Grunnlag for veileder. . NGI (Norge geotekniske institutt).
MOLAB. (2011) Chemical analysis and leaching tests of H150, H400 and the main waste. .
Naidu R, Semple KT, Megharaj M, et al. (2008) Bioavailability: Definition, assessment and implications for risk assessment. In: Hartemink AE, McBratney AB and Naidu R (eds) *Developments in Soil Science*. Elsevier, 39-51.
Natarajan KA and Bangalore I. *Eh-pH Diagrams - Fundamental Aspects*. Available at: https://www.scribd.com/document/167508734/Lecture5Eh-Ph-Diagrams.
NGU. (2015a) *Gruvedeponi*. Available at: https://www.ngu.no/emne/gruvedeponier.
NGU. (2015b) Ørtfjell Deposit no. 40 in Rana (1833) municipality. *The Ore Database*.
Palinkaš AL, Bermanec V and Galović L. (2016) The Alpine Wilson cycle and NW Tethyan Metallogeny. *Geologia Croatica* 69: 1-2.
Paradis S and Goodfellow W. (2012) SEDEX Deposits in the Cordillera: Current concepts on their geology, genesis, and exploration. *Geological Survey of Canada, Geology of Canada* 7144.
Pedersen B. (2018) *Kobber*. Available at: https://snl.no/kobber.
Pedersen B and Kofstad PK. (2018) *Mangan*. Available at: https://snl.no/mangan.

Peters SE and Loss DP. (2012) Storm and fair-weather wave base: A relevant distinction? *Geology* 40: 511-514.
Pichler H and Schmitt-Riegraf C. (2012) *Rock-forming minerals in thin section*: Springer Science & Business Media.
Posth NR, Konhauser KO and Kappler A. (2011) Banded iron formations. *Encyclopedia of Geobiology*. Springer, 92-103.
Poulton SW and Canfield DE. (2011) Ferruginous Conditions: A Dominant Feature of the Ocean through Earth's History. *Elements* 7: 107-112.
Radulescu M. (2010) Formation of a stratiform Zn–Pb–Ag sedex deposit—numerical simulation. *Carpathian Journal of Earth Environmental Sciences* 5: 67-82.
Ramberg IB, Bryhni I, Nøttvedt A, et al. (2013) *Landet blir til*, Norway: Norsk geologisk forening.
Ramirez-Llodra E, Trannum HC, Evenset A, et al. (2015) Submarine and deep-sea mine tailing placements: a review of current practices, environmental issues, natural analogs and knowledge gaps in Norway and internationally. *Marine Pollution Bulletin* 97: 13-35.
RanaGruber. *Dunderland Valley*. Available at: http://ranagruber.no/index.php?id=50&L=1%3Btx_news_pi1%5Bcontroller%5D%3DNews%3Btx_news_pi1%5Baction%5D%3Ddetail%3Btx_news_pi1%5Bnews.
Rickard D. (2012) Chapter 17 - The Evolution of the Sedimentary Sulfur Cycle. In: Rickard D (ed) *Developments in Sedimentology*. Elsevier, 685-766.
Robb L. (2005) *Introduction to ore-forming processes*: Blackwell Publishing
Roberts D. (2003) The Scandinavian Caledonides: event chronology, palaeogeographic settings and likely modern analogues. 365: 283-299.
Roberts D, Nordgulen O and Melezhik V. (2007) The Uppermost Allochthon in the Scandinavian Caledonides: From a Laurentian ancestry through Taconian orogeny to Scandian crustal growth on Baltica. *MEMOIRS-GEOLOGICAL SOCIETY OF AMERICA* 200: 357.
Rose AW, Hawkes HE and Webb JS. (1979) *Geochemistry in mineral exploration*: Academic press London.
Sangster D. (2002) The role of dense brines in the formation of vent-distal sedimentary-exhalative (SEDEX) lead–zinc deposits: field and laboratory evidence. *Mineralium Deposita* 37: 149-157.
Scott M. *Magnetite R060656*. Available at: http://rruff.info/magnetite/display=default/R060656.
Shervais J, Kolesar P and Kyle Andreasen A. (2005) *A Field and Chemical Study of Serpentinization—Stonyford, California: Chemical Flux and Mass Balance*.
Sintef. *NYKOS*. Available at: https://www.sintef.no/projectweb/nykos/.
Skei J. (2013) The dilemma of waste management in the mining industry-criteria for sea disposal. *Mineralproduksjon* 3: 1-4.
Skei J. (2014) Norwegian experiences with sea disposal of mine tailings. 1 ed. NBI (Norsk Berg Industri): Deposition Working Group.
Skinner BJ. (2015) *Mineral deposit*. Available at: https://www.britannica.com/science/mineral-deposit/Mississippi-Valley-type.
Smith KS. (2007) Strategies to predict metal mobility in surficial mining environments. *Reviews in engineering geology* 17: 25-45.
SOEST. (2010) *Chemical composition of seawater; Salinity and the major constituents* Available at: http://www.soest.hawaii.edu/oceanography/courses/OCN623/Spring2012/Salinity2012web.pdf.
Stephens M, Furnes H, Robins B, et al. (1985) Igneous activity within the Scandinavian Caledonides. *The Caledonide orogen—Scandinavia related areas* 2: 623-657.
Stephens M and Gee D. (1989) Terranes and polyphase accretionary history in the Scandinavian Caledonides. *Geological Society of America, Special Paper* 230: 17-30.
Taylor S. (1964) Abundance of chemical elements in the continental crust: a new table. *Geochimica et cosmochimica acta* 28: 1273-1285.

Trendall A. (1973) Varve cycles in the Weeli Wolli Formation of the Precambrian Hamersley Group, Western Australia. *Economic Geology* 68: 1089-1097.
Vogt C. (2012) International assessment of marine and riverine disposal of mine tailings. *Proceedings of the 34th Meeting of the London Convention and the 7th Meeting of the London Protocol, London, UK.*
Vogt C. (2013) International Assessment of Marine and Riverine Disposal of Mine Tailings. Final Report Adopted by the International Maritime Organization. London Convention/Protocol, IMO.
Walder I. (2012) *Standarder og veiledere for karakterisering av mineralavfall.* Available at: https://www.slideshare.net/geoforskning/ingar-walder.
Wilkinson J. (2013) Sediment-Hosted Zinc-Lead Mineralization: Processes and Perspectives: Processes and Perspectives.
Yang J, Large R and Bull S. (2004) Factors controlling free thermal convection in faults in sedimentary basins: implications for the formation of zinc–lead mineral deposits. *Geofluids* 4: 237-247.
Yang J, Large RR, Bull S, et al. (2006) Basin-Scale Numerical Modeling to Test the Role of Buoyancy-Driven Fluid Flow and Heat Transfer in the Formation of Stratiform Zn-Pb-Ag Deposits in the Northern Mount Isa Basin. *Economic Geology* 101: 1275-1292.
Young TP. (1989) Phanerozoic ironstones: an introduction and review. *Geological Society, London, Special Publications* 46: ix-xxv.
Zeng D, Zhou S, Ren B, et al. (2015) Bioaccumulation of antimony and arsenic in vegetables and health risk assessment in the superlarge antimony-mining area, China. *Journal of analytical methods in chemistry* 2015.